FREE CONVECTION HEAT TRANSFER FROM A VERTICAL SURFACE IN AN ENCLOSURE

DISSERTATION

Presented in Partial Fulfillment of the Requirements for the Degree Doctor of Philosophy in the Graduate School of The Ohio State University

By

DAVID JENKS MASSON, B.M.E., M.Sc.

The Ohio State University

1952

Approved by:

S. M. Marco

Adviser

The University assumes no responsibility for the accuracy or correctness of any of the statements or opinions expressed in this thesis.

ACKNOWLEDGMENTS

The author wishes to express his appreciation to Professor S. M. Marco, of the Mechanical Engineering Department of The Ohio State University, for his assistance, guidance and encouragement throughout the preparation of this dissertation.

Grateful acknowledgment is also due Professor W. Robinson of the Mechanical Engineering Department of The Ohio State University for his able counsel in connection with this work.

TABLE OF CONTENTS

LIST OF FIGURES

LIST OF SYMBOLS

a	Exponent
A	Constant
A	Area, square feet
b	Exponent
B	Constant
c	Specific heat at constant pressure, Btu per pound per ^{o}F
C	Constant
C'	Coefficient
d	Distance between top of model and top of duct, inches
D	Characteristic dimension
g	Acceleration of gravity, feet per hour squared
Gr_a	Grashof number based on total model height
Gr_p	Point Grashof number
h	Point heat transfer coefficient, Btu per hour per square foot per ^{o}F
k_m	Mean thermal conductivity based on average of model and duct temperatures, Btu per square foot-hour-^{o}F per foot
k_w	Thermal conductivity at temperature of heated surface, Btu per square foot-hour-^{o}F per foot
ℓ	Vertical distance from base to point on model surface, feet
ℓ'	Vertical distance from base to point on model surface, inches
L	Total height of model, feet
L'	Total height of model, inches

M	Length of model parallel to light beam, feet
Nu	Nusselt number, hD/k
Nu_{ave}	Nusselt number based on average heat transfer coefficient
Nu_p	Nusselt number based on point heat transfer coefficient
P	Pressure, pounds per square foot
q	Rate of heat transfer, Btu per hour
q'	Rate of heat transfer per unit area, Btu per hour per square foot
t_s	Duct wall temperature, ^oF
t_w	Model surface temperature, ^oF
T_r	Temperature of air surrounding interferometer, ^{o}Rankine
T_s	Duct wall temperature, ^{o}Rankine
T_w	Model surface temperature, ^{o}Rankine
ΔT	$t_w - t_r$
V	Velocity, feet per hour
x	Distance between vertical surfaces of model and duct, feet
x'	Distance between vertical surfaces of model and duct, inches
dt/dx	Temperature gradient, ^oF per foot
β	$1/T_w$, per degree Rankine
γ	Specific weight, pounds force per cubic foot
ϵ	Number of fringe displacements
η	Index of refraction
θ	$t_w - t_s$, ^oF
λ	Wave length, feet
μ	Absolute viscosity, pounds per foot hour

ν	Number of wave lengths
ρ	Density, pounds mass per cubic foot

SUMMARY

A Zehnder-Mach interferometer with eight-inch optical flats was used to gather the data. The configuration studied was a heated vertical rectangular prism confined by a floor, side wall, and top as shown in Figure 7, page 22. Table 1, page 22, gives the range of the variables investigated in this study.

The most significant results are:

1. The free convection heat transfer decreases from the value for a vertical wall in free air, for wall distances of something over one inch, to a minimum value which generally occurs for wall distances from three-eighths to one-half inches and then increases quite rapidly for very close spacings.

2. The free convective heat transfer is unaffected by the distance between the top of the heated wall and the top of the confining duct for distances greater than three-quarters of an inch. The free convective heat transfer from the top portion of the heated wall is considerably reduced as the top distance is reduced below three-quarters of an inch. This reduction is handled for computation purposes by graphical methods given in Figure 16.

3. The point value of the free convection heat transfer coefficient is given in terms of Nusselt and Grashof numbers by the empirical equation,

$$Nu_p = (k_m/k_w)(\ell/x) + 0.37\ \mathrm{Tanh}36x\ Gr_p^{0.25-0.0008x^{-1.43}} \qquad (15)$$

4. Integration of the value of h from the equation in (3) gives

$$Nu_{ave} = (k_m/k_w)(L/x) + \frac{(0.37\ \mathrm{Tanh}36x)Gr_a^n}{3n} \qquad (22)$$

where $n = 0.25 - 0.0008\ x^{-1.43}$

which fits the experimental values for the average heat transfer by free convection obtained by plotting point values and averaging by use of a polar planimeter.

Figure 17, page 46, is a graphical solution of the equation for the average Nusselt number which may be used for the determination of the average heat transfer coefficient. This chart is probably the most significant result of this work since it gives a simple means by which the desired results may be obtained. Although the actual experimental data do not extend over the complete range that the chart covers, it is felt that the trends have been so definitely established in the correlation of the experimental data that the extrapolation necessary to the extension of the chart is justified.

FREE CONVECTION HEAT TRANSFER FROM A VERTICAL SURFACE IN AN ENCLOSURE

SECTION I

INTRODUCTION

There has been a large number of works published by various experimenters in the field of free convection heat transfer. Most of the work in the past has been actuated by the necessity for information concerning its application to large constructions such as building, room heating, etc. Many experimental data are available in this field of heat transfer. For the most part equations have been presented by the authors that will express these data to a satisfactory degree of accuracy for engineering work. Most of these expressions are derived by using the tools of dimensional analysis and the constants determined by experimentation.

The evaluation of heat transfer by free convection by use of previously established equations is usually restricted to simple or special configurations since the equations have been set up for only the most commonly encountered shapes or special configurations for which there has been a particular need.

Most published free convective heat transfer data have been for bodies in free space. Some information for heat transfer between parallel walls at different temperatures is available but not for very closely spaced walls.

There is an almost complete lack of information concerning the free convective heat transfer between parallel walls that are closely spaced (less than a half inch) and also walls of small height (less than one foot). There is no information available concerning the free convective heat transfer for vertical surfaces that are completely confined.

This study came about due to this lack of data for short bodies closely confined. The results of this study are directly applicable to the problem of heat transfer by free convection from electronic components.

Free-convection heat transfer from individual electronic components to ambient air such as occurs in open vented equipment is losing its importance in current design of airborne electronic equipment because of its low magnitude at high operating altitudes and the reduction of temperature differentials available for heat dissipation at high flight speeds. However, many types of pressurized equipment have internal free-convective conditions since for moderate heat concentrations and at the relatively high internal pressure level free convection, radiation, and conduction are sufficient to transmit heat to be dissipated from components to the equipment case. In such equipments, the same modes cause heat transfer among components, i.e., between those of high heat dissipation and those of little or no heat dissipation in close proximity. In hermetically sealed sub-assemblies heat is transferred from internal components to the enclosure which is of similar size may also occur partly by free convection.

Electronic components and sub-assemblies are short bodies, one to five inches high, approaching cylindrical or prismatic shape. They are usually mounted on finite horizontal surfaces with their principal axes vertical. They are exchanging heat to surrounding surfaces mainly oriented parallel or normal to their axes in relatively close proximity.

It is one of the objects of this study to give information as to the best spacings to use in locating the various components of electronic equipment in their cabinets. Further, the information should be of general interest because it is unique in that it deals with short bodies that are confined.

SECTION II

EXPERIMENTAL TECHNIQUE

As stated above most of the experimental data and expressions for the evaluation of free convection heat transfer are concerned with large bodies in free space. Almost all of the data in the past have been correlated on the basis of the Grashof number and the Nusselt number (see Section III, page 36, for definitions).

Probably one of the reasons for the small amount of information on free convective heat transfer is the difficulty involved in obtaining it.

Data that are available are sometimes correlated with a small number of experimental points because enough analyses have been available so that generally only a verification of the validity of the analyses have been necessary.

For getting the free convection heat transfer from large bodies the usual method has been to make a heat balance involving corrections for radiation and conduction. These corrections usually are relatively large compared to the free convection heat transfer being investigated and are subject to a considerable amount of uncertainty.

In the past the methods of probing the temperature field near the surface with a thermocouple and of determining the heat input have been used for some studies on small bodies. This method may be criticized because of the fact that since the probe cannot measure the surface

temperature accurately (due to radiation to the probe), it is necessary to resort to extrapolation in order to evaluate the temperature gradient at the wall. Probing of the temperature field requires very steady conditions and is extremely tedious.

In evaluating the heat transfer for any small body the end effects are always a very difficult problem since the small body is often little more than two ends. End effects do not lend themselves readily to mathematical analysis.

From the above it is seen that if some method can be developed to obtain the whole temperature field adjacent to a body without corrections for other phenomena, such as radiation or conduction, around a body, the problem of collecting data for free convection heat transfer would be made much easier.

Optical methods are available to do just this. They fall into three general systems - the shadowgraph, schlieren, and interferometer.

The shadowgraph and schlieren are for the most part instruments that give a qualitative picture of what is happening while the interferometer gives a picture that is more readily evaluated from a quantitative standpoint.

1. The shadowgraph* consists of a high-intensity light beam passing through the subject and onto a photographic plate or screen. The differences in the rate of change in density causes

---

* For more detailed descriptions of these methods, see reference (16) and Appendix I.

different deflections of the light and therefore give a projection on the screen that has various intensities; the greater the rate of change of the density gradient the greater the contrast. This method is very suitable for the interpretation of what is happening in the field from a qualitative standpoint.

2. The schlieren* consists of a system whereby rays that are deflected to give less light at a particular point in the field on the screen are cut out so as to give more contrast than the shadowgraph. Likewise the bright regions are made brighter. Schlieren photographs can be evaluated but it involves tedious computations or measurements. The method is therefore best suited to qualitative work.

3. The Zehnder-Mach interferometer* was originally conceived in Germany in order to study gas flow. Its principle of operation depends on the fact that the refractive index of light varies with the density of the medium through which the light passes. As early as 1931 Kennard(1) published some results of studies of free convective heat transfer obtained with the interferometer. The interferometer is eminently suited to the study of free convective heat transfer, since in this case the variation of the density of a fluid is due only to variations in temperature, while the pressure is uniform. In accordance with the laws of perfect gases, density and temperature are inversely proportional to

---

* For more detailed descriptions of these methods, see reference (16) and Appendix I.

each other at constant pressure. Therefore, the temperature field surrounding a body at a temperature different from that of the convective fluid can be explored by means of the interferometer.

Appendix I gives the details of the application of the Zehnder-Mach interferometer as applied to this study.

SECTION III

TEST APPARATUS

Interferometer

The Zehnder-Mach interferometer used in this study had an optical system made up of five plane parallel optical plates 200 millimeters in diameter, manufactured of BS6-2 fine annealed optical glass. Two plates are partially coated on one surface for selective transmission. The other three are totally reflecting plane mirrors. All surfaces are ground flat to within less than one-quarter wave length of green light (5790 angstroms). The surfaces of the partially reflecting plates are parallel to each other to within 20 seconds of angle. The thickness of all plates is 25 millimeters.

The field of view of the interferometer as determined by the size of the plates is an ellipse with axes of 7.44 and 4.50 inches.

The supporting frame for the optical system has a box section made of half-inch steel plate. As shown in Figure 1, the frame is U-shaped so that the test configuration to be investigated may be placed in the open side. This instrument can be used in either the horizontal or vertical position.

For the experiments in the present investigation the interferometer frame was placed in the horizontal position. The

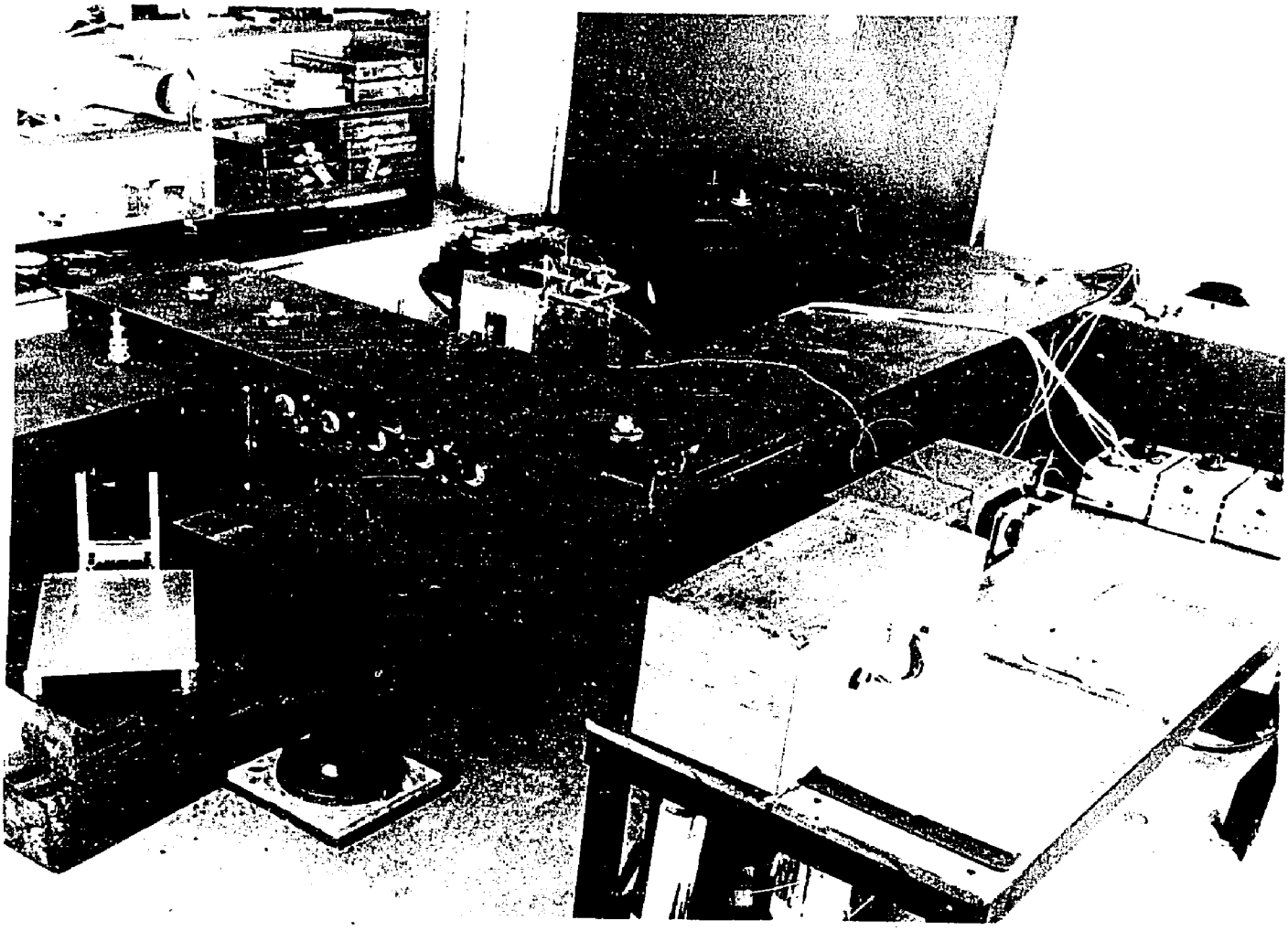

FIGURE 1.

GENERAL VIEW OF INTERFEROMETER WITH TEST MODEL AND AUXILIARY EQUIPMENT IN PLACE

test model was set in the open side as shown in Figure 1. Instrumentation and auxiliary control equipment were located on a separate table adjacent to the interferometer as shown in Figure 1.

Test Model

The configuration which was investigated was a heated vertical prismatic object of small height, mounted on a finite horizontal surface and surrounded by two cooled vertical surfaces and one cooled horizontal surface, all in relatively close proximity. The constructional features of the apparatus were such that the various distances between heated and cooled surfaces could be adjusted and prismatic objects of various heights could be used.

1. Determination of Length of Model

As pointed out in Appendix I, the interferometer required a configuration which could be considered to be equivalent to a two-dimensional system. Therefore, the lengths of the surfaces parallel to the light beam in the test section were of critical importance. It was realized that a very short model would introduce considerable difficulty in the interpretation of the interferograms since thermal gradients would exist in the field parallel to the test surfaces and hence it would be impossible to assign representative temperatures defined by the fringe patterns. In addition, the amount of refraction of light rays in a line parallel to the light bundle of the interferometer would depend on the difference in temperature between the test model and surroundings and

on the length for which this temperature difference existed (see Appendix I). The length of the model and the temperature difference would determine the distance between fringes. Thus for a minimum fringe spacing, determined by the resolving power of the photographic film to be used to record the interferograms for interpretation, the maximum allowable temperature difference would be smaller the longer the model. The refraction of the light would in effect be an integration of the temperature distribution along the length of the model. Therefore, the ideal temperature distribution along any light beam would be one which was constant for the length of the model and changed abruptly at both ends. In order to ascertain how closely this condition could be approximated, the initial phase in the development of the test apparatus was concerned with the determination of a suitable length for the test model.

The basic data for the design of the model were obtained by thermal probings in which temperature distributions around a prototype model were determined. The model was constructed of a 3/4-inch thick Transite core with embedded heating wires and 1/8 inch thick copper face plates. It was mounted on a flat plate, as shown in Figure 2. The temperature distribution in the air around the model was found by means of an iron-constantan thermocouple made of 0.004-inch wire located accurately with a micrometer in reference to the model. A precision potentiometer was used for measurement of the thermal e.m.f.'s. The results of the probings are given in Figures 26 through 29 in Appendix II. These results

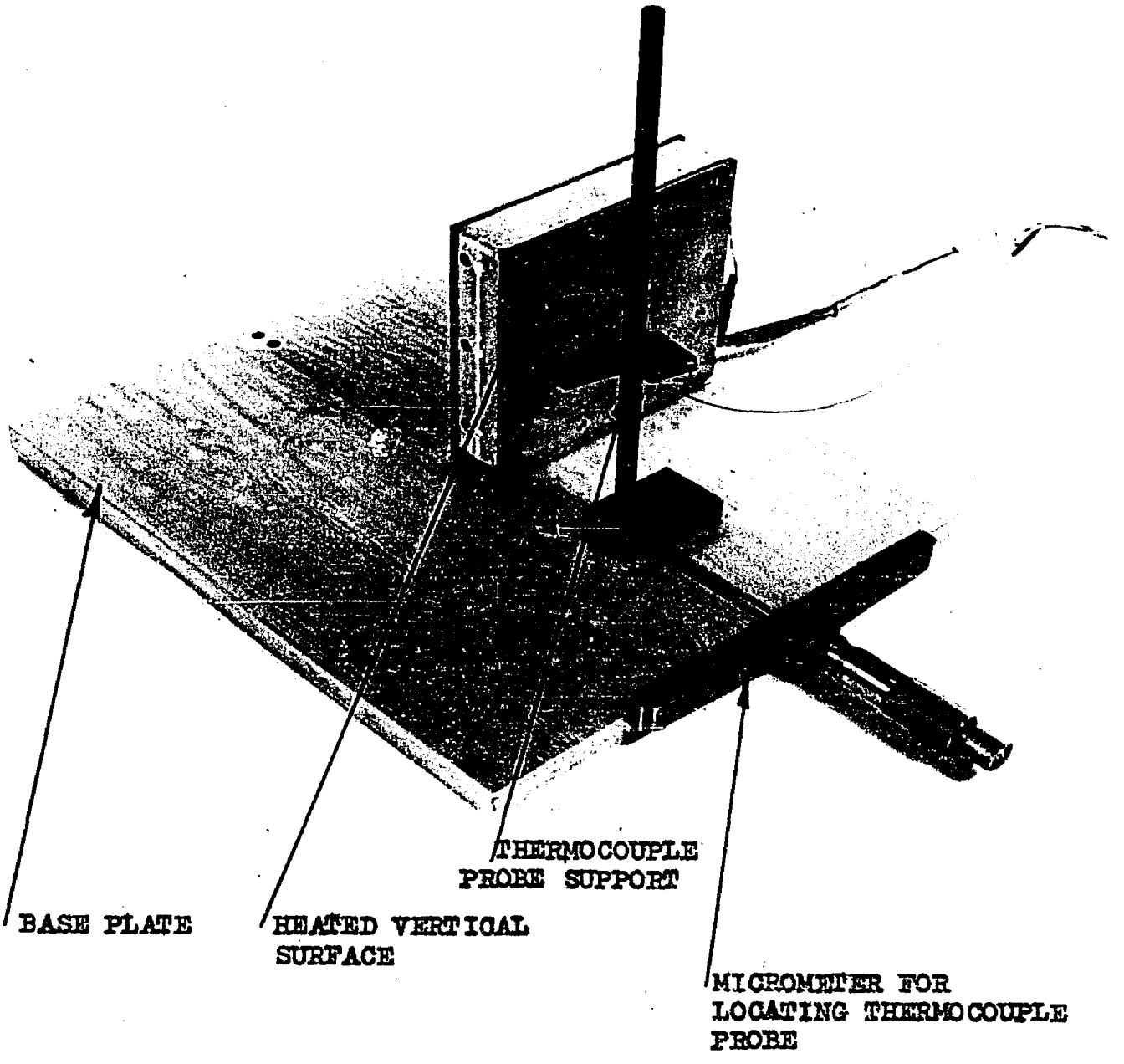

FIGURE 2.

VIEW OF PROTOTYPE MODEL WITH THERMOCOUPLE PROBE AND LOCATING MICROMETER

indicated that the ideal temperature distribution was best approached when the copper surface-plates of the model projected 1/16-inch beyond the Transite core. The model length was selected as 10 inches since this was the shortest length for which the errors discussed in Appendix I would not be in excess of 2.5 per cent. The lengths of the cooled surfaces were made equal to the length of the heated model.

2. Construction of Test Model

The sides and top of the heated prismatic vertical model were made of 1/8-inch copper plate screwed to the Transite core in which the heating elements were imbedded. The Transite core was made 5/8 inch thick, 3-3/4 inches wide, and 9-7/8 inches long. Longitudinal grooves 0.025 inch wide with 1/8-inch spacings were milled in the sides and top of the core to accomodate the 0.007-inch diameter Ni-Chrome V resistance heating wire. The heating elements were wired so that the top of the model, the top halves of each side and the bottom halves of each side could be controlled separately. The wires were cemented in place with a porcelain cement. The Transite core was then ground on both sides to within 0.001 inch of being flat and parallel. Thermocouples were peened into the inside surface of the copper plates and their leads brought out of the ends of the Transite core of the model. After the copper sides and top, which were 10 inches long, were fastened to the Transite core, the flatness of the model was checked on a surface plate. The surfaces were scraped to within 0.002 inches of being flat and parallel.

Figure 3 shows the two models used in this study. The 4-inch high model was used to collect most of the data and the 2-inch high model was used to confirm the correlation established for the 4-inch model.

Cooled confining surfaces were made to form a duct 7 inches high and 2 inches wide. The duct, shown in Figure 4, was made of 1/4-inch brass plate which was flat to within 0.0015 inch in the total length of 10 inches. All joints were sealed with soft solder since the cooling medium was to be water circulated in a tank built up around the duct. The duct sides were parallel to each other to within 0.0005 inches after final assembly. The temperature of the duct was measured with 13 thermocouples spaced around the center of the sides and top of the duct.

3. Compensation for End Effects

A picture showing the fringe configuration with the model set normal to the light beam shows qualitatively the end effect beyond the end of the test model. Such a picture is shown in Figure 5, where the model is in a duct and its long dimension is set normal to the light path. It was found that by rounding the top of the duct's end to a 3/8-inch radius, the effect of the flow of heated air from the top of the duct, i.e., the distance from the end of the model to where the ambient temperature exists, as shown in Figure 5, was reduced. In this manner, the change from ambient temperature to the temperature within the duct was effected in the shortest distance.

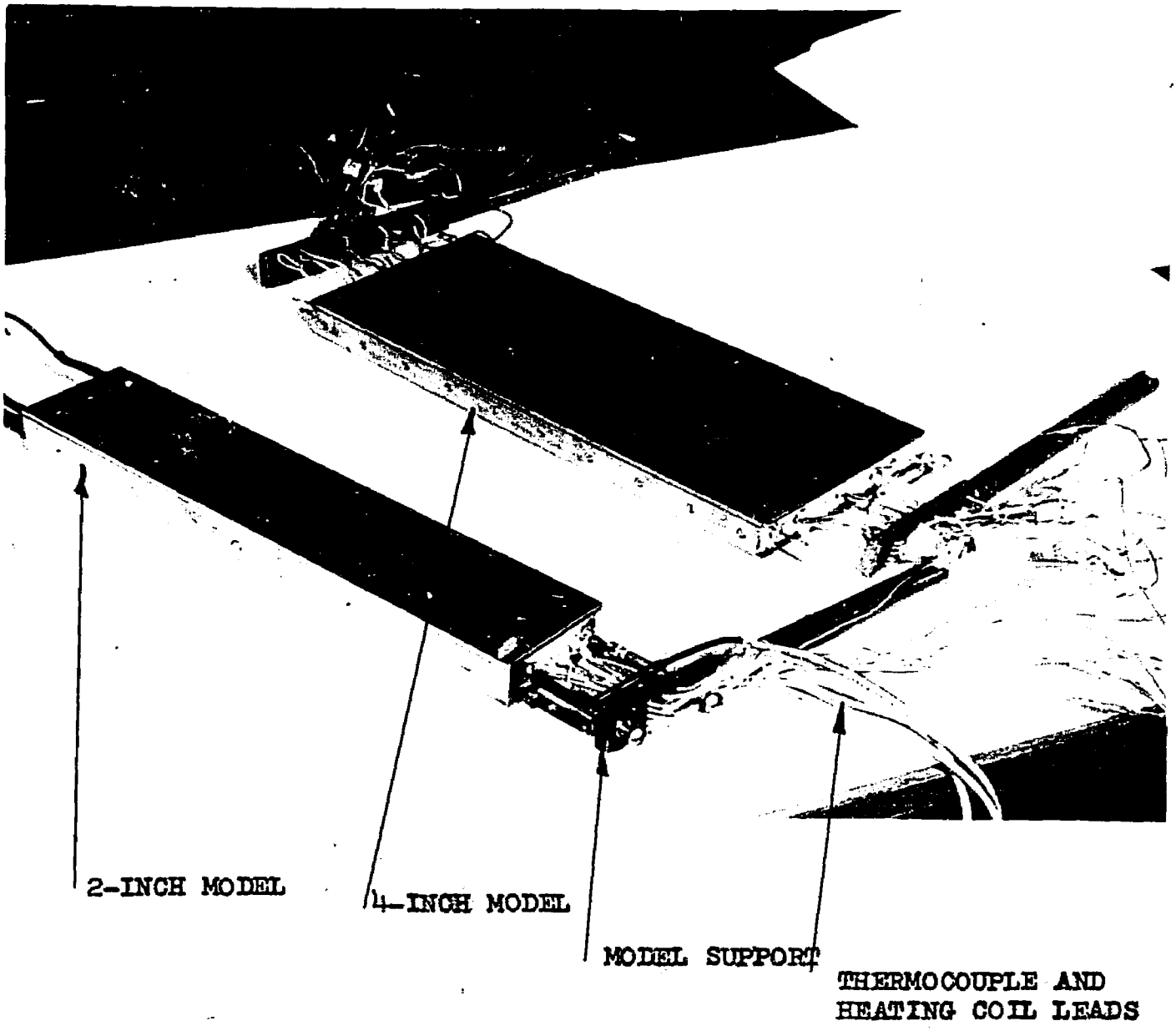

FIGURE 3.

PRISMATIC MODELS OF 2- AND 4-INCH HEIGHT

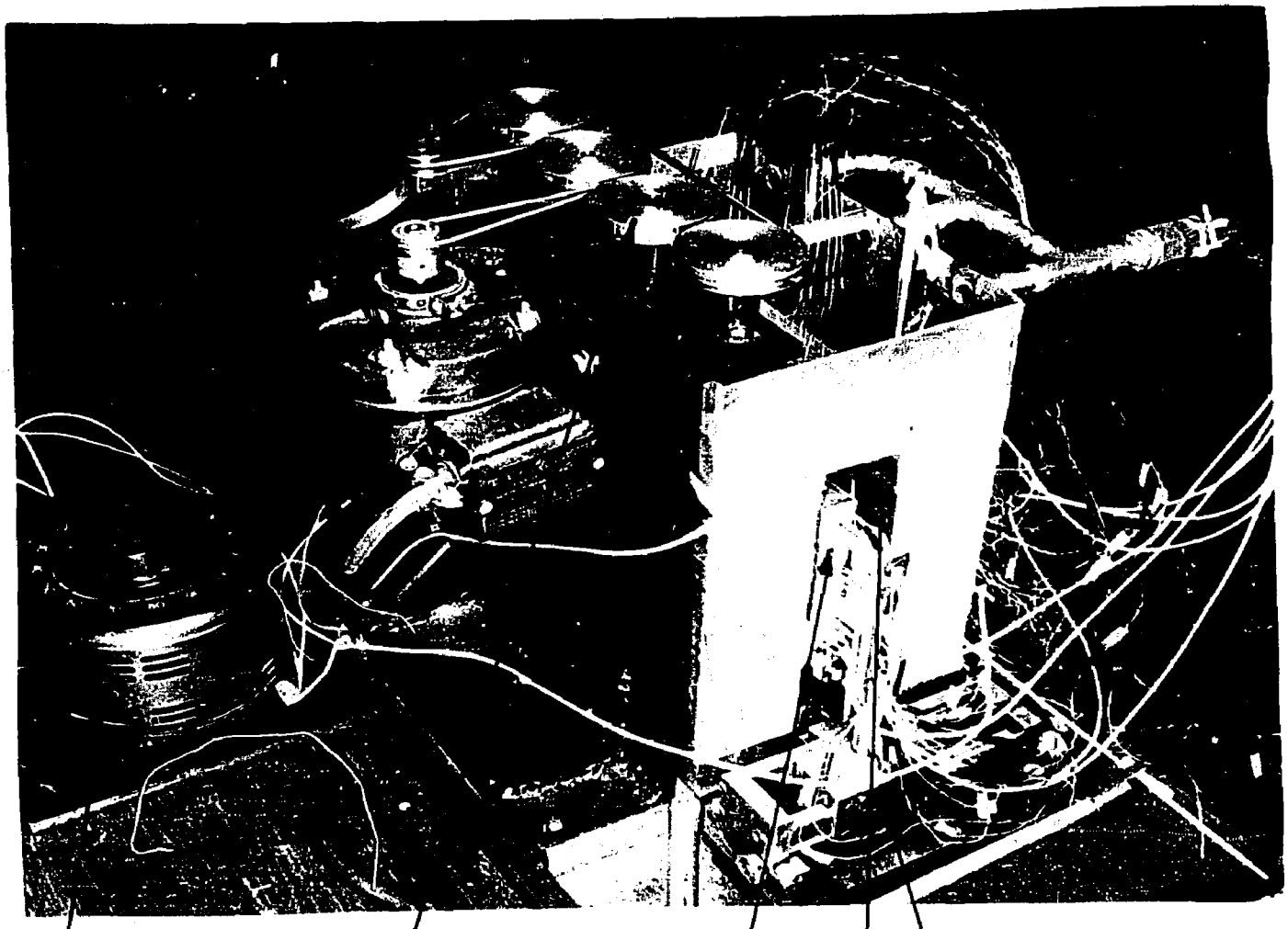

FIGURE 4.

TEST APPARATUS

FRINGE CONFIGURATION WITH MODEL SET NORMAL TO LIGHT BEAM

FIGURE 5

After the model was placed in the duct the temperature distribution parallel to the length of the duct was probed and found to be considerably different from those obtained on the model in the open, since the end effect was greater. Various arrangements were tried on the ends of the test section to reduce this effect. These included shielding the opening except for the region around the model where the temperature gradient was to be explored interferometrically; extending the duct sides to a greater length than the model; extending the top and bottom of the duct; and extending the top only and the bottom only. The use of thin optically-flat glass windows was considered but abandoned due to the expense and

time involved to secure them. The best arrangement was found to be a series of horizontal resistance wires of 0.004-inch diameter spaced at about 3/8-inch intervals across the ends of the duct. Electrical heating of the wires produced a convective end effect with a steep temperature gradient in the direction of the light beam. Also, the in-flow of air at the bottom and the out-flow at the top of the duct sharply decreased. Optimum voltages across the grid for particular model temperatures were determined by thermal probings at various levels along the model and at various distances from the model. In each case the optimum voltage was taken as that which gave an area under the temperature distribution curve equal to the area under the ideal temperature distribution curve. In accordance with the theory outlined in Appendix I, the ideal temperature distribution was based on the air temperature at the center of the model, since the interferograms were taken with the instrument focused at that point. Figure 6 shows some typical results of these thermal probings.

4. Adjustment and Control of Test Conditions

The test apparatus shown in Figure 4 was constructed so that the heated model and duct could be held at a constant temperature difference and the model could be located any place in the duct by lateral and vertical screw adjustment of the supports. The surface temperature of the model was uniform and was produced by adjustment of the input voltage to the embedded heating coils by means of variable-voltage transformers. The temperature of the duct walls was also uniform and was maintained so by means of an

agitated water bath controlled by an adjustable continuous supply of fresh water.

The position of the duct and the model relative to the light beam was critical since non-parallelism could cause undesirable optical reflections from the model and duct surfaces. Therefore, the duct was carefully located by means of two reference blocks with cross hairs which were brought into optical alignment by producing coincidence of their images. The model was located by measurements relative to the duct walls.

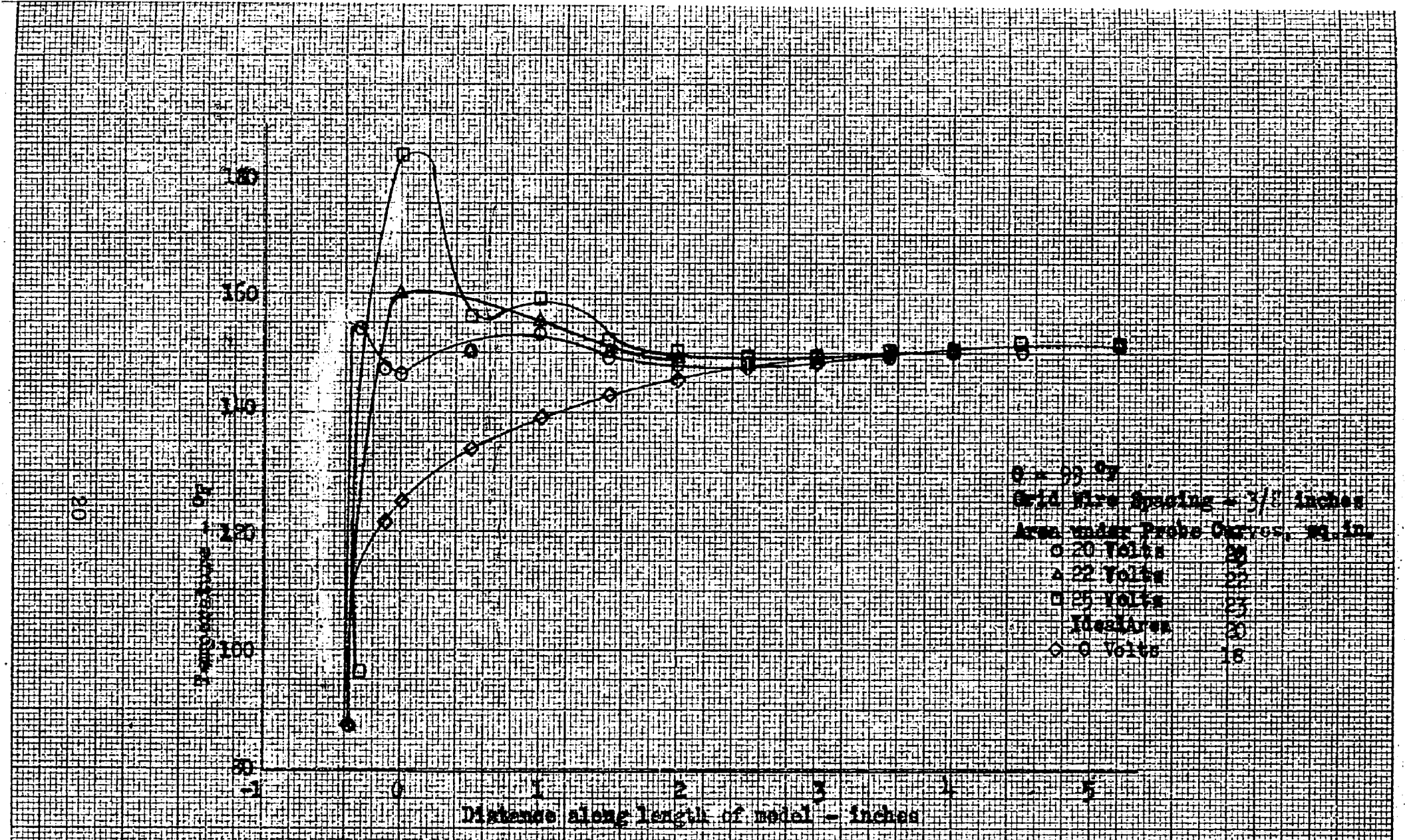

SAMPLE RESULTS OF PROBES PARALLEL TO LENGTH OF MODEL

FIGURE 6.

SECTION IV

TEST DATA

Procedure and Scope

Tests were carried out with the apparatus shown in Figure 4 to determine the effect of several variables on the point value of the convective heat transfer coefficient. The variables to be investigated were:

1. Distance x between the parallel vertical surfaces of the model and the duct.
2. Distance d between the top of the model and the top of the duct.
3. Height L of the model.
4. The vertical distance, ℓ, from the bottom of the model to the point in question.
5. Temperature difference θ between the model and the duct.
6. Temperature T_w of the model.

The dimensional variables x, d, ℓ and L are shown in the diagram of Figure 7.

Model surfaces and duct walls were maintained at uniform but different temperatures. Except when the heated model was in the center of the duct, data for two side distances x were obtained with each photograph.

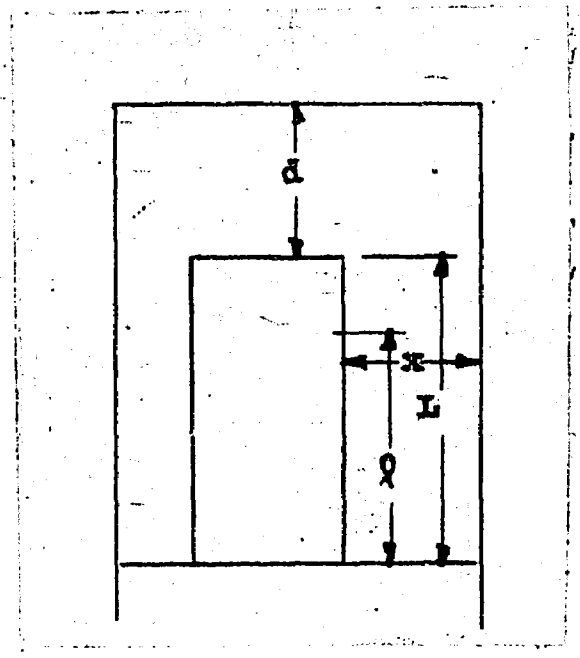

FIGURE 7

DIAGRAM OF CONFIGURATION

Quiescence was maintained in the room while the data were collected and ample time was allowed between photographs for thermal equilibrium to be established.

Table 1 contains the range of conditions of the test data. The conditions for each individual data point are given in Table 4 in Appendix V.

Table 1. Range of Test Data

Model Height, inches	Variable	Number of Settings	Range of Settings
4	x	14	0.135 to 1.015 inches
4	d	4	0.125 to 1.866 inches
4	θ	4	50 to 112°F
2	x	14	0.125 to 0.875 inches
2	d	4	0.125 to 1.8 inches
2	θ	2	100°F (70° and 108°F for one distance, d)

The photographs of the interferometric patterns were made on Kodak Super Speed Ortho Portrait films with a Speed Graphic 45 camera having a focal plane shutter. The camera was installed without the lense board so that the image from the interferometer was focused at the focal plane of the camera. Exposures of 1/50 second were used. A typical interferogram is shown in Figure 23, Appendix I. All told, 150 photographs were taken.

Interpretation of Interferograms

1. Heat Transfer Mechanism

The fluid at the heated surface is assumed to have no motion. The fluid in the film immediately adjacent to the surface is assumed to have little motion. Therefore, practically all heat transfer through the film, which under the free convective conditions such as used in the investigation may have a thickness in the order of 0.075 inch, takes place by conduction. The fundamental expression for one-dimensional conductive heat transfer is

$$q = - kA\, dt/dx \qquad (1)$$

where q = rate of heat transfer, Btu per hour

k = thermal conductivity, Btu per hour per square foot per degree F per foot

A = area, square feet

dt/dx = temperature gradient, ^{o}F per foot

The rate of heat transfer q from the heated model to the cooled duct may also be defined in terms of a heat transfer coeffi-

cient h, the surface A, and the temperature difference between the heated model and the cooled duct $t_w - t_s$. Thus,

$$q = hA(t_w - t_s). \tag{2}$$

The heat transfer at any point is obtained by equation (2) and may be equated to equation (1). Therefore,

$$h\,(t_w - t_s) = -k\,dt/dx \tag{3}$$

since the heat transfer at a particular point must pass through the air adjacent to the model surface.

2. Evaluation Procedure

With thermocouples located on the model and duct, the temperatures t_w and t_s were measured directly. Tables were available giving values of the thermal conductivity k. The values for k and other physical properties of air used in the analysis are given in Table 3, Appendix III. Referring to equation (3), it is seen that the only term which remained to be determined in order to compute the heat transfer coefficient was dt/dx. In other words, the temperature gradient in the air film adjacent to the surface of the model had to be determined.

Equation (36), Appendix I, gives an expression for computing the temperature difference between any point in the field of an interferogram and the ambient temperature, the latter being the temperature of the air surrounding the interferometer at the time the interferogram was taken. Curves of the variation of this tem-

perature difference ΔT with ambient temperature and density were made up for values of ϵ, fringe shifts from ambient condition, ranging from 1 to 30. From these curves, since t_w was known, the number of fringe shifts ϵ corresponding to the difference between the temperature at the model surface and the ambient temperature, in a direction could be chosen. By counting normal to the model surface on the interferogram the number of fringes, the temperature at each fringe could be determined.

To obtain plots of the temperature gradients, it was also necessary to determine accurately the location of each fringe relative to the model surface. For that purpose, the negatives of the interference photographs were enlarged by 10 to 1, by projection on a screen. The positions of the fringes were obtained by scaling the projected images. Actually the positions were transferred by pin marks to a scale strip on which distances were measured with an accuracy of 0.01 inch, corresponding to 0.001 inch in the actual temperature field.

For each interferogram, after measuring the distances between the fringes at various elevations on the surface of the model, a table of temperature versus distance normal to the model surface was set up. These values were plotted and slopes of the tangents to these temperature distribution curves at the model surface were measured. These slopes gave values of the temperature gradients dt/dx. A typical plot of the reduced data is shown in Figure 8.

The temperature gradients determined by the above method were found to vary with the dimensional variables indicated on

L' = 4 Inches
t_w = 128 °F
t_s = 72 °F
θ = 52 °F
ℓ' = 2 Inches
d = 0.781 Inches

Temperature at fringe, °F.	Distance from surface to fringe, inches. $x' = 1.015$	$x' = 0.146$
128	0	0
122.6	0.021	0.015
117.3	0.044	0.029
112.2	0.068	0.042
107.3	0.089	0.057
102.3	0.117	0.070
97.5	0.144	0.084
92.8	0.182	0.098
88.2	0.223	0.109
83.5	0.299	0.138
79.1	0.893	0.

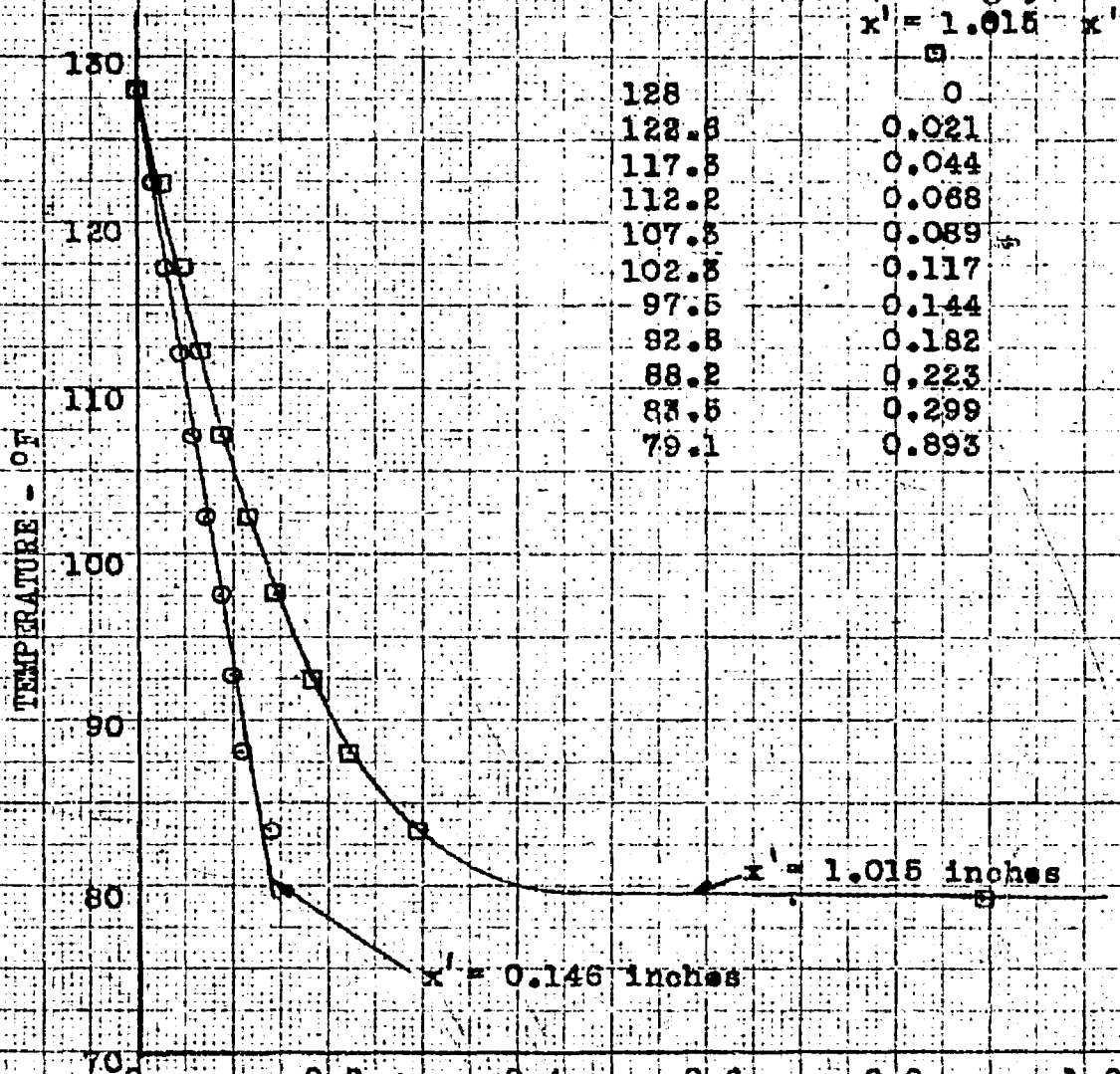

TYPICAL PLOT OF TEMPERATURE DISTRIBUTION NORMAL TO HEATED SURFACE OF MODEL.

FIGURE 8.

page 21. A typical plot of the variation of temperature gradient versus distance x between model and duct wall for various elevations ℓ from the base is shown in Figure 9. From the faired temperature gradient-curves such as shown in Figure 9, values of dt/dx for constant values of distance x were determined and tabulated, as given in Table 4 in Appendix V.

Discussion of Reduced Heat Transfer Data

From the shape of the curves in Figure 9 it may be seen that the temperature gradient and, therefore, the local heat transfer coefficient varies little with the distance x when the latter is large. As the distance x is decreased, the heat transfer coefficient decreases, reaching a minimum at a distance between the vertical surfaces, which for the test data, is in the range of 1/4 to 1/2 inch. With further decrease of the distance x the temperature gradient increases rapidly. As may be expected, it would be infinite if the distance were decreased to zero.

When the distance between the vertical surfaces is very small, the flow of heat, other than by radiation, should occur by pure conduction through the air space. Then, essentially, a straight-line temperature distribution would exist between the two surfaces for temperature differences used in the investigation. The rate of heat transfer per unit area would be given by

$$q = k_m (t_w - t_s)/x \ , \qquad (4)$$

where k_m is the thermal conductivity evaluated at the mean tempera-

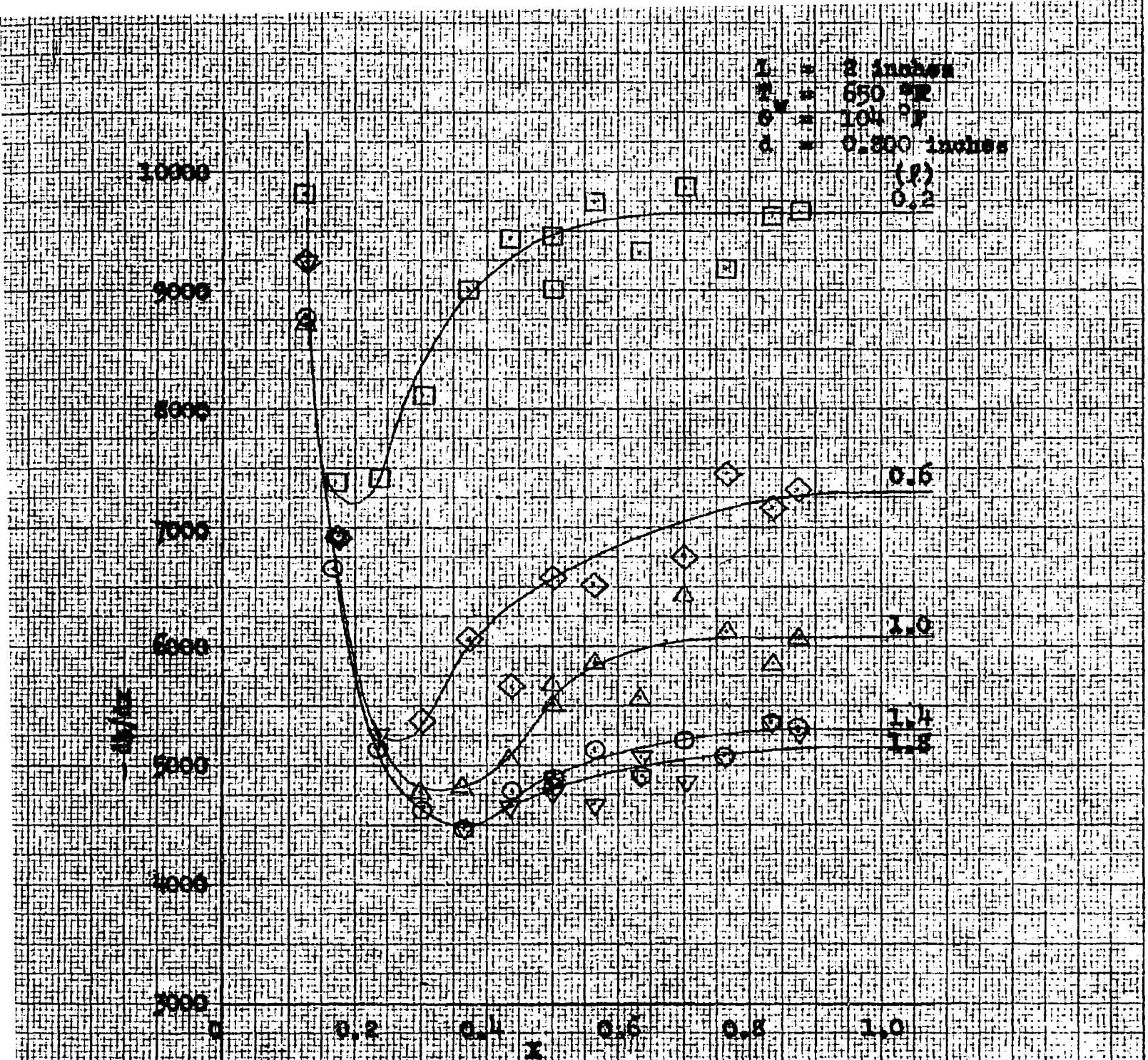

VARIATION OF TEMPERATURE GRADIENT WITH DISTANCE BETWEEN MODEL AND DISC FOR VARIOUS DISTANCES FROM BOTTOM OF MODEL

FIGURE 9.

ture of the air space. In equation (4), $(t_w - t_s)/x$ would be equivalent to - dt/dx for small distances which when plotted versus x gives a hyperbola for any particular temperature difference. When plotted with the experimental curves, such as those shown in Figure 9, the hyperbolas become tangent to the corresponding experimental curves at small values of the distance x. This is shown for a typical data plot in Figure 10. When the gradient-curve due to conduction is subtracted from the total gradient-curve, as obtained experimentally, a resultant curve is found which is tangent to the total gradient-curve at large values of surface distance. This latter curve resulting from the difference between the total gradient and the conduction gradient is designated for the purpose of this study, as the free-convection effect.

The effect of reducing the distance between the top of the model and the top of the duct is to decrease the heat transfer coefficients in the upper portion of the model while those near the base remain unaffected. This is illustrated by the typical curves in Figure 11.

As shown from the curves in Figure 11, obtained from a crossplot of the data in Figure 9, the local temperature gradient decreased with increase of the elevation from the base. The rate of decrease is reduced at greater elevations.

The model height appears to have no effect on point heat transfer coefficients. At top distances 3/4 inch and greater, the gradient curves are found to coincide, for both models used, at equal elevations from the base, all other conditions being the same.

This is shown by the solid-line curve in Figure 12. The model height does affect the heat transfer from the lower portion of the model when the top distance is small, as shown in Figure 13.

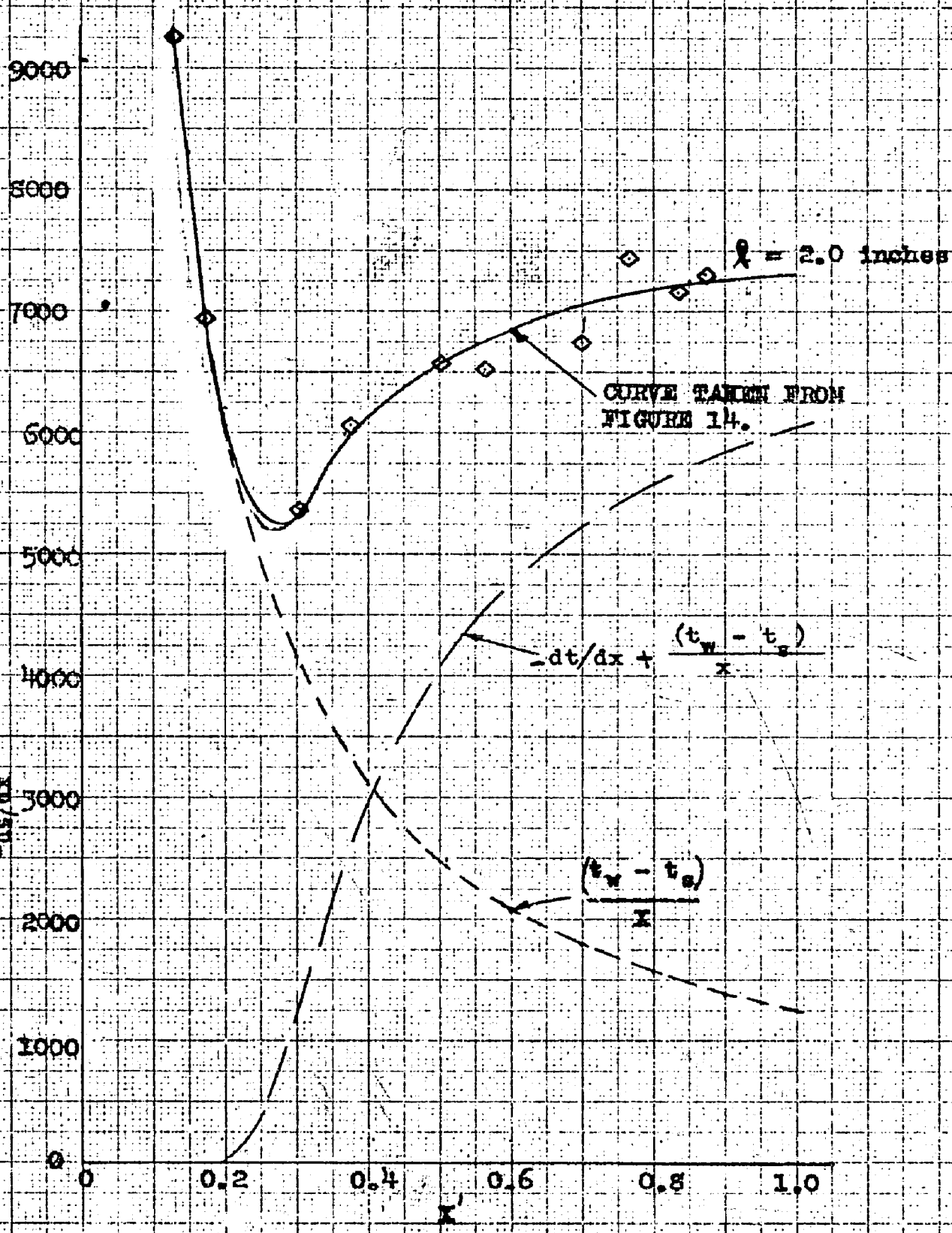

TYPICAL PLOT OF CONDUCTION EFFECT TO SHOW TANGENCY TO EXPERIMENTALLY DETERMINED TEMPERATURE GRADIENT CURVE.

FIGURE 10.

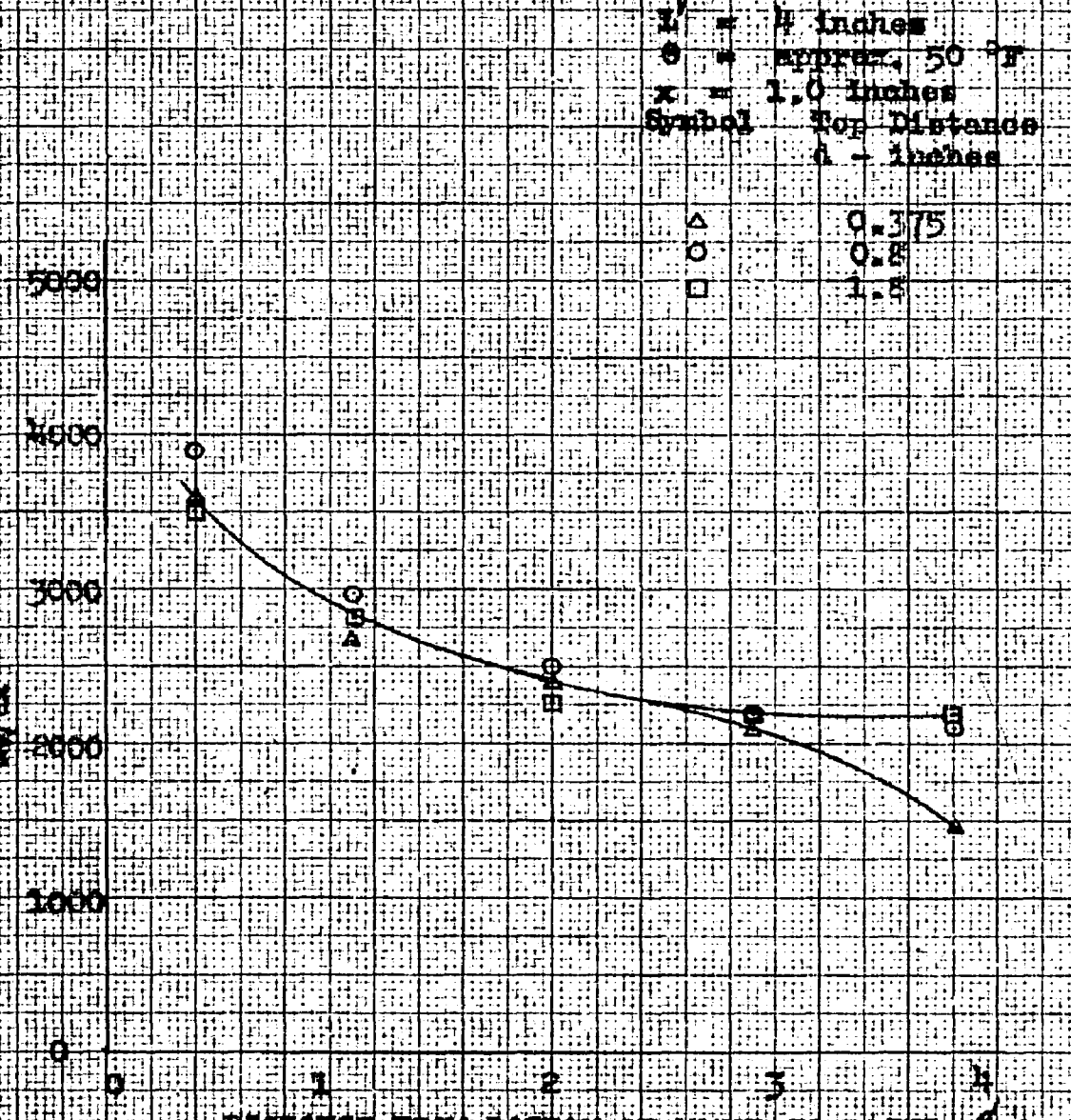

EFFECT OF TOP DISTANCE, d, ON TEMPERATURE GRADIENT

FIGURE 11.

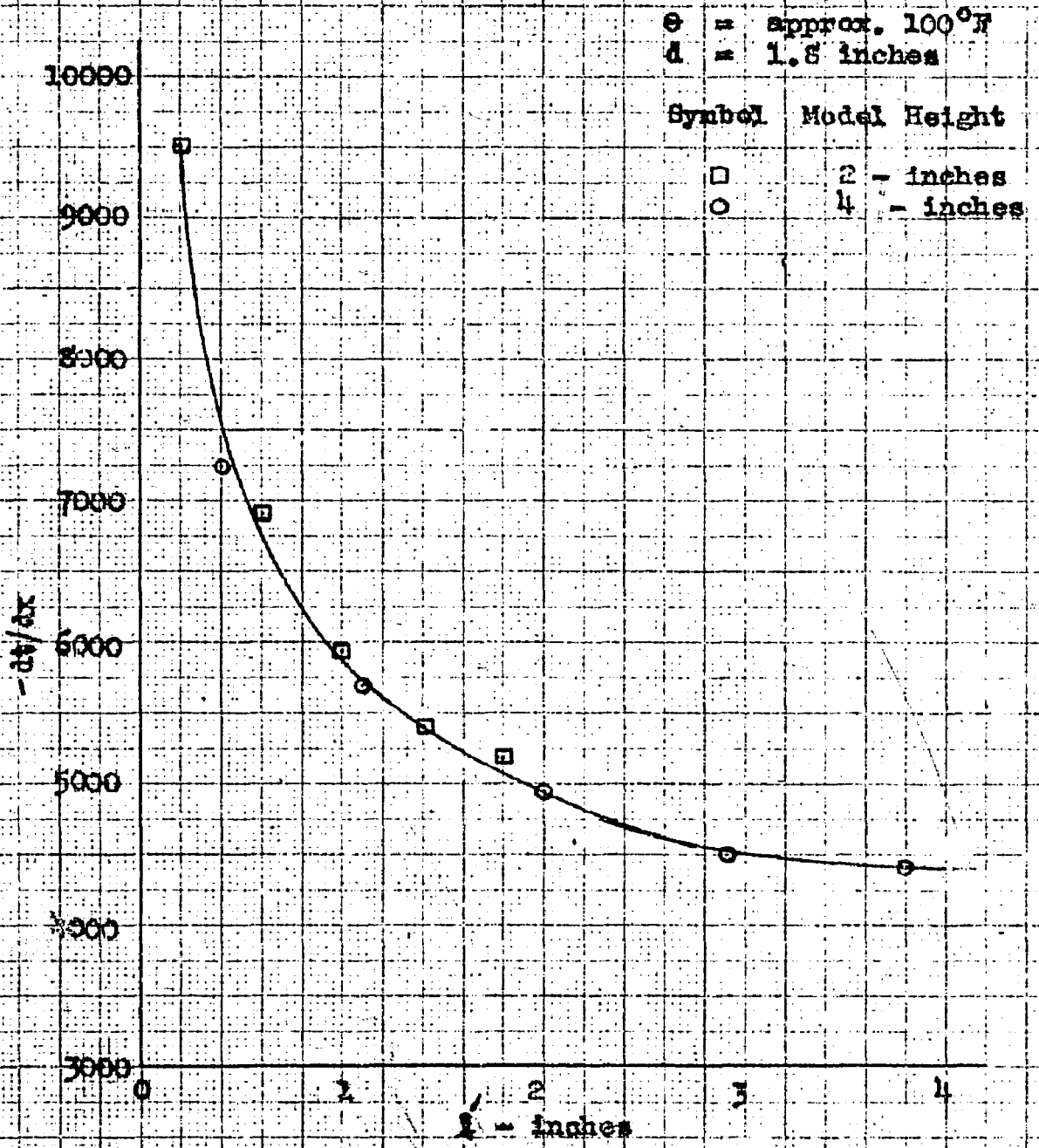

VARIATION OF TEMPERATURE GRADIENT ALONG SIDE OF MODEL FOR 2- AND 4-INCH MODELS WITH LARGE TOP SPACING.

FIGURE 12.

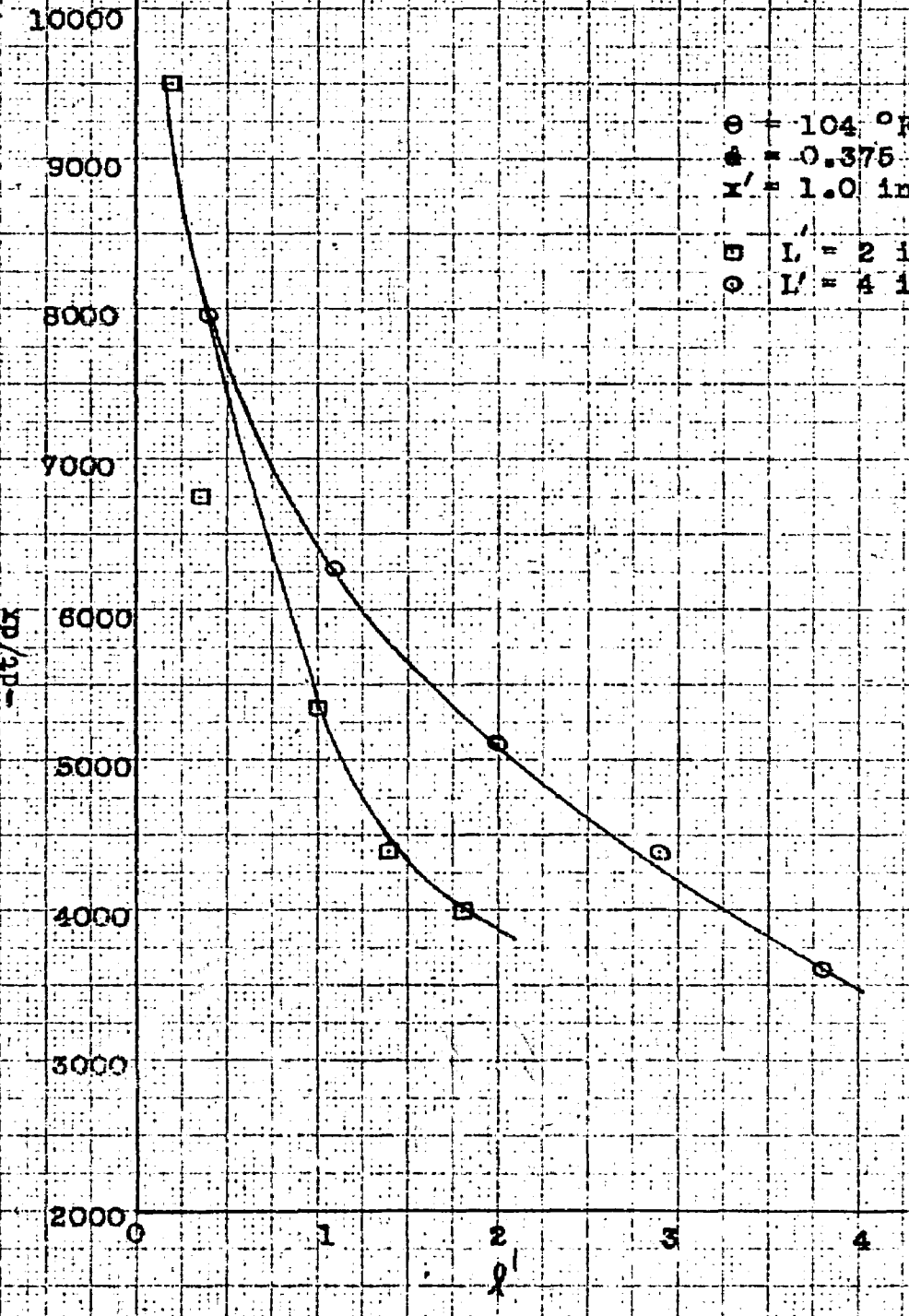

VARIATION OF TEMPERATURE GRADIENT ALONG SIDE OF MODEL FOR 2- AND 4-INCH MODELS WITH SMALL TOP SPACING

FIGURE 13.

SECTION V

DATA CORRELATION

Point Heat Transfer Coefficients

In general we speak of free convection heat transfer as that heat transferred by virtue of the motion of the fluid and conduction combined. As mentioned previously, for purposes of this study it is found that by separating the pure conduction and free convection a better correlation results. This comes about because the configurations in this study were such that the heated and cooled walls were brought close to each other and the conduction of heat between the walls contributed much more of the heat transfer than it normally does, and in very close spacings almost all of the heat transfer is by conduction, as is shown on Figure 10 by the tangency of the pure conduction temperature gradient to the total temperature gradient. Most free convection heat transfer work has been carried out with models in free space or with large distances between heated and cooled surfaces so that not much information is available for the purpose of comparison.

For free convection heat transfer data the tools of dimensional analysis have been used to develop methods of expression. From dimensional analysis the following dimensionless groups occur.

1. $\frac{VD\rho}{\mu}$ Reynolds number

2. $\frac{g\beta\theta L^3\rho^2}{\mu^2}$ Grashof number

3. $\frac{c\mu}{k}$ Prandtl number

and 4. $\frac{hL}{k}$ Nusselt number.

In the above dimensionless groups the Grashof number is really the same as the Reynolds number. Grashof number is used to express the Reynolds number in free convection work. The difference between the two lies in the fact that the velocity is taken care of in the Grashof number by expressing it in terms of the velocity resulting from the bouyant force, due to change in density in the fluid.

Nusselt expressed the heat transfer by free convection by the equation

$$Nu = C\ Gr^a\ Pr^b \qquad (5)$$

This is the conventional method for expressing free convection data and gives good correlation for bodies in free space for temperature differences above 20^oF.(4)

The Prandtl number is made up of terms that are dependent on the temperature of the air and should be constant according to Reynolds' analogy. Actually there is a small variation as shown in Table 3 (about 1 per cent + in the range of temperatures used). This variation was not considered in the correlation of the present data and therefore Nusselt's equation could be written as

$$Nu = C' (Gr)^a \qquad (6)$$

For purposes of this report the heat transfer by conduction is expressed by a Nusselt number. It should be noted though that since there is no motion of the fluid in the case of conduction, these Nusselt numbers should not show a correlation with the Grashof number and are used only to add continuity to the equations used to express the data.

From equation (4)

$$q_{cond} = - k_m \frac{\Theta}{x} = h_{cond} (\Theta) \qquad (7)$$

Multiplying by ℓ and dividing by k_w gives

$$\frac{h_{cond}}{k_w} = (k_m/k_w)(\ell/x) = Nu_{conduction} \qquad (8)$$

The total rate of heat transferred per unit area is given by

$$q = - k_w (dt/dx) = h (\Theta t) \qquad (9)$$

Multiplying by ℓ and dividing by k_w gives

$$(dt/dx)(\ell/\Theta) = h \ell/k_w = Nu_{tot.} \qquad (10)$$

$$Nu_{total} - Nu_{conduction} = Nu_{convection} \qquad (11)$$

By using the Grashof numbers for the various test conditions the plot of Nusselt numbers for free convection only, versus Grashof number, gives a straight line on log-log coordinate paper.

This is what one would expect since the Grashof number is the dimensionless parameter which is the basis of correlation for most free convective data. The correlation is good for a particular distance between the side of the model and the side of the duct but fails when the experimental data for various wall distances are superimposed. Not only does the slope of the line through the data vary with wall distance, but the intercept also varies.

By plotting, the values of the intercepts for various wall distances and by reasoning that the value of the convective Nusselt number must approach zero for very small wall distances, the shape of the curve of the intercept of x is established. The expression that best fits this curve is of the form A Tanh Bx where A and B are constants. A is the value of the coefficient ahead of the Grashof number for the case of the model wall in the free space, i.e., x very large. Tanh Bx varies from zero to one with different degrees of rapidity depending on the value of B. For the experimental data presented here the expression

$$A \tanh Bx = 0.37 \tanh 36x \qquad (12)$$

best fits the data (Figure 14).

A plot of the variation of slope with the wall distance is given in Figure 15. The expression that best fits these data is given by

$$n = 0.25 - 0.0008x^{-1.43} . \qquad (13)$$

VARIATION OF COEFFICIENT AHEAD OF GRASHOF NUMBER WITH DISTANCE BETWEEN MODEL AND DUCT

FIGURE 14.

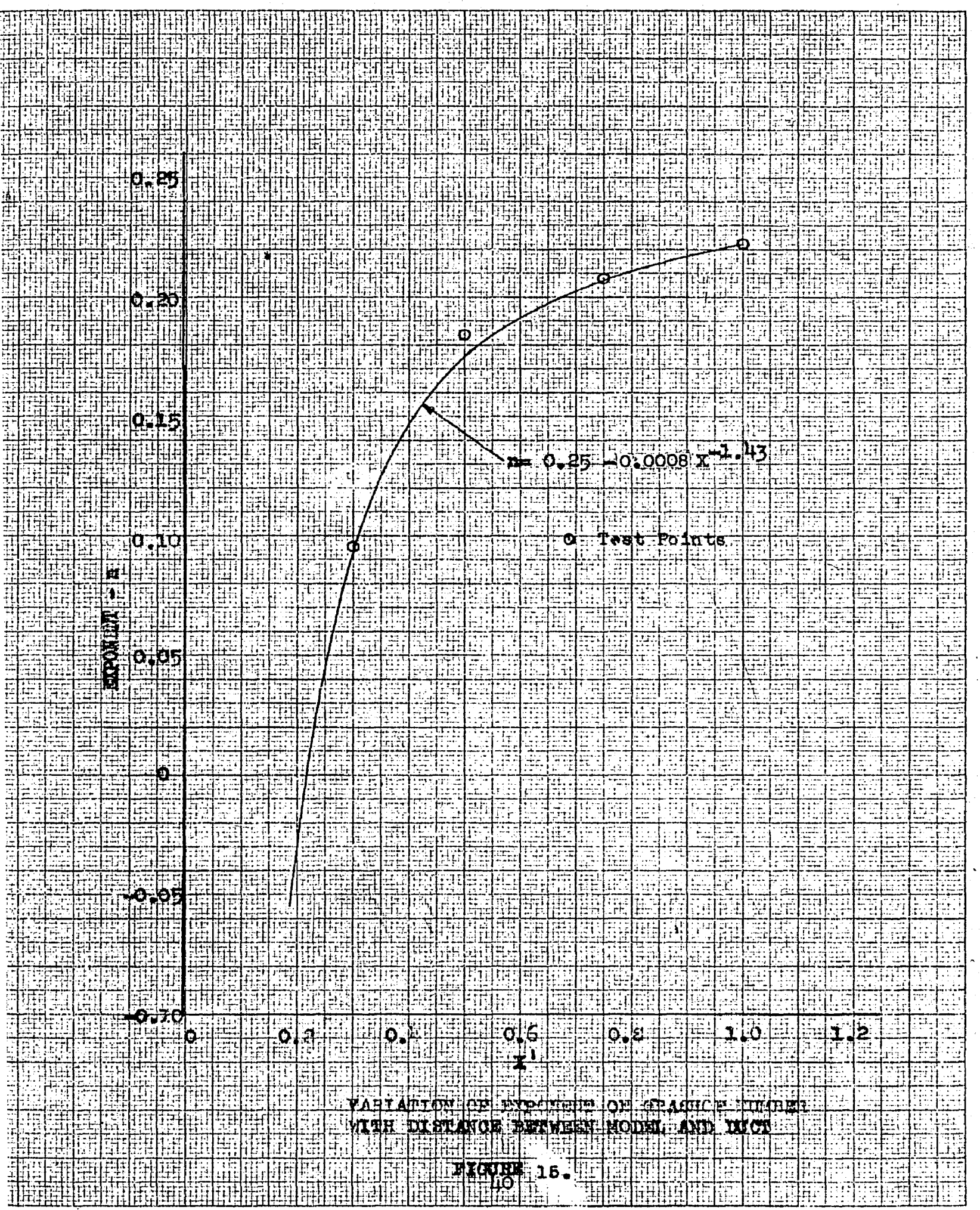

VARIATION OF EXPONENT OF GRADIENT FUNCTION WITH DISTANCE BETWEEN MODEL AND DUCT

FIGURE 15.

where the first term is the same as the exponent that is almost universally used for free convection from bodies in free space with the same range of Grashof number as has been used for this experimental work.

This gives then the expression

$$Nu_{conv} = 0.37 \text{ Tanh } 36x \, Gr_p^{0.25} - 0.0008 x^{-1.43} \qquad (14)$$

which is the equation which best expresses the free convection part of the experimental data.

If we now add in the conduction part of the heat transfer in terms of Nusselt numbers we get

$$Nu_p = (h \, \ell / k_w)$$

$$= (k_m/k_w)(\ell/x) + 0.37 \text{ Tanh } 36x \, Gr_p^{0.25} - 0.0008x^{-1.43} \qquad (15)$$

By multiplying equation (15) by the thermal conductivity at the wall temperature and dividing by the distance from the bottom of the wall to the point at which the heat transfer coefficient is desired, one obtains that coefficient, h, in Btu per ^{o}F per square foot. If ℓ is divided into both sides of equation (15) and set equal to zero, the value of the heat transfer coefficient comes out equal to infinity. Theoretically this should be true but practically it does not happen. Therefore the value of ℓ to be used should probably not be less than 0.10 inch since the experimental data from which this equation was obtained went down only to values of ℓ in

the vicinity of 0.2 inch. Values of dt/dx for smaller values of have been checked and it is found that extrapolation much beyond 0.10 inch does not give results that agree with experimentation.

It should be pointed out that equation (15) is empirical and is suitable for expressing the data that were gathered for this study. Since it is empirical any extrapolation should be done with caution.

The effects of all the variables that were encountered in this study are satisfactorily correlated by equation (15), except for the effect of the top distance. This end condition was such that it was not considered practical to include it in the expression for the heat transfer. It can, however, be compensated for by multiplying values obtained for the Nusselt number for free convection by the values indicated in Figure 16. Figure 16 is a chart for correction due to top distances as a function of wall and top distances.

Average Heat Transfer:

The average heat transfer coefficient was found by integrating equation (15) modified to the form of equation (18). Since the point Nusselt number is

$$Nu = h \ell / k_w \qquad (16)$$

where h = point heat transfer coefficient

ℓ = distance from the bottom of the model

k_w = thermal conductivity at temperature t_w

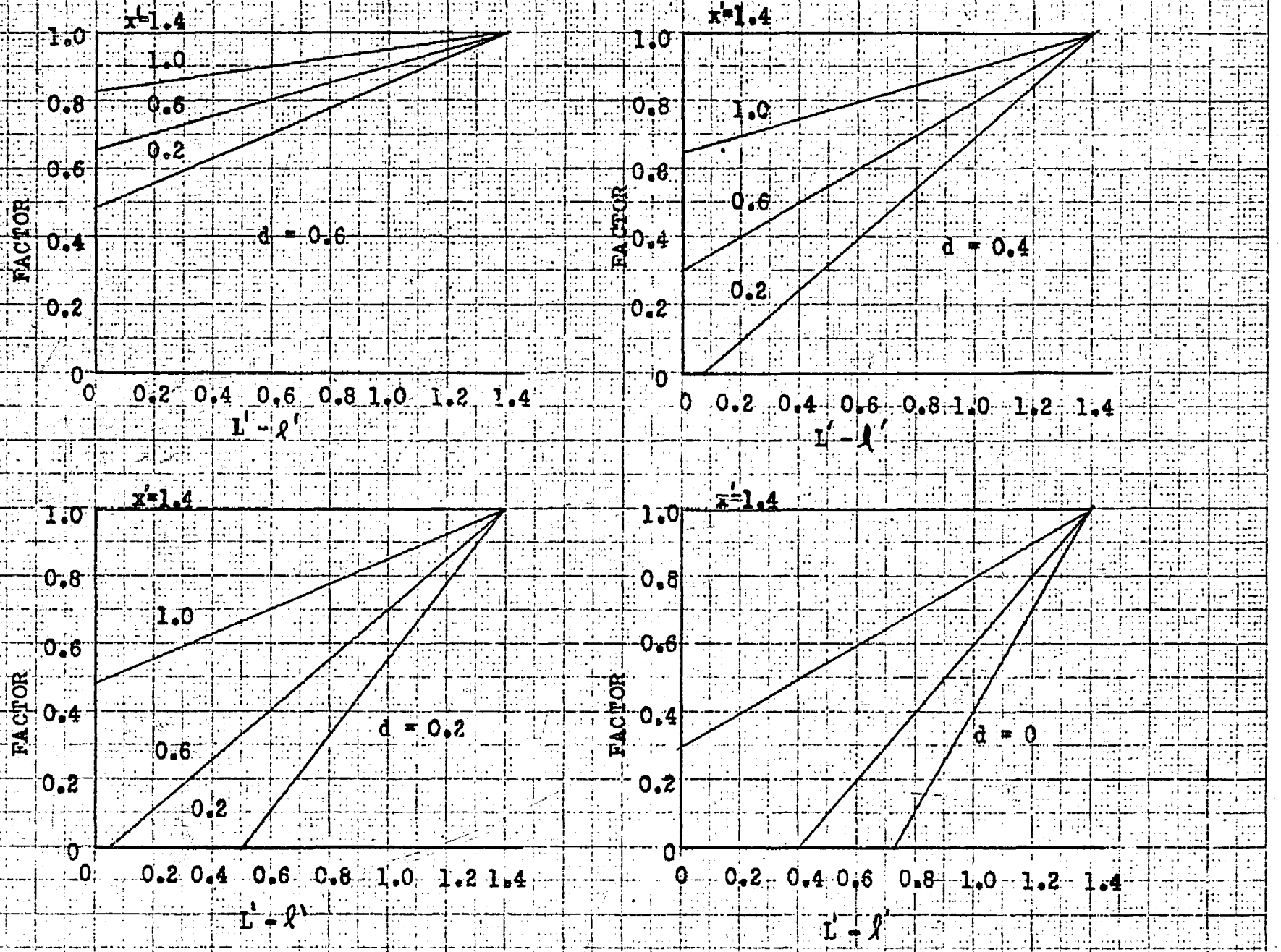

FACTOR BY WHICH NUSSELT NUMBER SHOULD BE MULTIPLIED WHEN VALUE OF d IS LESS THAN 0.8 INCHES.

FIGURE 16.

the expression is

$$\frac{h\ell}{k_w} = \frac{k_m}{k_w}\frac{\ell}{x} + 0.37 \tanh 36x \left(\frac{g\beta\Theta\rho^2}{\mu^2}\right)^n \ell^{3n} \qquad (17)$$

Dividing both sides by ℓ and multiplying by k_w gives

$$h = \frac{k_m}{x} + k_w (0.37 \tanh 36x) \left(\frac{g\beta\Theta\rho^2}{\mu^2}\right)^n \ell^{3n-1} \qquad (18)$$

which is the expression for the point heat transfer coefficient.

Integrating equation (18) from 0 to L gives

$$\int_0^L h\,d\ell = \frac{k_m \int_0^L d\ell}{x} + k_w (0.37 \tanh 36x) \left(\frac{g\beta\Theta\rho^2}{\mu^2}\right)^n \int_0^L \ell^{3n-1}\,d\ell \qquad (19)$$

$$\int_0^L h\,d\ell = \frac{k_m L}{x} + k_w (0.37 \tanh 36x) \left(\frac{g\beta\Theta\rho^2}{\mu^2}\right)^n \frac{L^{3n}}{3n} \qquad (20)$$

Dividing by L gives

$$h_{avg} = \frac{1}{L}\int_0^L h\,d\ell = \frac{k_m}{x} + \frac{k_w}{3nL} (0.37 \tanh 36x)(Gr_a)^n \qquad (21)$$

where h_{ave} = average heat transfer coefficient, Btu/ft^2/°F/hr

k_w = thermal conductivity at model surface

k_m = thermal conductivity at mean temperature between the model and the duct

x = distance between model and duct, feet

n = $0.25 - 0.0008(x)^{-1.43}$

L = total height of model, feet

n = exponent on the Grashof number.

The expression for the Nusselt number based on the average heat transfer coefficient is therefore

$$Nu_{avg} = \frac{h_{ave}\, L}{k_w} = \frac{k_m}{k_w}\,\frac{L}{x} + \frac{0.37\ \tanh 36x}{3n}\, Gr_a{}^n \qquad (22)$$

The solution of equation (21) is given in the form of a computation chart, Figure 17, where the average heat transfer coefficient can be obtained without the necessity of having to carry out cumbersome computations or use tables for physical properties.

In using the above method for finding the amount of heat transfer from an isothermal surface, the spacing, x, at which minimum heat transfer occurs might be of great interest. The location of this point can be found by differentiation, with respect to x, of equation (22). This differentiation gives

$$\frac{dNu_{avg}}{dx} = \frac{-k_m}{k_w}\,\frac{L}{x^2} + \frac{0.37 Gr_a{}^n}{3n}\left\{3\ \mathrm{sech}^2 36x + (.000096x^{-2.43})\tanh 36x\left[\mathrm{Log}_e Gr_a - \frac{1}{n}\right]\right\} \qquad (23)$$

which cannot be solved explicitly for x. Since a trial and error solution is necessary, Figure 18 has been prepared in order to facilitate the solution for x at which minimum heat transfer occurs.

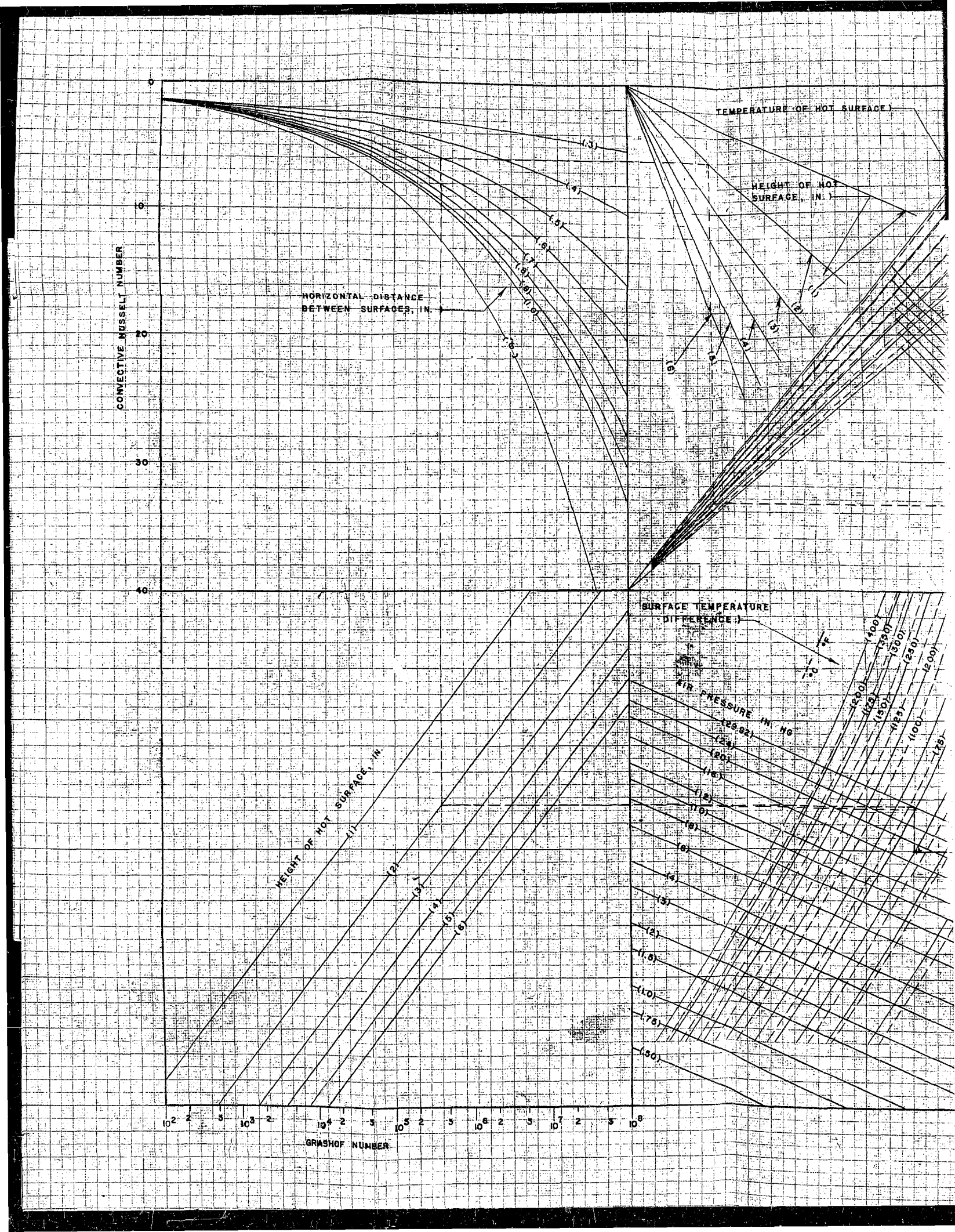
CONVECTIVE NUSSELT NUMBER
0
10
20
30
40
HORIZONTAL DISTANCE BETWEEN SURFACES, IN.
(.3)
(.4)
(.5)
(.6)
(.7)
(.8)
(.9)
(1.0)
(1.5)
(2)
TEMPERATURE OF HOT SURFACE)
HEIGHT OF HOT SURFACE, IN.)
(3)
(4)
(5)
(6)
SURFACE TEMPERATURE DIFFERENCE)
1.5
1.0
AIR PRESSURE IN HG
(29.92)
(28)
(26)
(24)
(22)
(20)
(18)
(16)
(14)
(12)
(11)
(10)
(9)
(8)
(7)
(6)
(5)
(4)
(3)
(2)
(1.5)
(1.0)
(.75)
(.50)
1200
1250
1300
1350
1400
1100
1150
HEIGHT OF HOT SURFACE, IN.
(1)
(2)
(3)
(4)
(5)
(6)
10^2 2 5 10^3 2 5 10^4 2 5 10^5 2 5 10^6 2 5 10^7 2 5 10^8
GRASHOF NUMBER

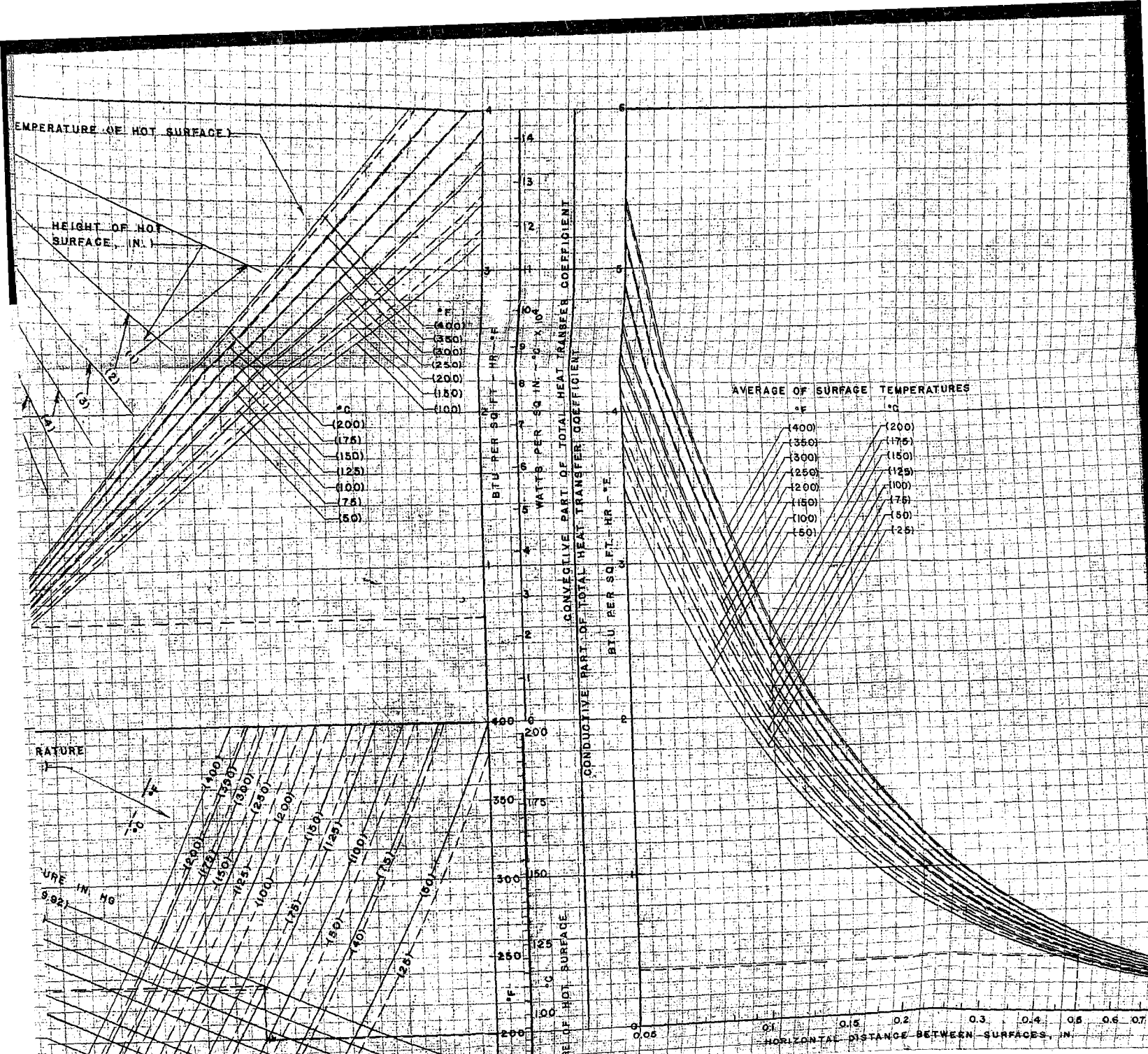

FIGURE 17.

AVERAGE HEAT TRANSFER COEFFICIENT
COMPUTATION CHART.

METHOD FOR USE:

1. Enter lower right block at temperature of heated surface.
2. Move horizontally to the left to the proper line designating the temperature difference between the heated and cooled surfaces.
3. Move vertically to the proper line designating the pressure.
4. Move horizontally to the left to the line designating the height of the surface.
5. Move vertically to the proper line designating the spacing between the heated and cooled surfaces.
6. Move horizontally to the right to the proper surface height.
7. Move vertically to the line designating the proper temperature of the heated surface.
8. Move horizontally to the right and read the convective heat transfer coefficient.
9. Enter the block at the upper right hand corner at the proper value for the distance between the heated and cooled surfaces.
10. Move vertically to the average of the temperatures of the heated and cooled surfaces.
11. Read on the left hand ordinate, the heat transfer coefficient due to conduction.
12. Add results of steps 8 and 11 for total heat transfer coefficient.

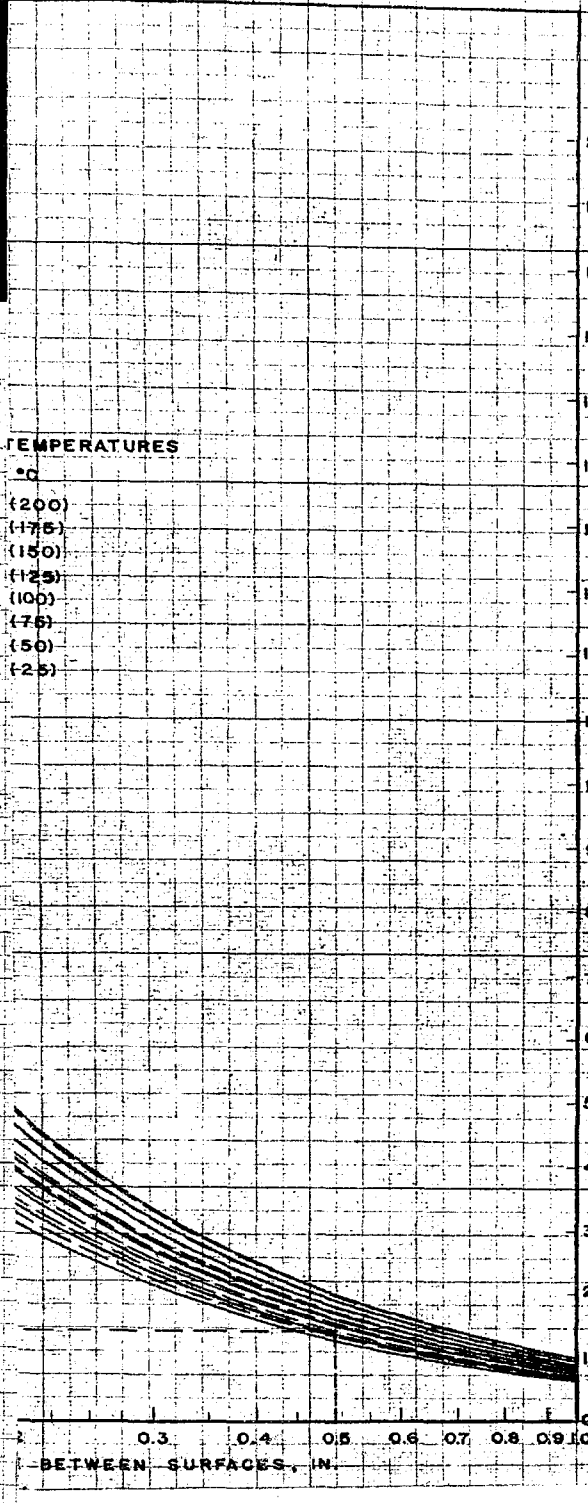

ure of heated surface.
he proper line designating
the heated and cooled surfaces.
designating the pressure.
he line designating the height

designating the spacing between

the proper surface height.
ating the proper temperature of

read the convective heat transfer

hand corner at the proper value
d and cooled surfaces.
the temperatures of the heated

he heat transfer coefficient due

total heat transfer coefficient.

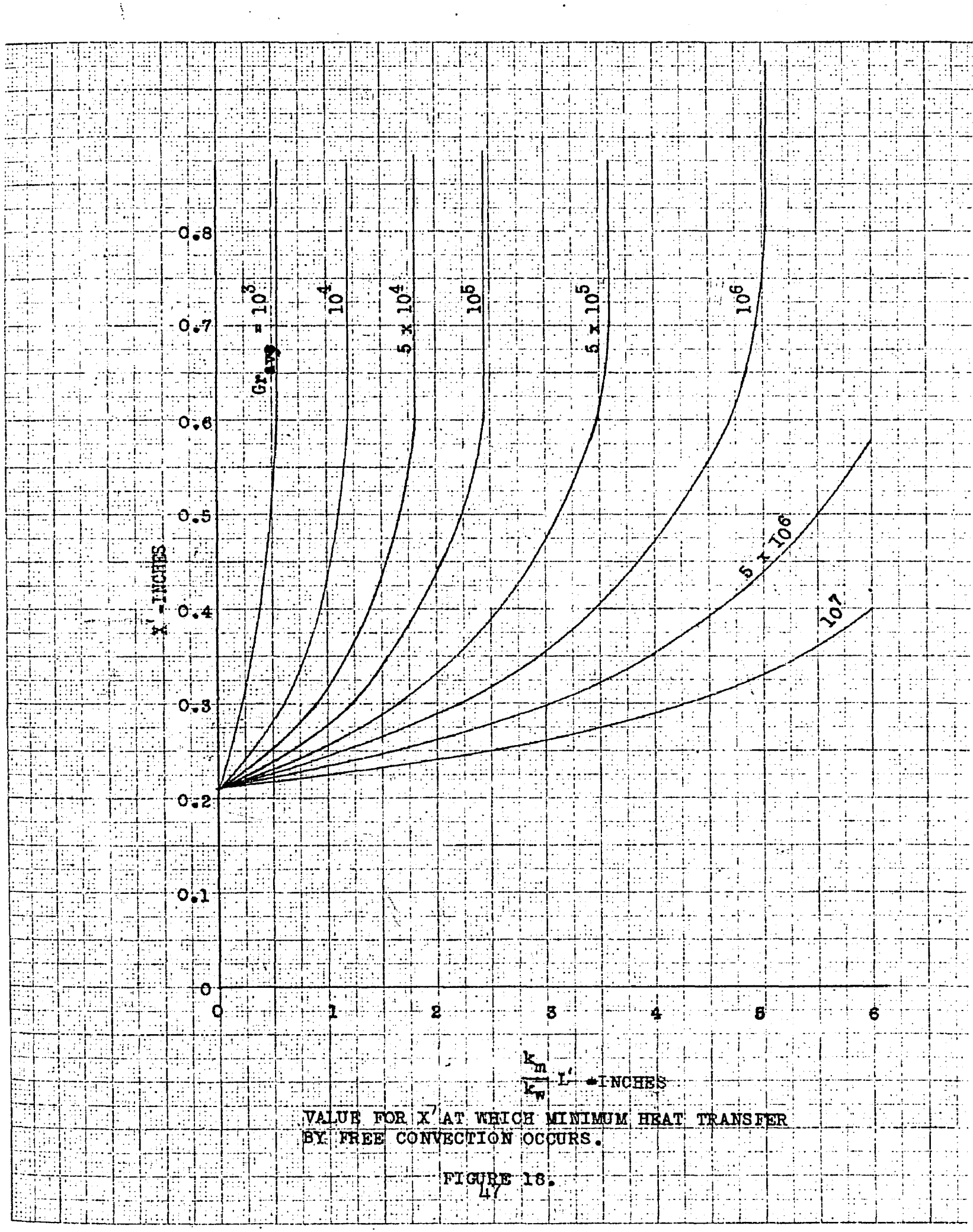

VALUE FOR X' AT WHICH MINIMUM HEAT TRANSFER BY FREE CONVECTION OCCURS.

FIGURE 18.

SECTION VI

DISCUSSION OF RESULTS

1. Point Heat Transfer Correlation

The total Nusselt numbers could not be plotted against the Grashof number and give a correlation that is valid because the total Nusselt number as it is expressed is made up of a convection part and a conduction part. The conduction part is independent of the Grashof number and therefore must either be plotted separately from the convection part or plotted with it for equal values of elevation from the bottom of the model. This is true for small values of x but for larger values the conduction part of the total heat transfer becomes less and less significant.

Figure 19 was made up in order to show how well equation (14), page 41, represents the data taken for this investigation.

By inspection of equation (15), page 41, it is seen that it applies for all values of x. For large values of x the conduction part of the equation reduces to zero and the convection part takes the familiar form of $c\,Gr^n$ where n is 1/4 and c is 0.37,

$$Nu_{p,c} = 0.37\ Gr_p^{1/4} \quad . \tag{24}$$

This value for c corresponds to that which we would obtain for a very large value of x or for a vertical surface on a base plate. This value of c is in general greater than those values that are published by other investigators for free plates. It should be

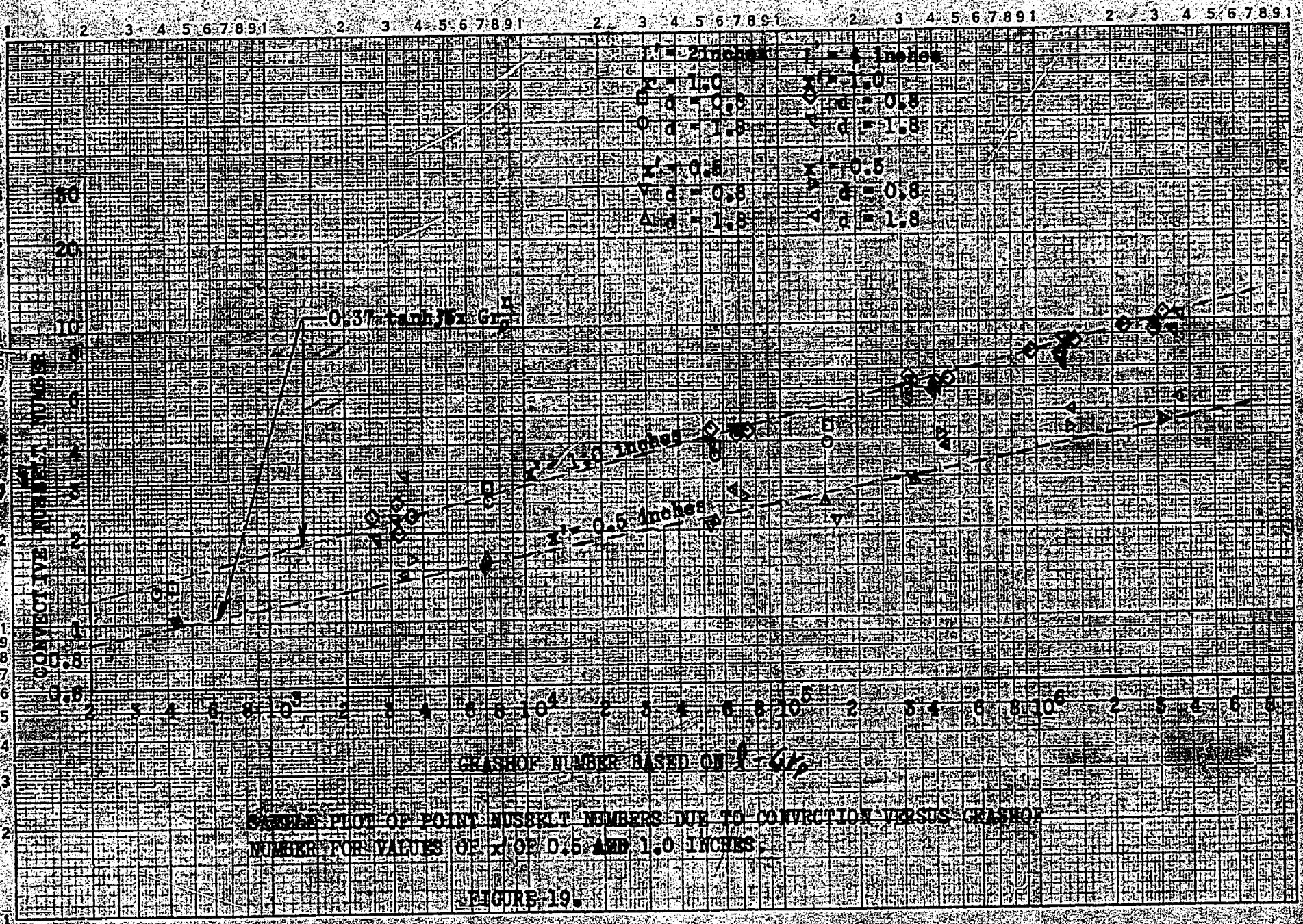

SAMPLE PLOT OF POINT NUSSELT NUMBERS DUE TO CONVECTION VERSUS GRASHOF NUMBER FOR VALUES OF x OF 0.5 AND 1.0 INCHES.

FIGURE 19.

remembered that these are point values of the Nusselt number and very few results are published, since most free convection data have been obtained as average values.

For point values of the Nusselt number Schmidt and Beckman[6] obtained the equation

$$Nu_{\rho} = 0.36\ Gr_{\rho}^{1/4} \tag{25}$$

for a vertical free surface. The method of collecting data was by probing with a thermocouple.

Average Heat Transfer

Most investigations have been carried out by evaluating the average heat transfer coefficient on a free vertical surface. By integrating equation (18), page 44, for large values of x we obtain equation (24). All the investigations in the past have obtained the value 1/4 for the exponent on the Grashof number. There is no uniform agreement as to the constant ahead of the Grashof number, however. In the table below are given some of the values of c that have been published, along with the values obtained in this study.

TABLE 2

Value of c for this investigation	0.494
Schmidt and Beckman[6]	0.48
King[5]	0.507
Lorenz[5]	0.501

As pointed out in the references, the equation that King presents was determined by including the experimental data of a number of investigations. The equation presented by Lorenz was determined analytically. In all the equations except the one presented for this report and the Schmidt and Beckman equation the Prandtl number ($c\mu/k$) was raised to the 1/4 power and multiplied by the Grashof number. In the range of temperatures used in this study the Prandtl number varied only from 0.71 to 0.67. A constant value of 0.70 was used on the equations mentioned in order to get the constants corresponding to those of this study and Schmidt and Beckman.

Jakob[4] correlated the data of Mull and Richer[4] for the average heat transfer between parallel surfaces spaced down to 0.5 inch apart. This correlation was made by using data which were taken on surfaces from 30 to 960 square inches and consisted of only 25 experimental points. Also the smallest spacing of the surfaces was only 0.5 inch. The comparison of the results from this study for the large values of Gr, which Jakob computed by using x instead of L, is good but for the small values of Gr_x the results obtained in this study are higher. Jakob's expression for the heat transfer is

$$hx/k = 0.18 (Gr_x)^{1/4} (L/x)^{1/4} \qquad (26)$$

When, for a particular set of conditions, values of Nusselt number are plotted versus side distance, x, the value for the Nusselt number in the case of a free vertical surface as found from an equation using King's value of the coefficient should be the

asymptote for the Nusselt number curve for a confined surface at large values of x. This is shown in Figure 20.

It should be pointed out that the integrated equation is such that it gives values of Nu that go to infinity and then negative for values of x approaching 0.215 inch from above and therefore should be limited to values of not less than 0.3 inch for x. At this point the error involved is less than 6 per cent for the smallest values of L shown in Figure 17. This error is on the conservative side and decreases rapidly as x gets smaller.

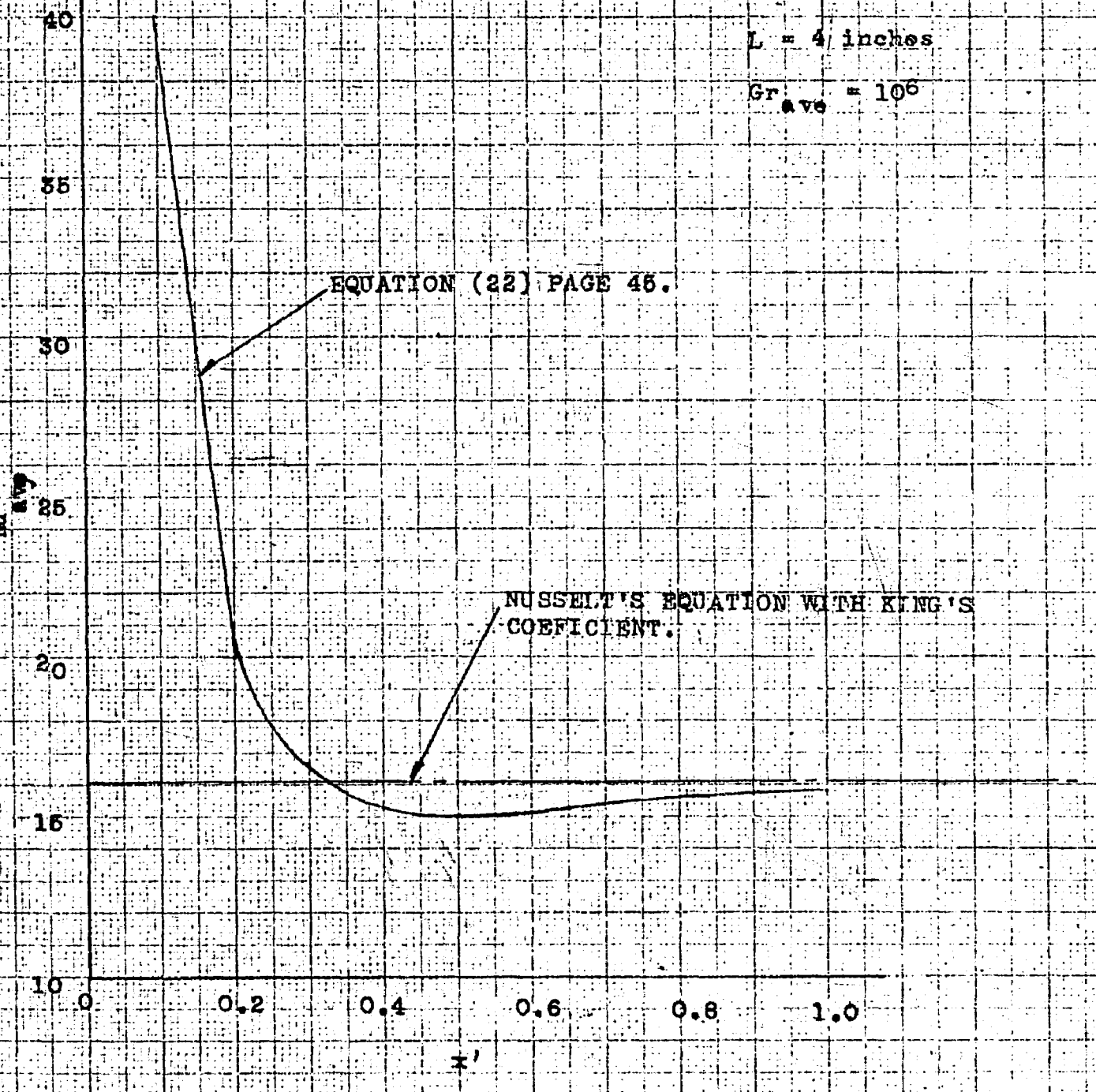

PLOT OF NUSSELT NUMBER BASED ON AVERAGE HEAT TRANSFER AS OBTAINED IN THIS STUDY VERSUS THAT FOR A FREE VERTICAL SURFACE.

FIGURE 20.

BIBLIOGRAPHY

1. Kennard, R. B., "An Optical Method for Measuring Temperature Distribution and Convective Heat Transfer", Bur. Standards J. Research, 8, 787-805, 1932.
2. Lorentz, H. A., The Theory of Electrons, 145, 1909.
3. Ladenburg, R., Winckler, J. and Van Voorhis, C. C., "Interferometric Study of Supersonic Phenomena", Naval Ordinance Report 69-46, April, 1946.
4. Jakob, M., Heat Transfer, Vol. 1, John Wiley and Sons, First Edition, 1949.
5. McAdams, W. H., Heat Transmission, McGraw-Hill Book Company, Second Edition, 1942.
6. Schmidt, E. and Beckman, W., "Das Temperatur- und Geschwindigkeitsfeld vor eine Wavme abgebenden senkrechten Platte bei Naturlicher Konvektion", Technische Mechanik und Thermodynamik, Vol. 1, No. 10, 341-364, 1930.
7. Schmidt, E., Thermodynamics, Oxford at the Clarendon Press, 1949.
8. Eckert, E. R. G., Drake, R. M. and Seehngen, E., "Design and Construction of an Interferometer", Air Force Technical Report 5721.
9. Eckert, E. R. G., Introduction to the Transfer of Heat and Mass, McGraw-Hill Book Company, 1950.
10. Jenkens, F. A. and White, H. E., Fundamentals of Physical Optics, McGraw-Hill Book Company, First Edition, 1937.
11. Jakob, M. and Hawkins, G. A., Elements of Heat Transfer and Insulation, John Wiley and Sons, Second Edition, 1950.

12. Brown, A. I. and Marco, S. M., Introduction to Heat Transfer, McGraw-Hill Book Company, First Edition, 1942.

13. Boelter, L. M. K., Cherry, V. H., Johnson, H. A. and Martinelli, R. C., Heat Transfer Notes, University of California Press, 1946.

14. Keating, T. J., "A Study of the Characteristics of the Boundary Layer on a Flat Plate With Forced Convection", Thesis for M. S. Degree, Ohio State University, Columbus, Ohio, 1948.

15. Kensch, R. B., "Interferometric Investigation of the Heat Transfer Coefficient in Free Convection Between Two Vertical Heated Flat Plates", Thesis for M. S. Degree, Ohio State University, 1949.

16. Liepman, Hans W. and Puckett, Allen E., Introduction to Aerodynamics of a Compressible Fluid, John Wiley and Sons, 1947.

APPENDIX I

THE USE OF THE INTERFEROMETER FOR FREE CONVECTION HEAT TRANSFER STUDIES

Figure 21 shows a diagram of a Zehnder-Mach interferometer. Light from the mercury lamp A passes through the condensing lenses B and a 5461 Angstrom filter C, converging on the illuminating mirror D. The illuminating mirror is located at the focal point of the parabolic mirror E which columnates the light. This light is then split into two bundles by the half-silvered mirror F. One bundle is reflected by the mirror G and the other by the mirror H. The bundles then rejoin at the half-silvered mirror I and are projected on the ground glass K from the spherical mirror J.

When the light in both bundles traverses identical optical paths, and when the mirrors F, G, H and I are all exactly parallel to each other, the field on the ground glass is either uniformly light or dark, depending on whether or not the path length FGI varies from the path length FHI by an odd or even number of half wave lengths. When a uniformly light field is obtained the interferometer is said to be adjusted for "zero-fringe". If the mirrors are not exactly parallel, a series of parallel interference fringes can be observed on the ground glass. The spacing and orientation of the fringes may be varied by rotation of mirror G about its horizontal and/or vertical axis.

In Figure 22, a fringe pattern obtained with non-parallel mirrors for a field of uniform temperature is shown. The object in the center is a prism which has appreciable length parallel to the light path. Similarly, the four enclosing surfaces are of the same lengths. All surfaces are at the same temperature as the air in-

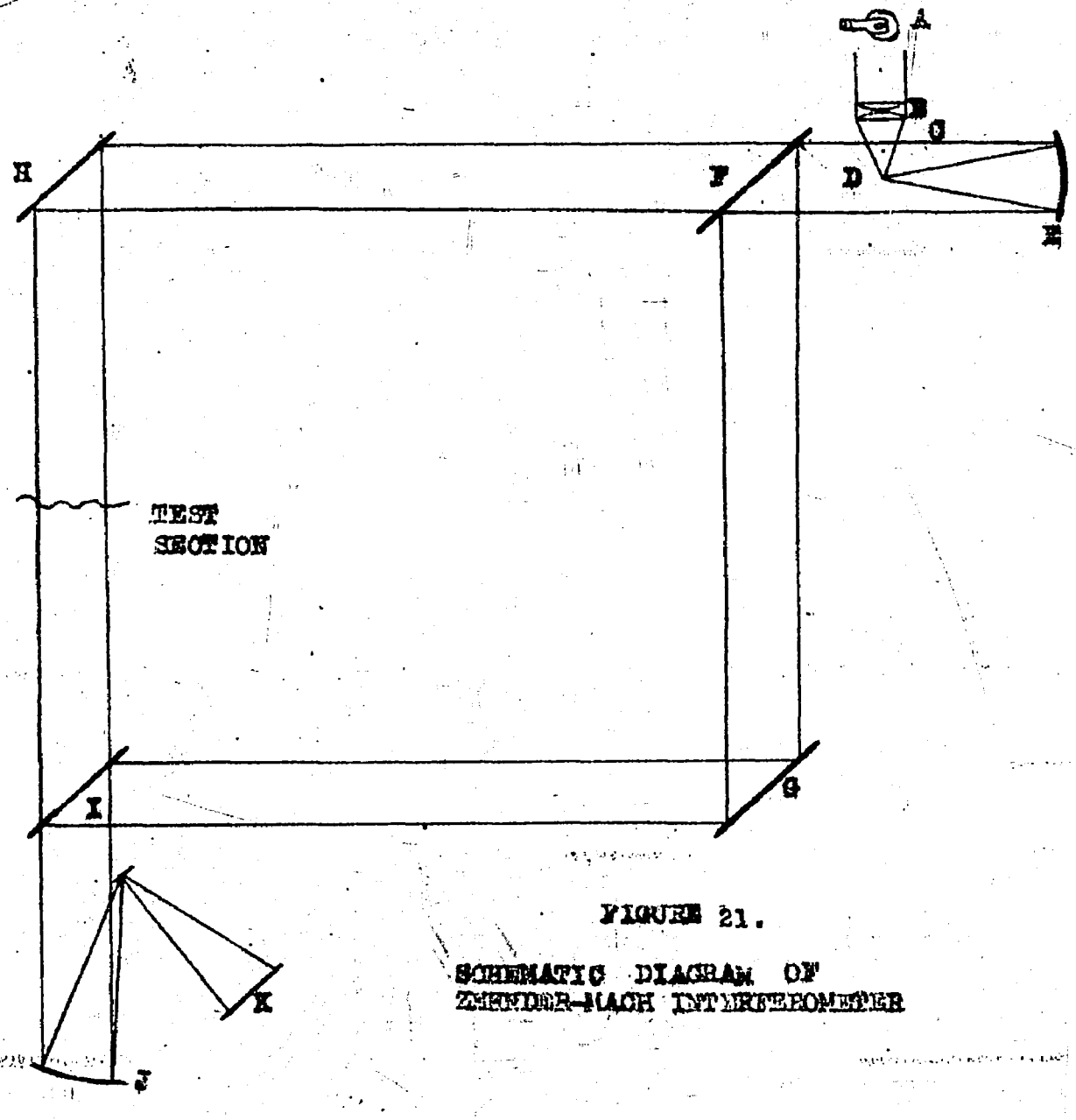

FIGURE 21.

SCHEMATIC DIAGRAM OF
ZEHNDER-MACH INTERFEROMETER

side the space between the prism and the surrounding vertical and horizontal walls. The assembly is located in portion FHI indicated in Figure 21.

The fringe pattern shown in Figure 22 is transformed to that in Figure 23 when the center prism is heated and the air acts as convective medium transmitting heat from the prism to the surrounding walls. Then, a temperature gradient exists between the prism, across the air space and to the walls. The distortion of the fringes is caused by the change of the refractive index of the air by virtue of its temperature change.

The index of refraction is given by the expression

$$\eta = \lambda_o/\lambda \tag{27}$$

where λ_o = wave length of the light in a vacuum

λ = wave length in air at any density.

The number of wave lengths in the length M of the light beam passing parallel, equal and adjacent to the prism is

$$\gamma = M/\lambda \tag{28}$$

The number of wave lengths in the same length of the air between mirrors FG which does not undergo a temperature change is

$$\gamma_r = M/\lambda_r \tag{29}$$

The difference in the number of wave lengths then is

$$\epsilon = \gamma_r - \gamma = M(1/\lambda_r - 1/\lambda) = M/\lambda_o\,(\eta_r - \eta) \tag{30}$$

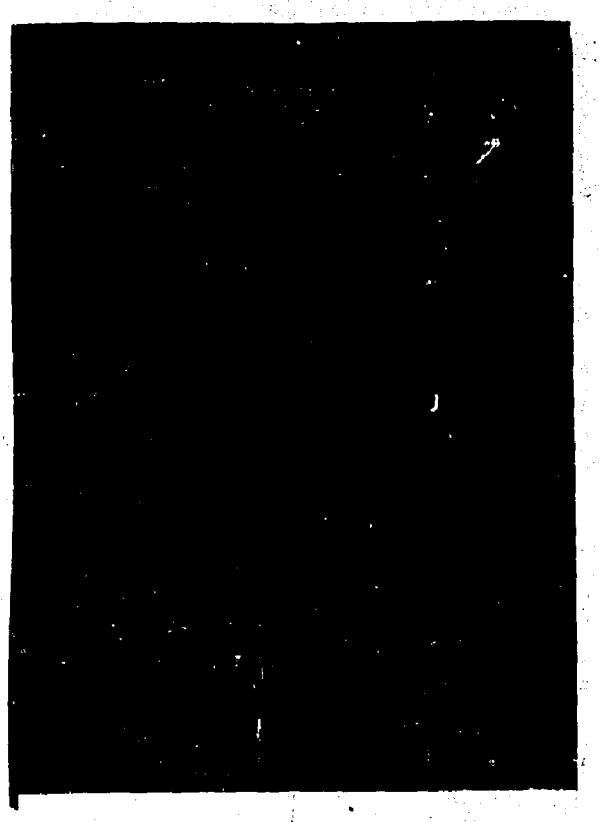

FIGURE 22.

INTERFEROGRAM WITH PARALLEL FRINGES WITH NO TEMPERATURE DIFFERENCE BETWEEN HEATED AND COOLED SURFACES.

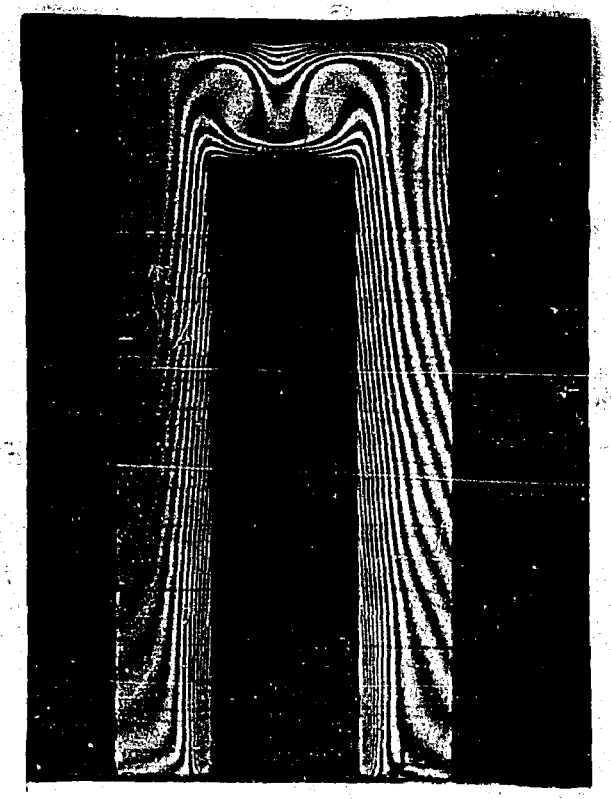

FIGURE 23.

INTERFEROGRAM SHOWING THE DISTORTION OF FRINGES, INITIALLY PARALLEL, WHEN A 50 °F TEMPERATURE DIFFERENCE EXISTS BETWEEN HEATED AND COOLED SURFACES.

This difference in the number of wave lengths can be determined from an interferogram such as that shown in Figure 23. It is the number of interference fringes between the point where the refraction coefficients are η_r and η, respectively, counted when passing on the interferogram parallel to the direction of the original undisplaced fringes.

Lorenz and Lorentz[2] give as the relation between η and the specific weight γ, the expression

$$\frac{\eta^2 - 1}{\eta^2 + 2} \, 1/\gamma = C_1 \tag{31}$$

Assuming that for air η is nearly unity and simplifying we obtain

$$\frac{\eta - 1}{\gamma} = C_2 \tag{32}$$

As a reference value for air at 0°C and 29.2 inches of mercury $\eta = 1.0002934$ and $\lambda_o = 5461$ angstroms $= 2.15 \times 10^{-5}$ inches. This gives for C_2 the value 0.003625 cubic feet per pound. Combining equations (30) and (32) we obtain

$$\gamma_r - \gamma = \frac{\epsilon \lambda_o}{C_2 M} \tag{33}$$

λ_o and M being expressed in the same units. From the gas laws

$$T = P/R\gamma \tag{34}$$

where T = absolute temperature, °Rankine

P = atmospheric pressure, pounds per square foot

R = gas constant, foot pounds per pound per °Rankine

γ = specific weight, pounds per cubic foot.

By substituting γ from equation (33) in equation (34) the following expression for the absolute temperature at any location in the interferogram identified by ϵ fringes counted from the reference point corresponding to T_r is

$$T = P/R\ 1/\gamma_r\ 1/(1 - \frac{\epsilon \lambda_o}{C_2 M \gamma_r}) = T_r\ 1/(1 - \frac{\epsilon \lambda_o}{C_2 M \gamma_r}) \qquad (35)$$

Therefore, expanding the denominator

$$\Delta T = T - T_r = (\frac{\lambda_o \epsilon}{C_2 M \gamma_r}) + (\frac{\lambda_o \epsilon}{C_2 M \gamma_r})^2 + (\frac{\lambda_o \epsilon}{C_2 M \gamma_r})^3 + \ldots \qquad (36)$$

Equation (36) may be used to compute any temperature fields from an interferogram and the location of known reference temperatures. It is valid for finding the temperature at a point in the field, whether the fringes are originally horizontal or a "zero-fringe" is used. In the case of horizontal fringes, the number of fringes from the reference point is counted, as the fringes are numbered, in the manner shown in Figure 24. In the case of the "zero-fringe", as reference conditions, the fringes are counted and numbered as shown in Figure 25.

It is noteworthy that in the preceding development of the basic relationships used for the interpretation of interferograms the determination of temperatures in the field is dependent on the difference in the number of wave lengths along two parallel light paths. The temperature distribution along the light path is not taken into account but rather is integrated by means of the interferogram. Consequently, only two-dimensional temperature fields

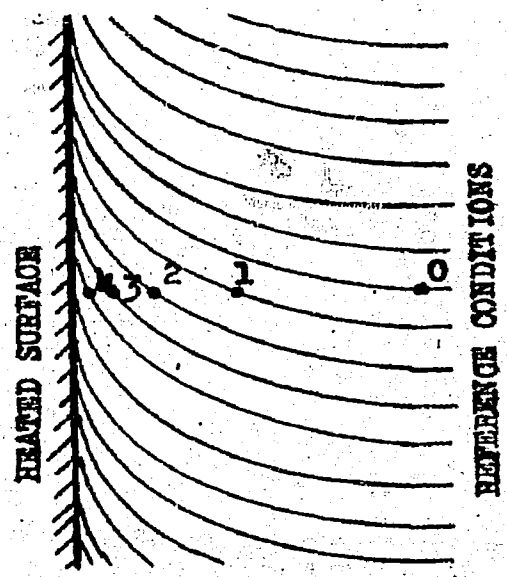

FIGURE 24

METHOD OF COUNTING FOR FRINGES INITIALLY HORIZONTAL

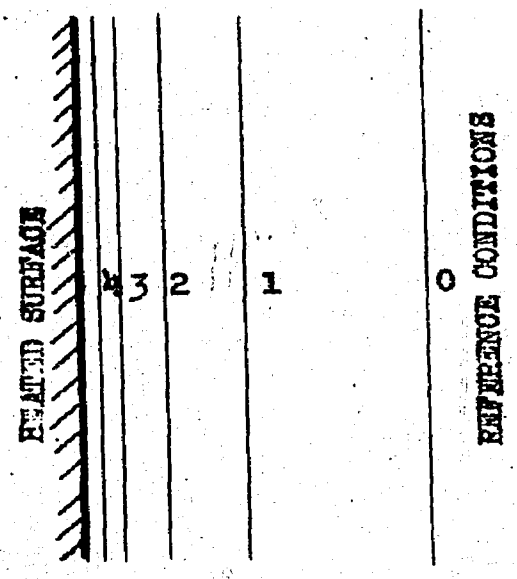

FIGURE 25

METHOD OF COUNTING FOR "ZERO FRINGE" AT REFERENCE CONDITIONS

can be explored conveniently since the length M of the temperature variation is essentially interpreted in terms of an abrupt change. Some experiments and methods for three-dimensional fields with an axis of revolution normal to the light bundle have, however, been carried out.(3)

The Zehnder-Mach interferometer has a number of distinct advantages as an experimental aid, as an entire temperature field may be recorded instantaneously on one negative. Its expense is only limited by the size of the mirrors. Large quantities of data can be obtained quickly since the time required is diminished by the time required to make settings and establish the required ther-

mal conditions. Since radiation effects are not recorded, no corrections are necessary and the free convection phenomena are isolated.

APPENDIX II

RESULTS OF PROBING IN THE TEMPERATURE FIELD AROUND THE PROTOTYPE MODEL

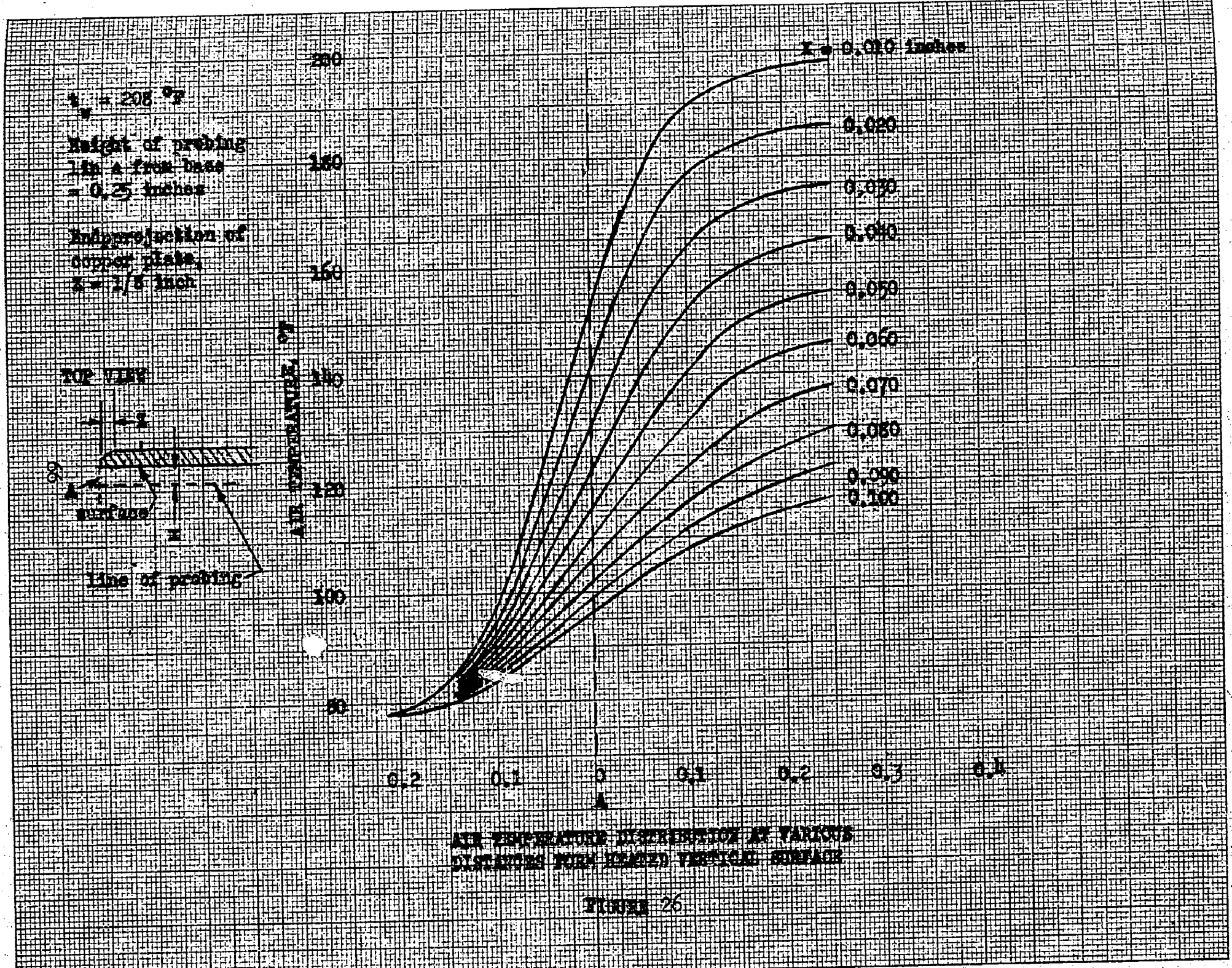

AIR TEMPERATURE DISTRIBUTION AT VARIOUS DISTANCES FROM HEATED VERTICAL SURFACE

FIGURE 26

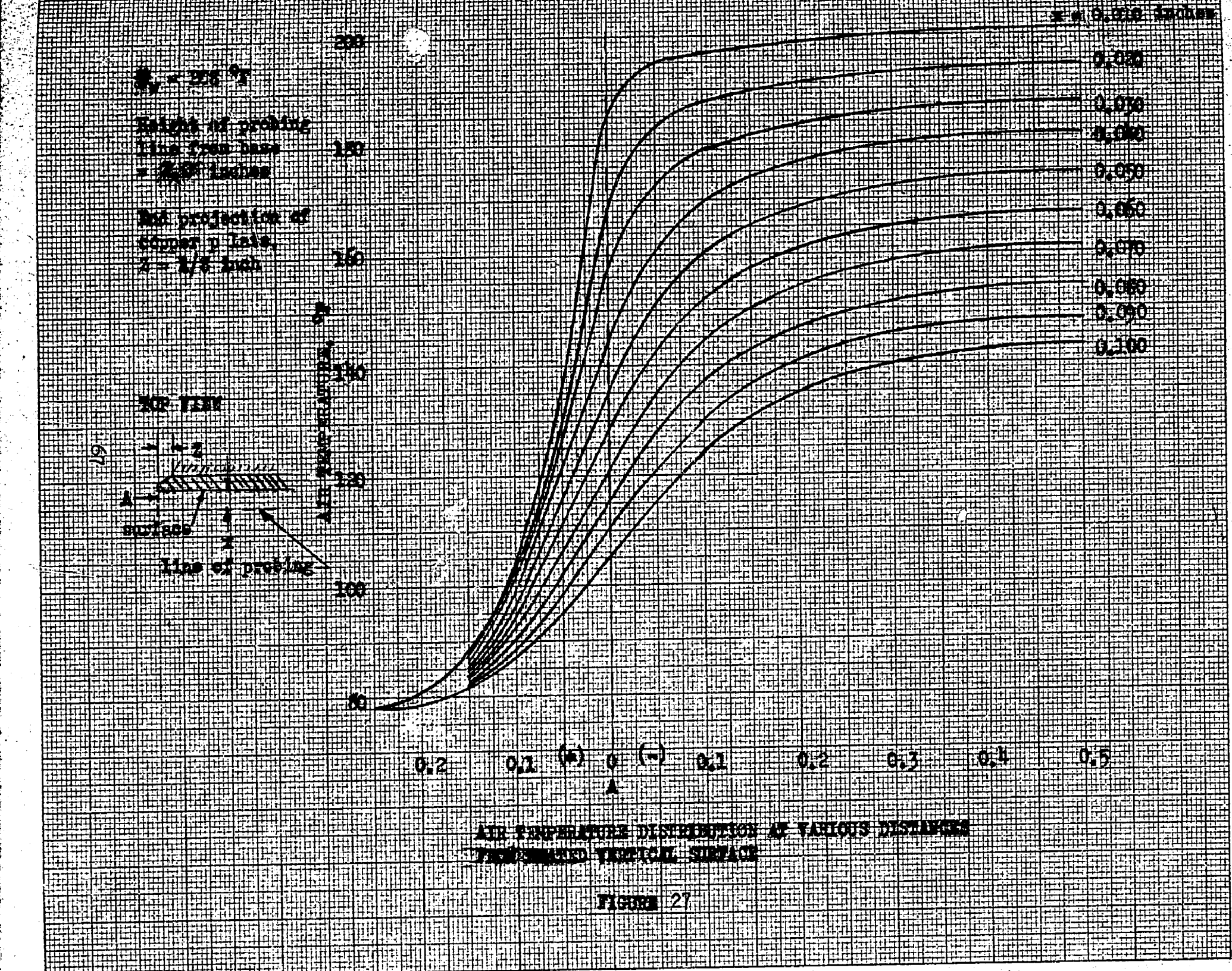

AIR TEMPERATURE DISTRIBUTION AT VARIOUS DISTANCES FROM HEATED VERTICAL SURFACE

FIGURE 27

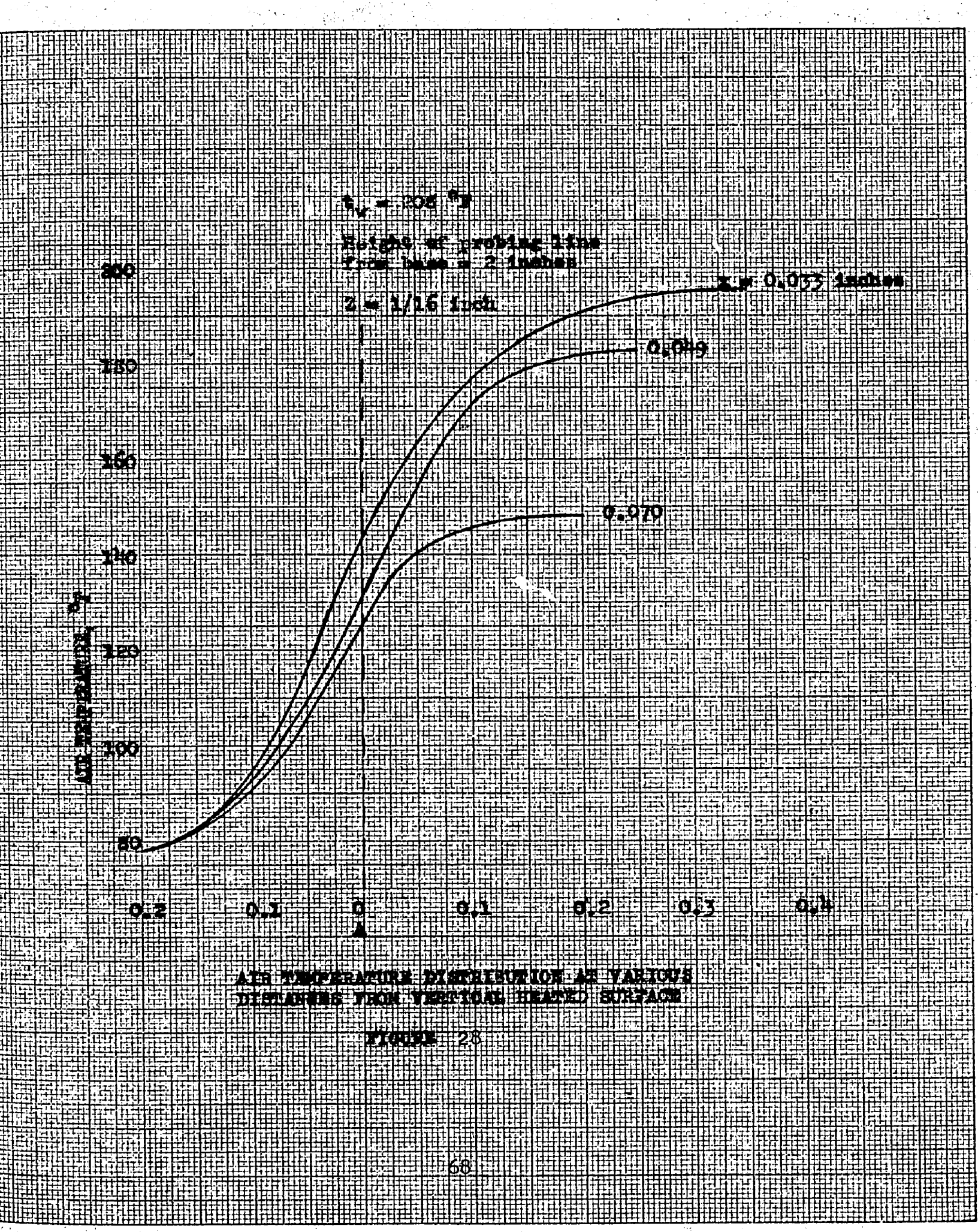

AIR TEMPERATURE DISTRIBUTION AT VARIOUS DISTANCES FROM VERTICAL HEATED SURFACE

FIGURE 28

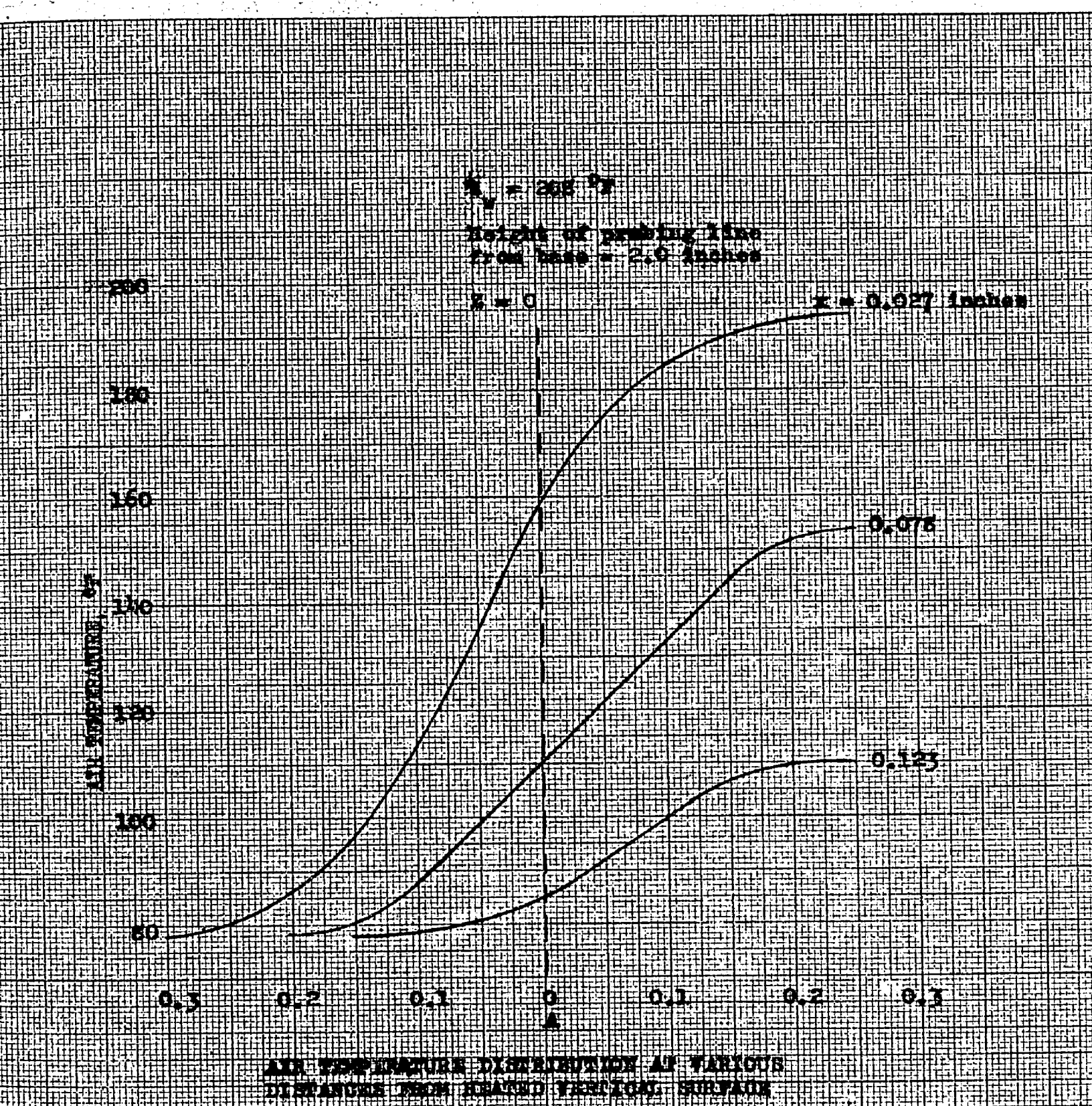

AIR TEMPERATURE DISTRIBUTION AT VARIOUS DISTANCES FROM HEATED VERTICAL SURFACE

FIGURE 29

APPENDIX III

PROPERTIES OF AIR

TABLE 3

Deg F	c $\frac{\text{Btu}}{\text{lb-deg F}}$	ρ * $\frac{\text{lb}}{\text{ft}^3}$	μ $\frac{\text{lb}}{\text{ft-hr}}$	k $\frac{\text{Btu}}{\text{hr-ft-deg F}}$	$\frac{c\,\mu}{k}$
0	0.239	0.0862	0.040	0.0132	0.72
20	0.240	0.0826	0.041	0.0138	0.71
40	0.240	0.0793	0.043	0.0143	0.71
60	0.240	0.0763	0.044	0.0148	0.71
80	0.240	0.0734	0.045	0.0153	0.70
100	0.240	0.0708	0.046	0.0158	0.70
120	0.240	0.0684	0.047	0.0162	0.70
140	0.240	0.0661	0.049	0.0168	0.70
160	0.241	0.0640	0.050	0.0172	0.70
180	0.241	0.0620	0.051	0.0177	0.69
200	0.241	0.0601	0.052	0.0182	0.69
250	0.242	0.0559	0.055	0.0192	0.68
300	0.242	0.0522	0.058	0.0204	0.68
350	0.243	0.0490	0.060	0.0216	0.68
400	0.245	0.0461	0.062	0.0227	0.67
450	0.246	0.0436	0.065	0.0239	0.67
500	0.247	0.0413	0.067	0.0250	0.66
600	0.250	0.0374	0.072	0.0271	0.66
700	0.253	0.0342	0.076	0.0291	0.66
800	0.257	0.0315	0.081	0.0312	0.66

* ρ is for 29.92 in Hg pressure.

Sources of Data:

c, μ and k - Gas Tables by Keenan and Kaye

ρ computed from simple gas law.

APPENDIX IV

VARIATION OF TEMPERATURE GRADIENT WITH DISTANCE BETWEEN MODEL AND DUCT FOR VARIOUS DISTANCES FROM BOTTOM OF MODEL FOR ALL TEST CONDITIONS COVERED IN THIS INVESTIGATION

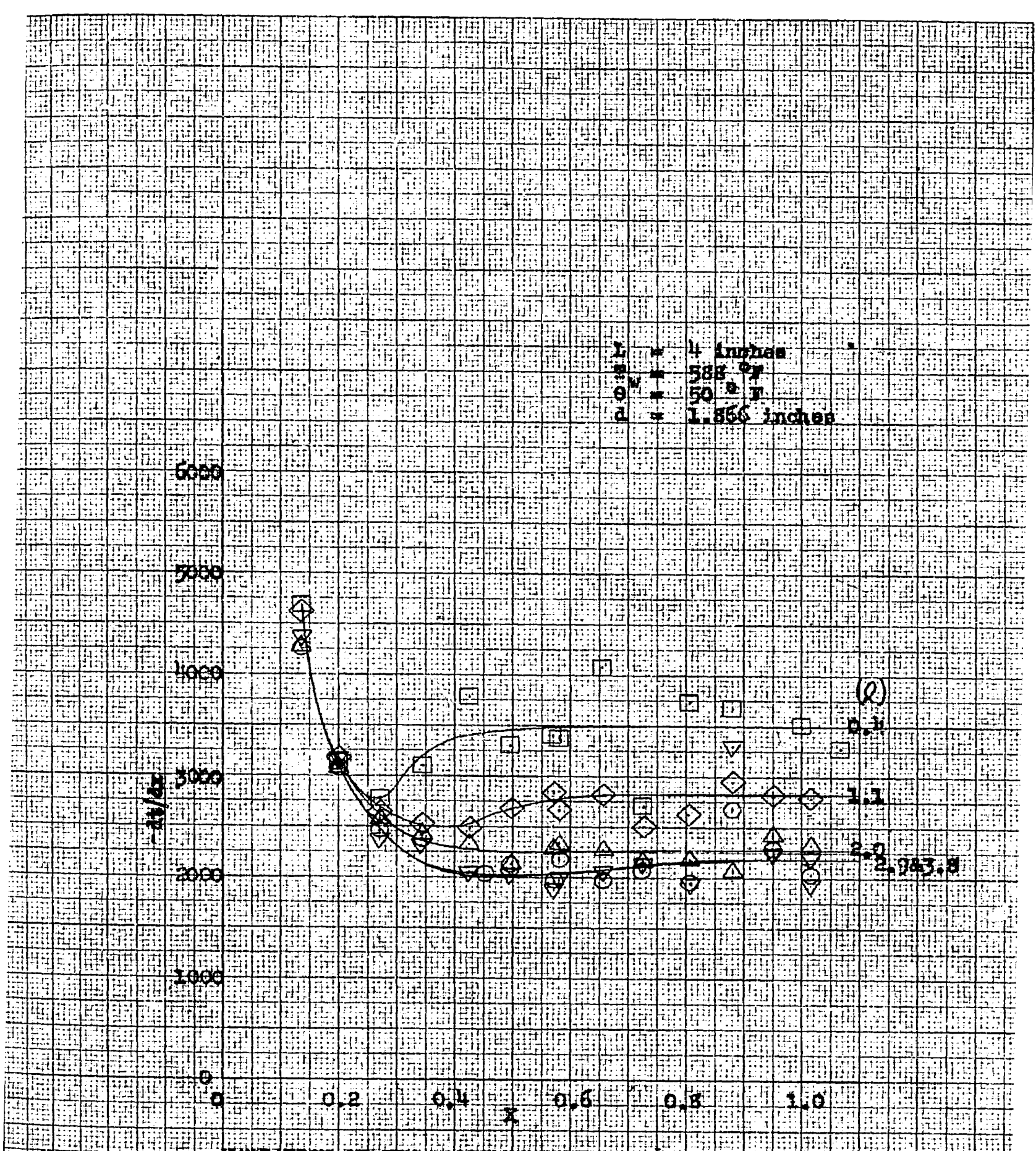

VARIATION OF TEMPERATURE GRADIENT WITH DISTANCE BETWEEN NOZZLE AND DUCT FOR VARIOUS DISTANCES FROM BOTTOM OF MOTOR

FIGURE 30

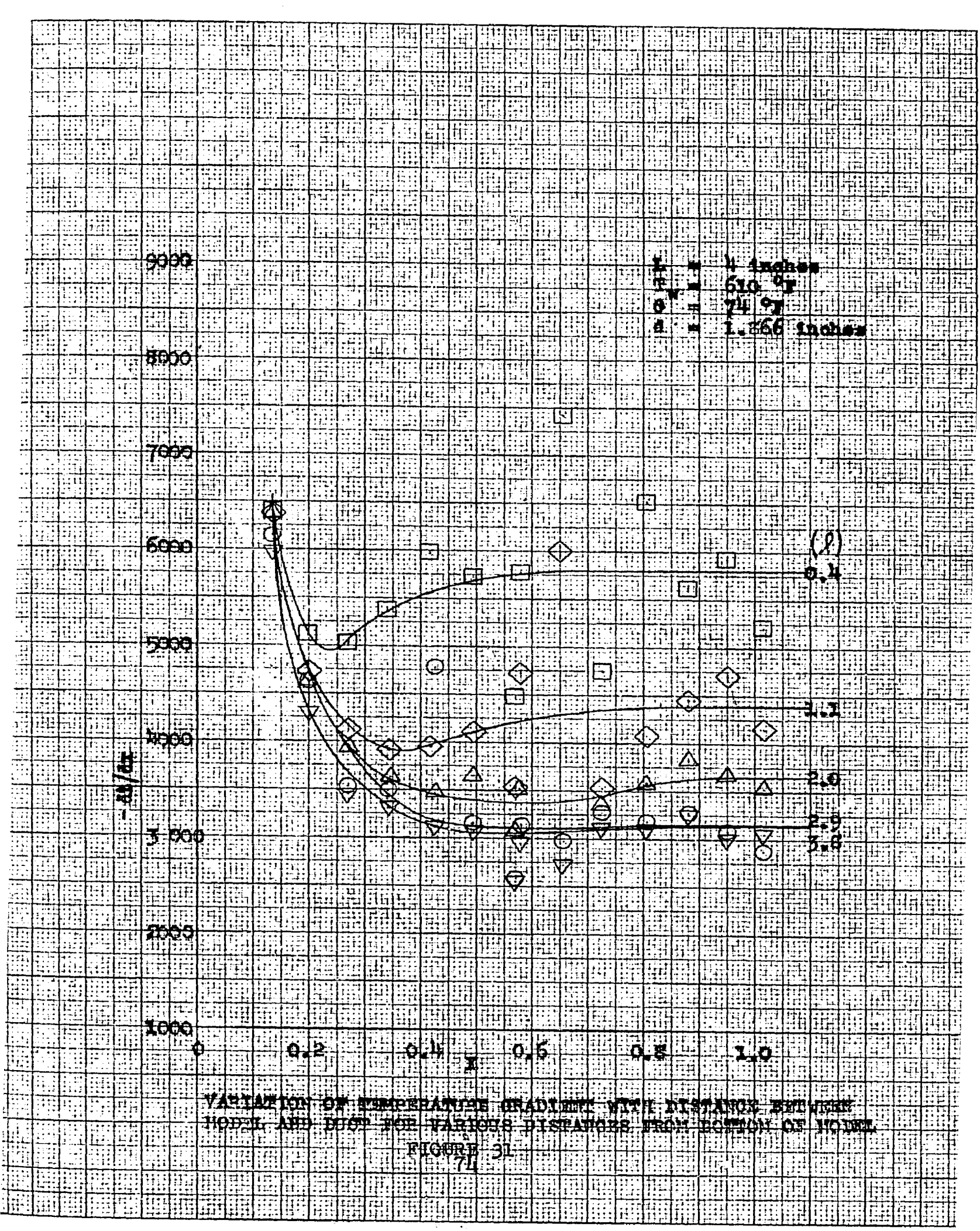

VARIATION OF TEMPERATURE GRADIENT WITH DISTANCE BETWEEN MODEL AND DUCT FOR VARIOUS DISTANCES FROM BOTTOM OF MODEL.

FIGURE 31

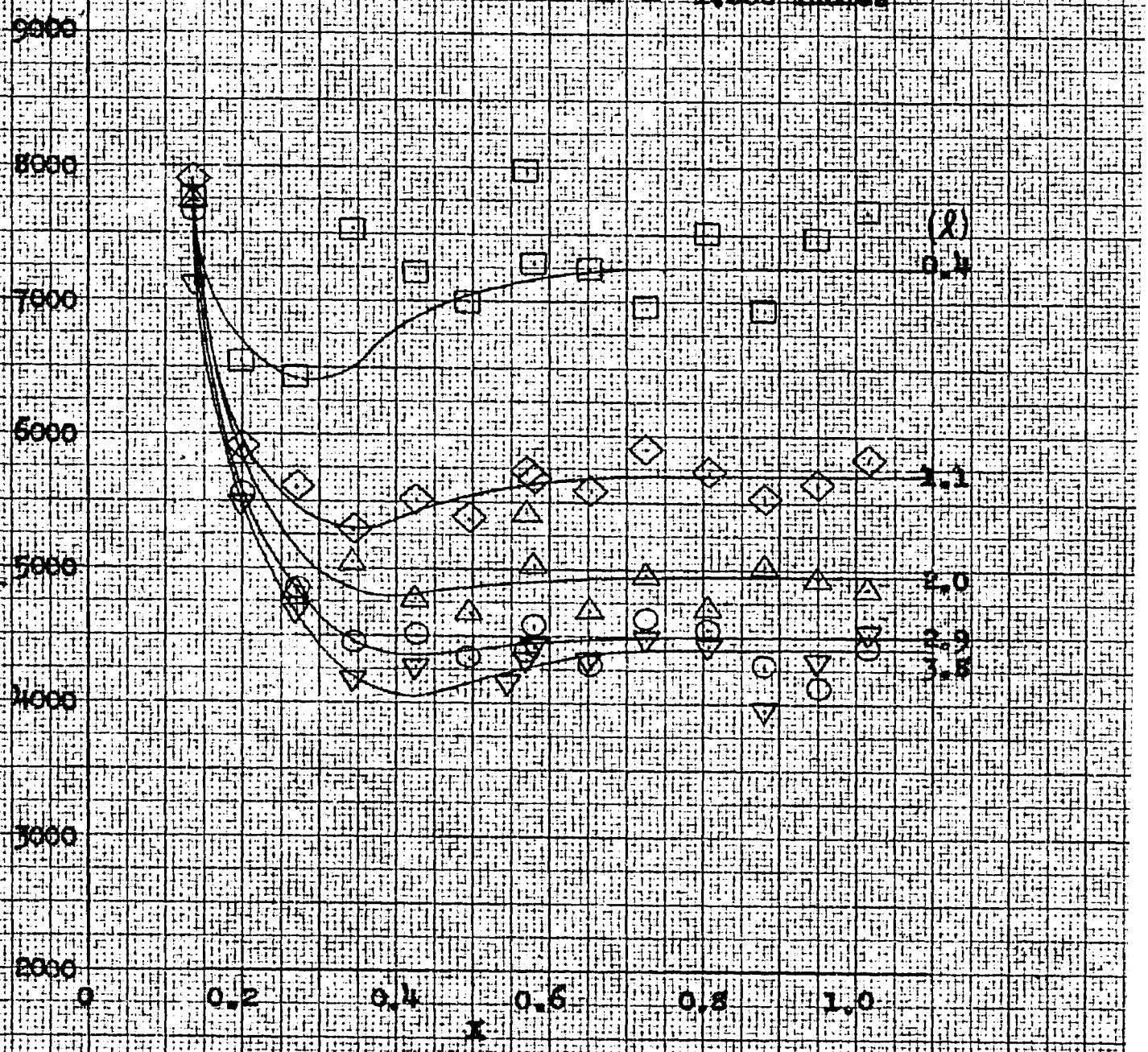

VARIATION OF TEMPERATURE GRADIENT WITH DISTANCE BETWEEN MODEL AND DUST FOR VARIOUS DISTANCES FROM BOTTOM OF MODEL.

FIGURE 32

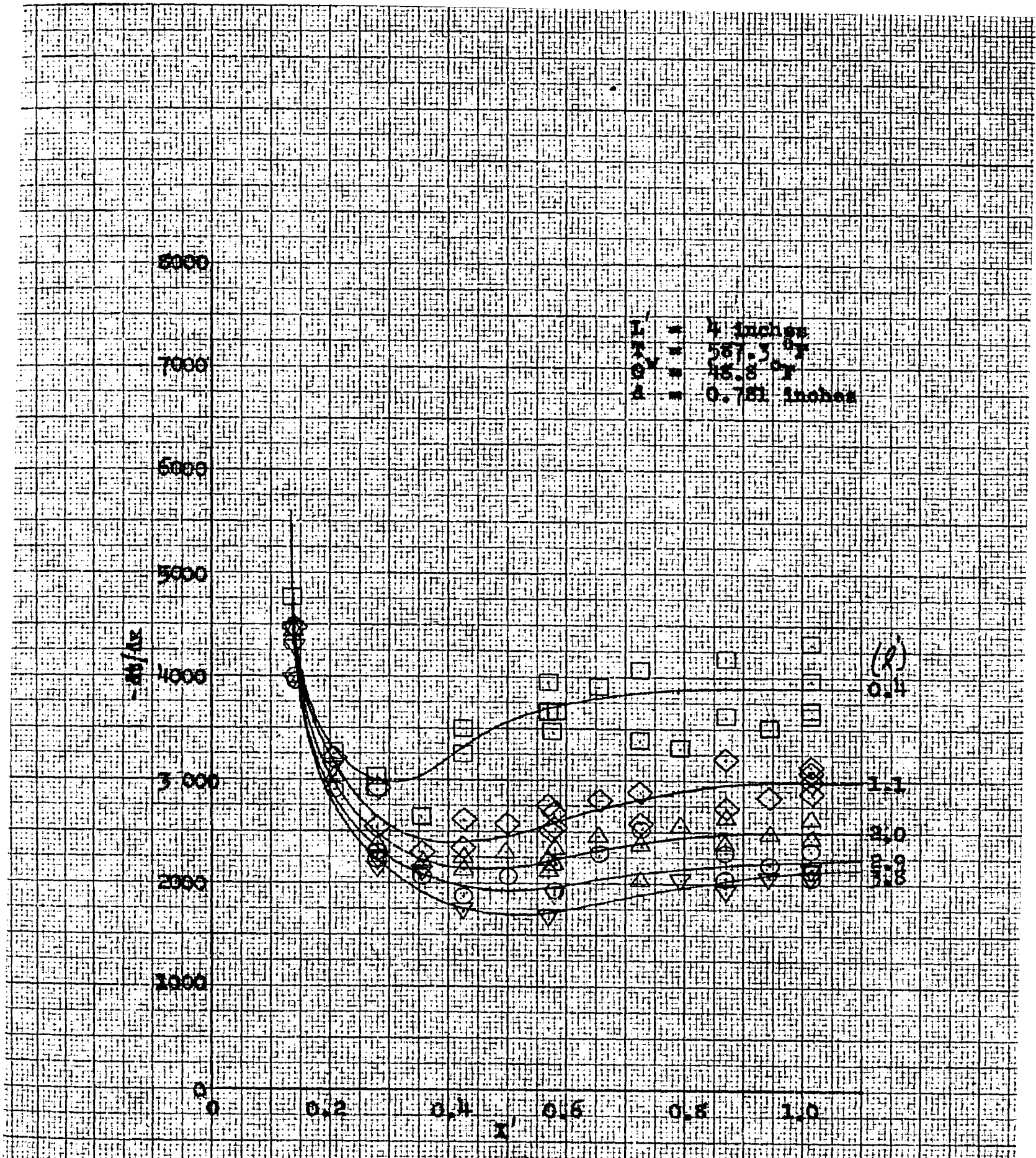

VARIATION OF TEMPERATURE GRADIENT WITH DISTANCE BETWEEN MODEL AND DUCT FOR VARIOUS DISTANCES FROM BOTTOM OF MODEL

FIGURE 33

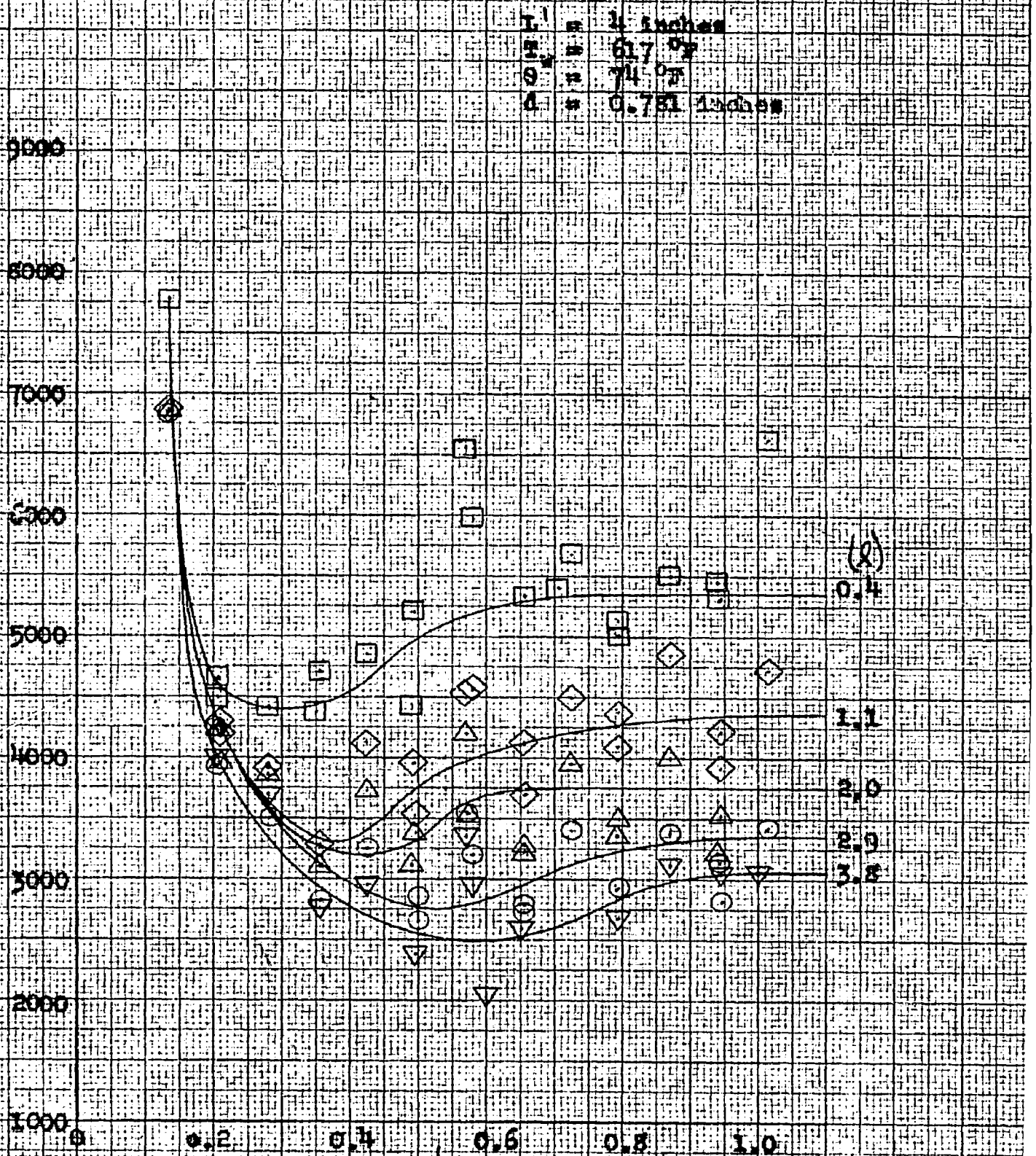

VARIATION OF TEMPERATURE GRADIENT WITH DISTANCE BETWEEN MODEL AND DUCT FOR VARIOUS DISTANCES FROM BOTTOM OF MODEL

FIGURE 31

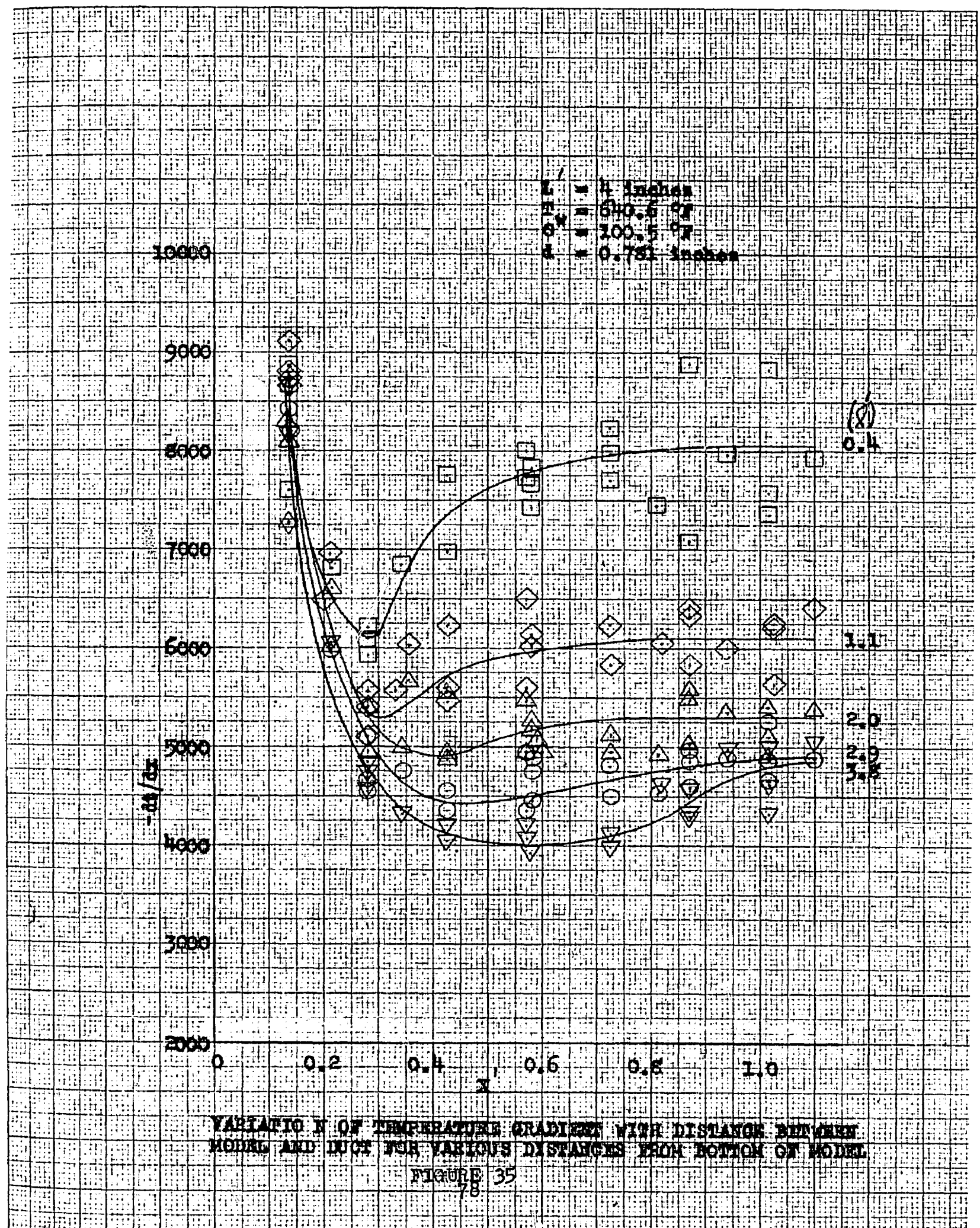

VARIATION OF TEMPERATURE GRADIENT WITH DISTANCE BETWEEN MODEL AND DUCT FOR VARIOUS DISTANCES FROM BOTTOM OF MODEL

FIGURE 35

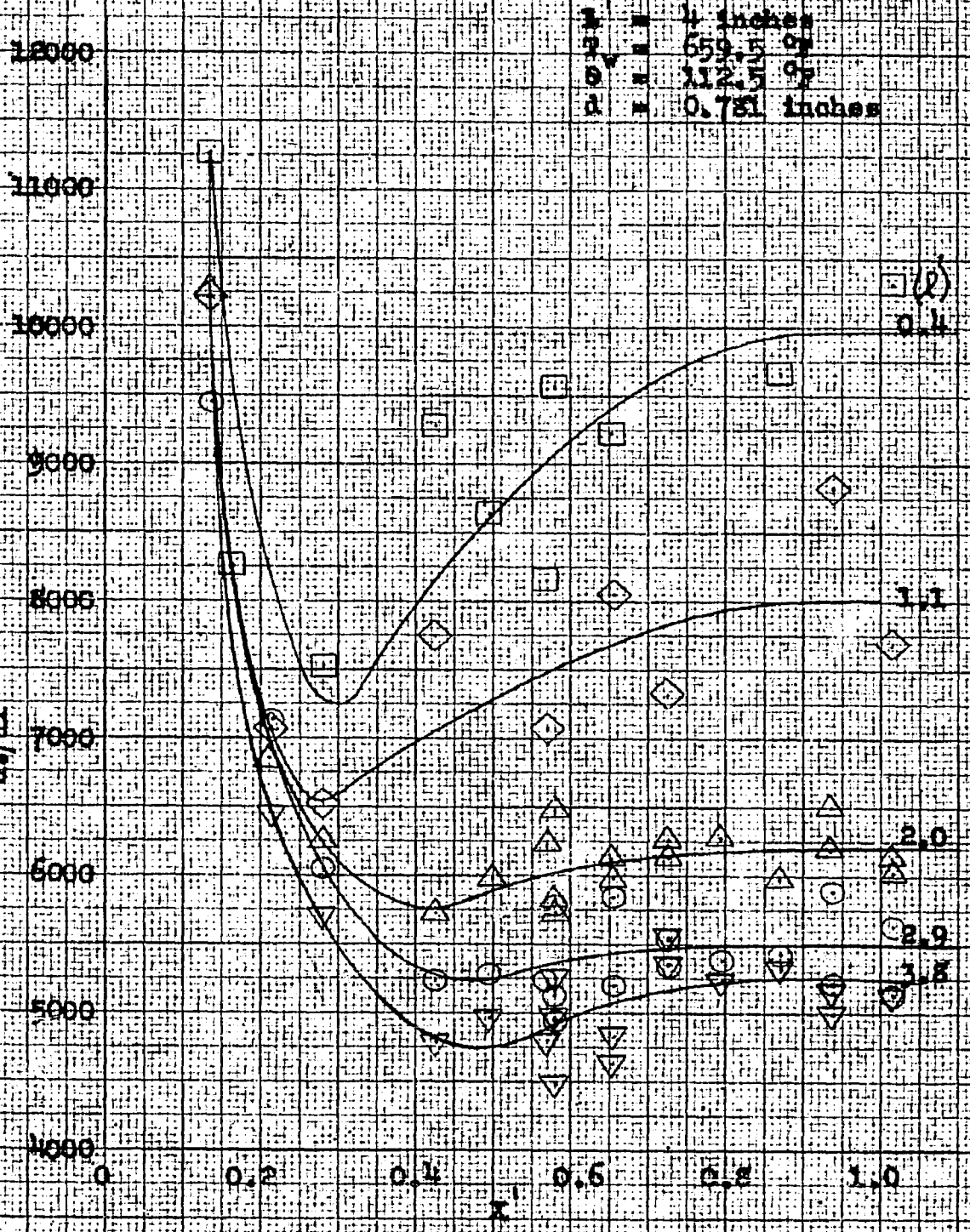

VARIATION OF TEMPERATURE GRADIENT WITH DISTANCE BETWEEN MODEL AND DUCT FOR VARIOUS DISTANCES FROM BOTTOM OF MODEL

FIGURE 36

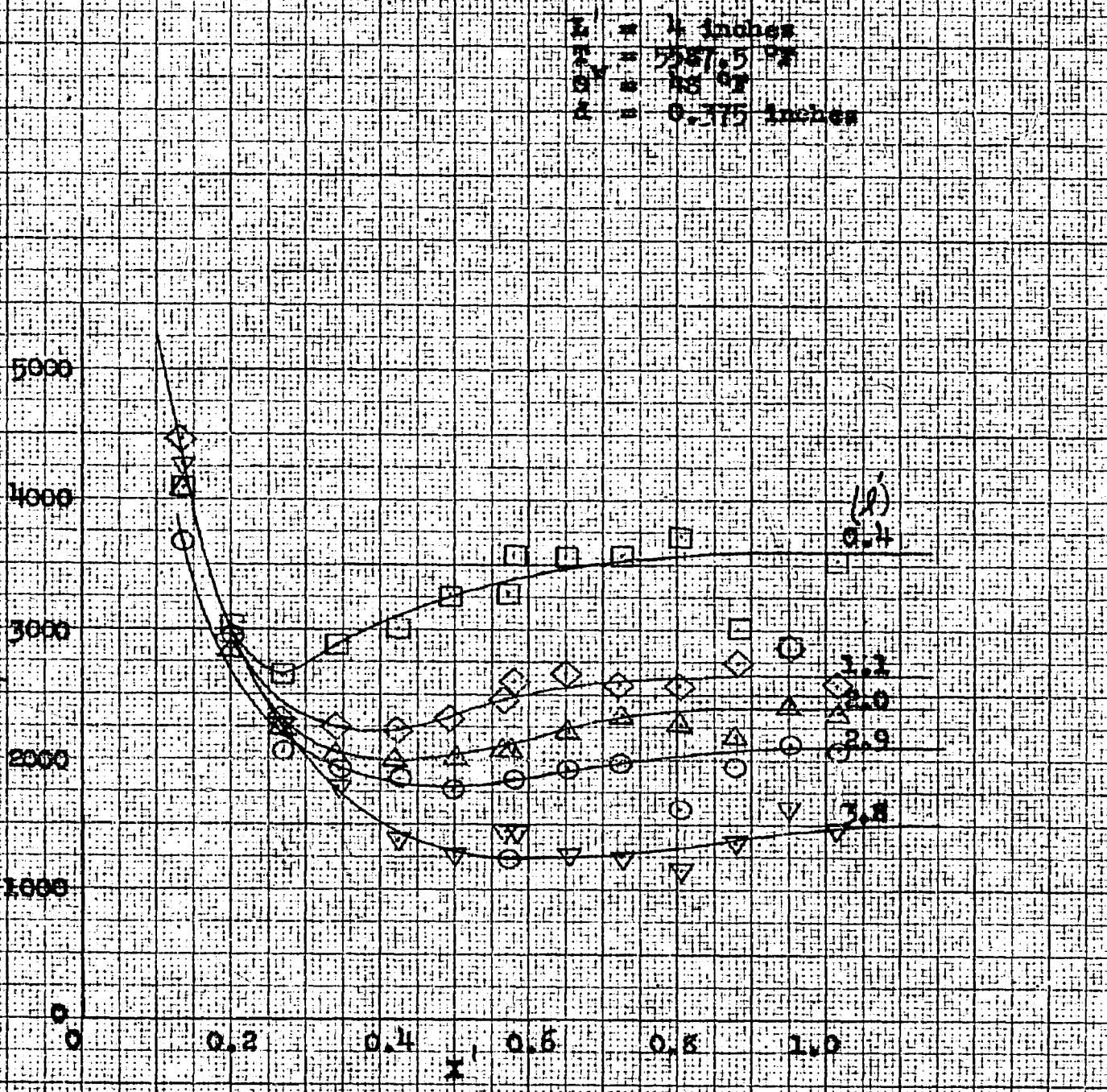

VARIATION OF TEMPERATURE GRADIENT WITH DISTANCE BETWEEN MODEL AND DUCT FOR VARIOUS DISTANCES FROM BOTTOM OF MODEL

FIGURE 37

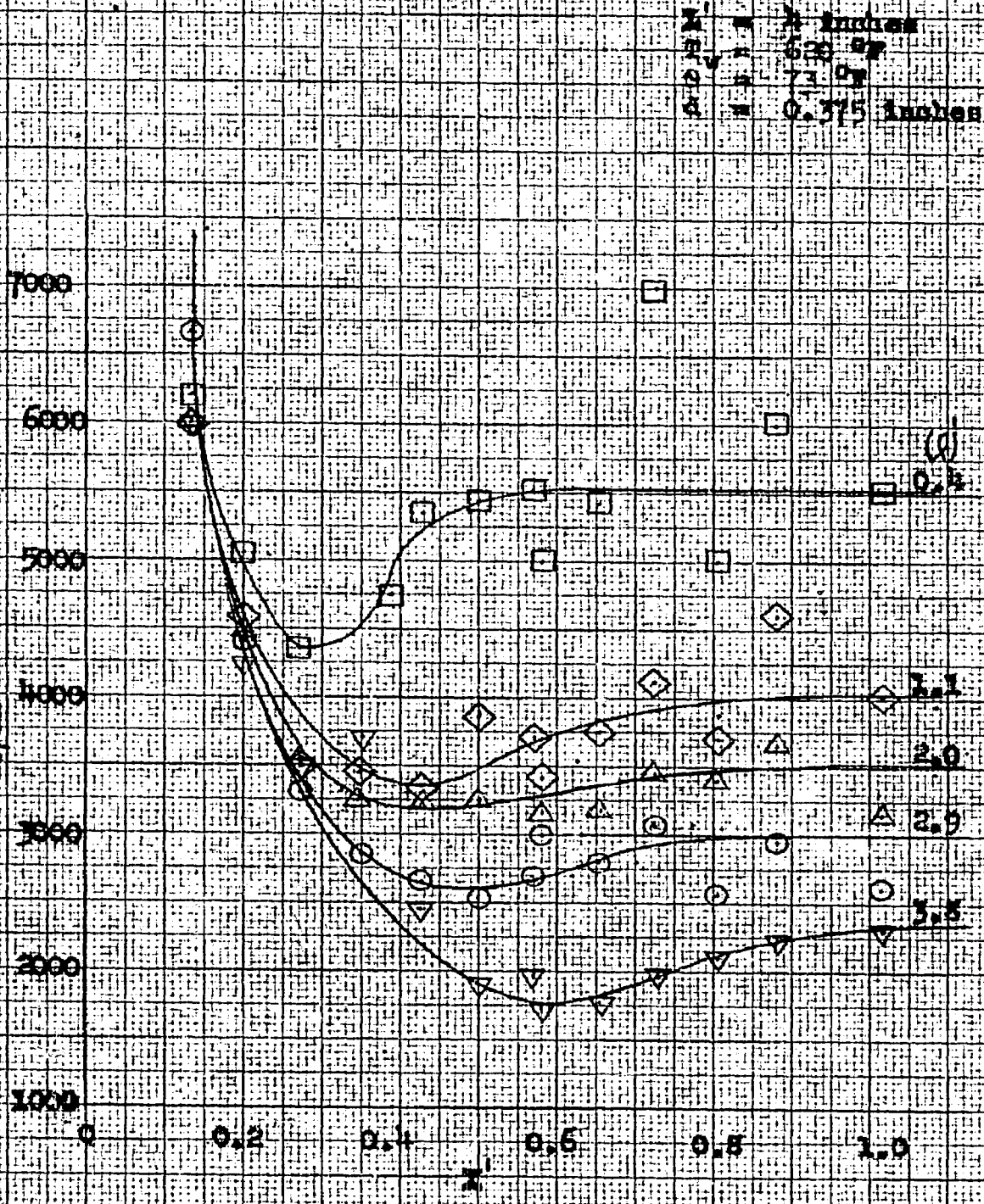

VARIATION OF TEMPERATURE GRADIENT WITH DISTANCE BETWEEN MODEL AND DUCK FOR VARIOUS DISTANCES FROM BOTTOM OF MODEL

FIGURE 38

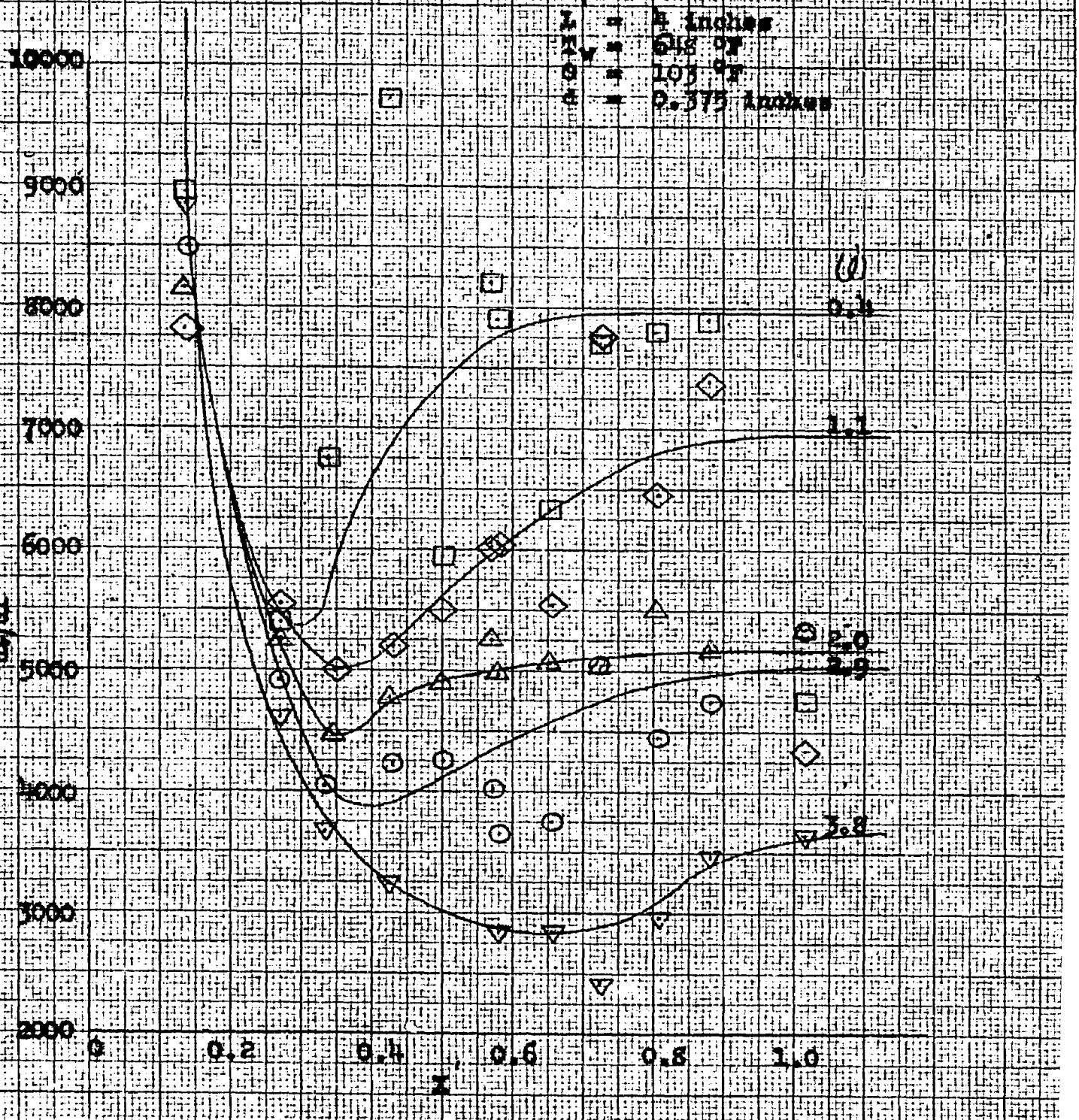

VARIATION OF TEMPERATURE GRADIENT WITH DISTANCE BETWEEN MODEL AND DUCT FOR VARIOUS DISTANCES FROM BOTTOM OF MODEL

FIGURE 39

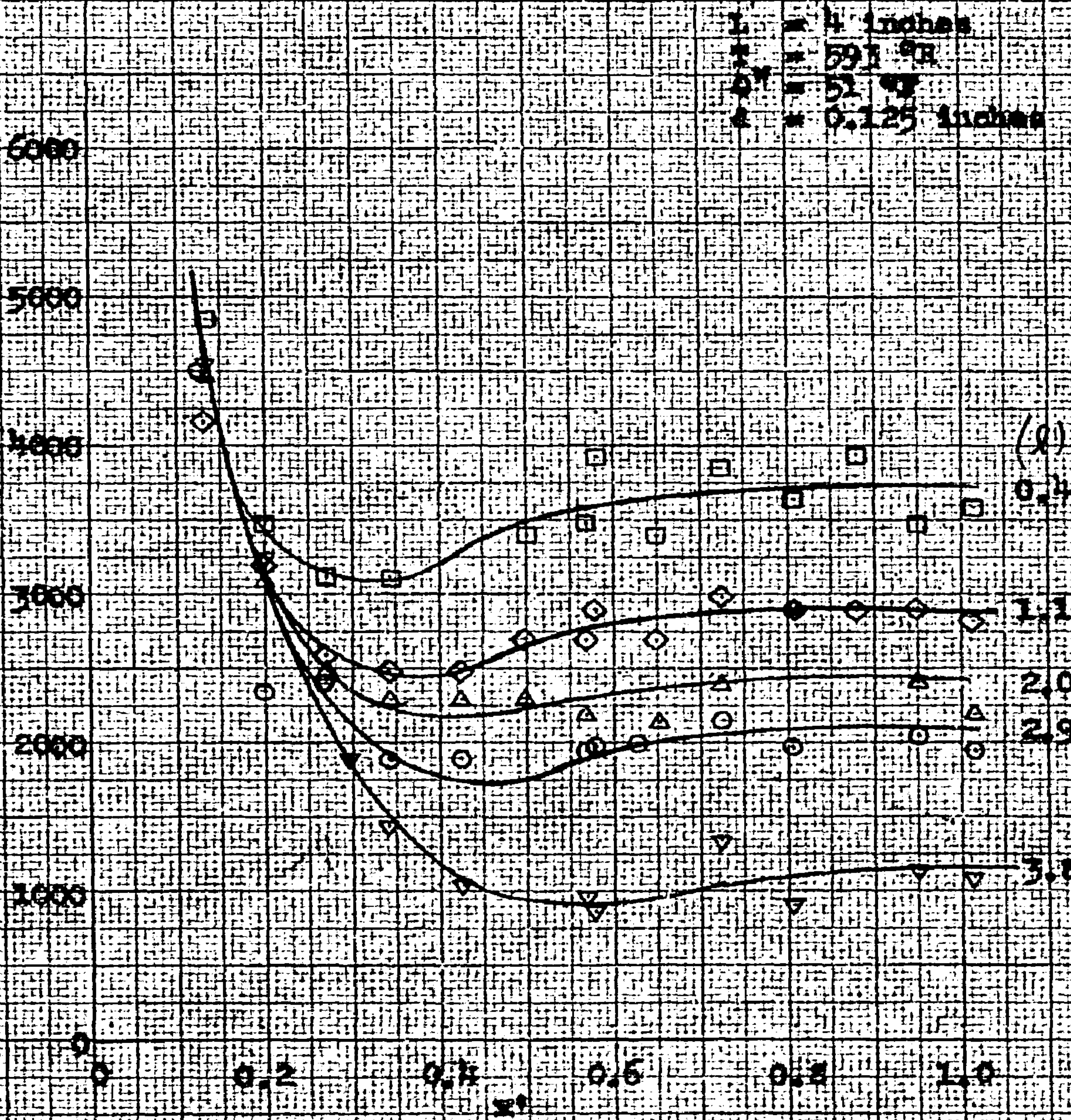

VARIATION OF TEMPERATURE GRADIENT WITH DISTANCE BETWEEN MODEL AND DUCT FOR VARIOUS DISTANCES FROM BOTTOM OF MODEL

FIGURE 49

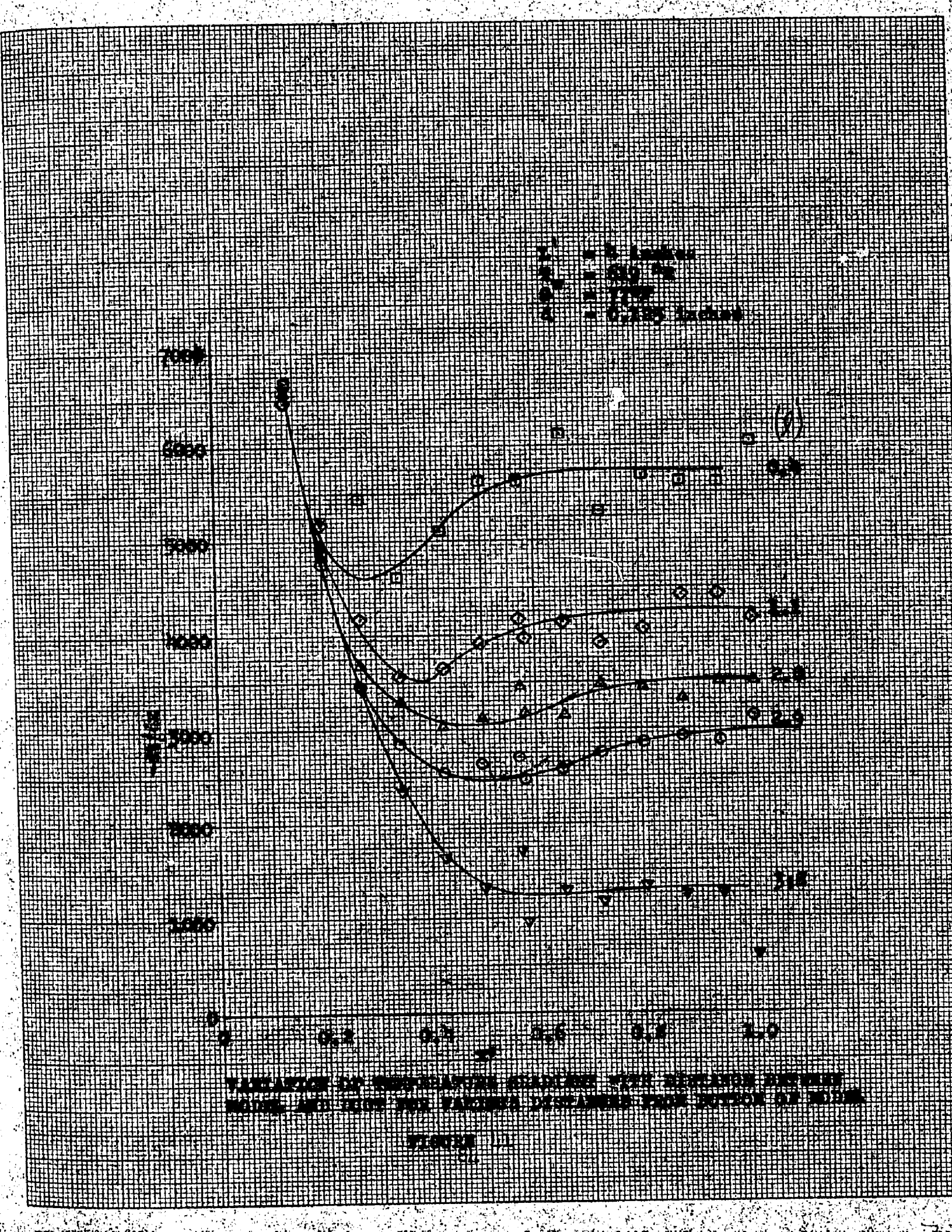
7000
6000
5000
4000
3000
2000
1000
0
0,2
0,4
2,6
0,8
3,0
2,5
2,0
1,5
1,0
0,5

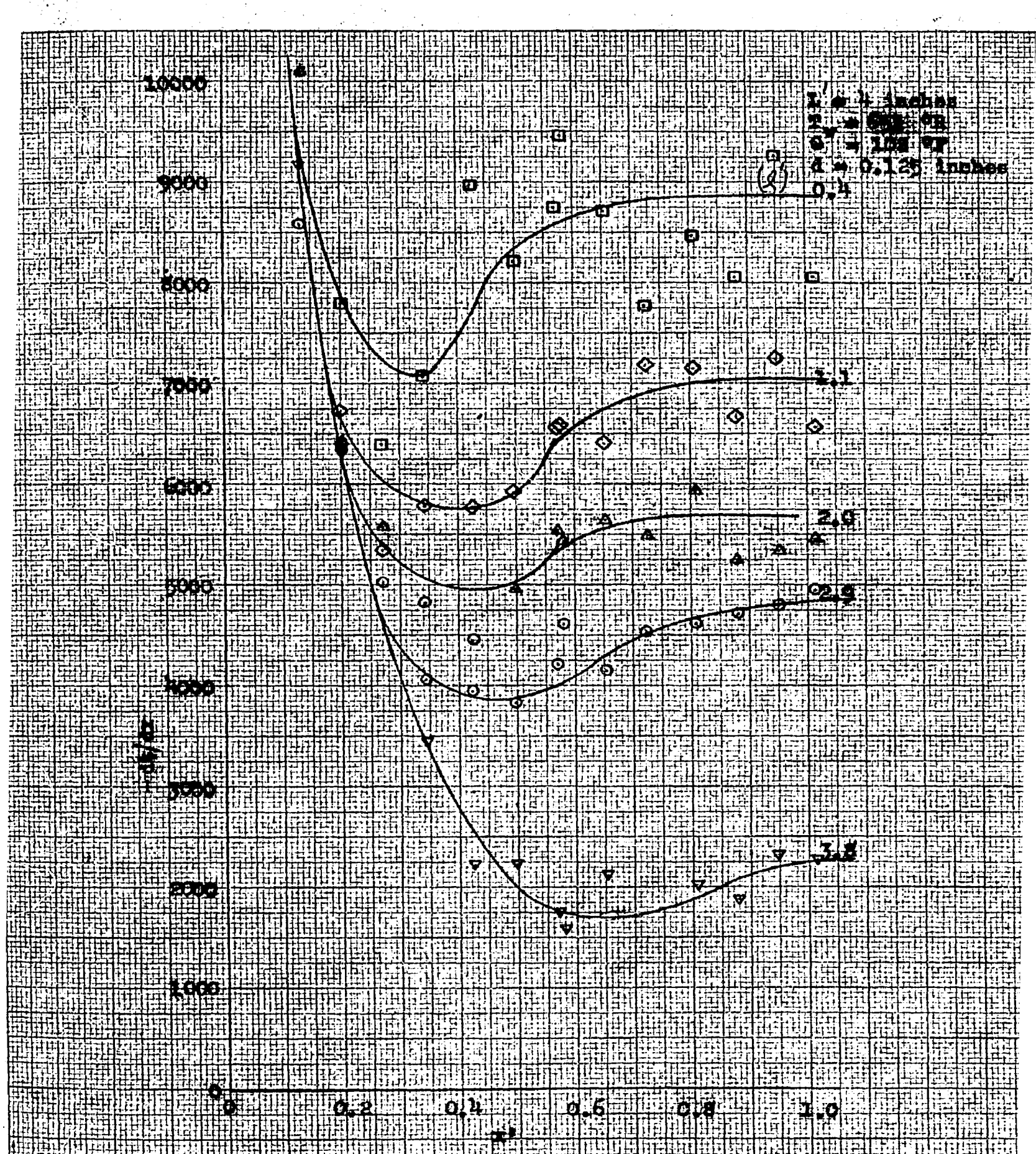

VARIATION OF TEMPERATURE GRADIENT WITH DISTANCE BETWEEN NOZZLE AND DUCK FOR VARIOUS DISTANCES FROM BOTTOM OF HOUSE

FIGURE 12

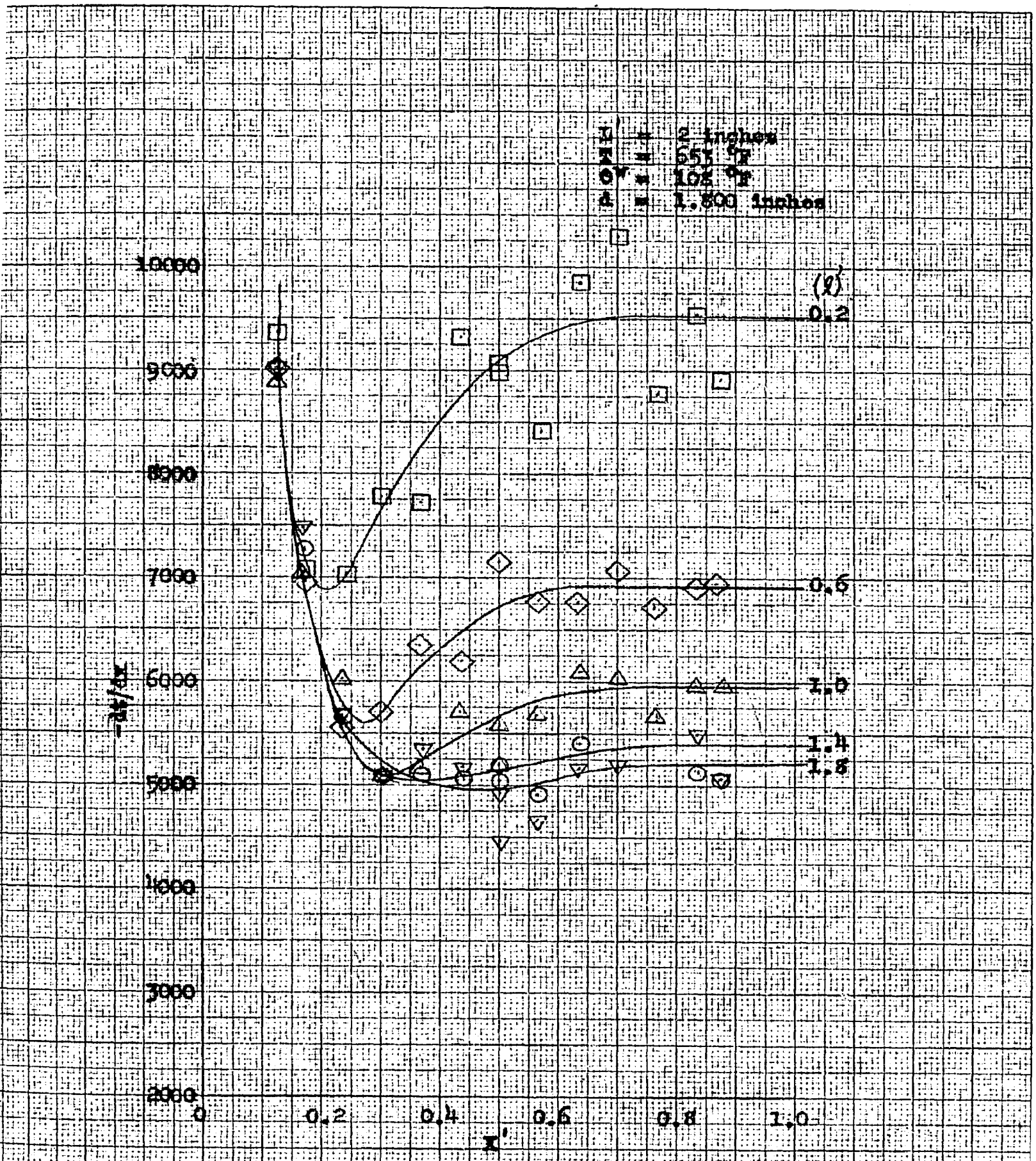

VARIATION OF TEMPERATURE GRADIENT WITH DISTANCE BETWEEN MODEL AND DUCT FOR VARIOUS DISTANCES FROM BOTTOM OF MODEL.

FIGURE 43

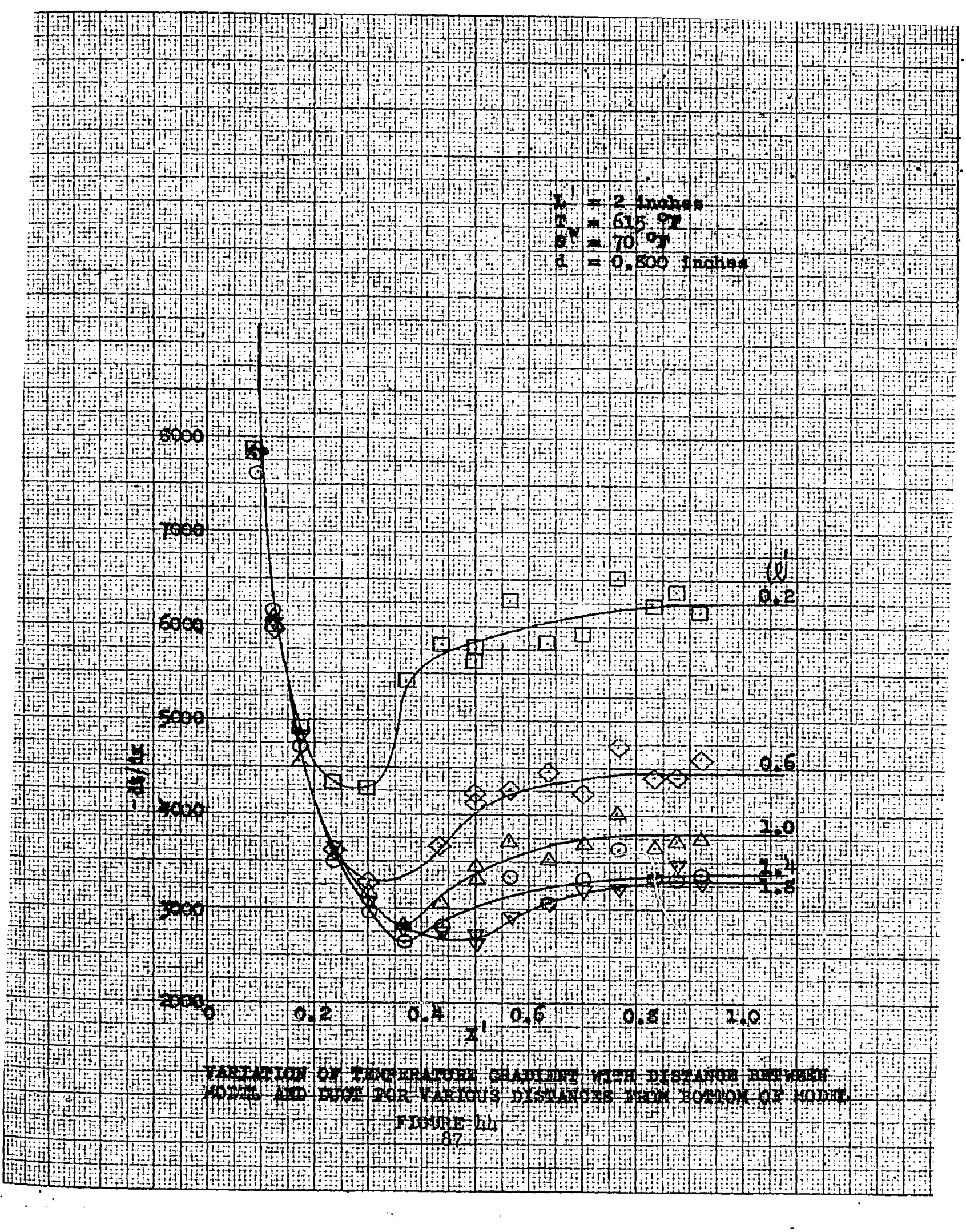

VARIATION OF TEMPERATURE GRADIENT WITH DISTANCE BETWEEN NOZZLE AND DUST FOR VARIOUS DISTANCES FROM BOTTOM OF HOOD.

FIGURE 14

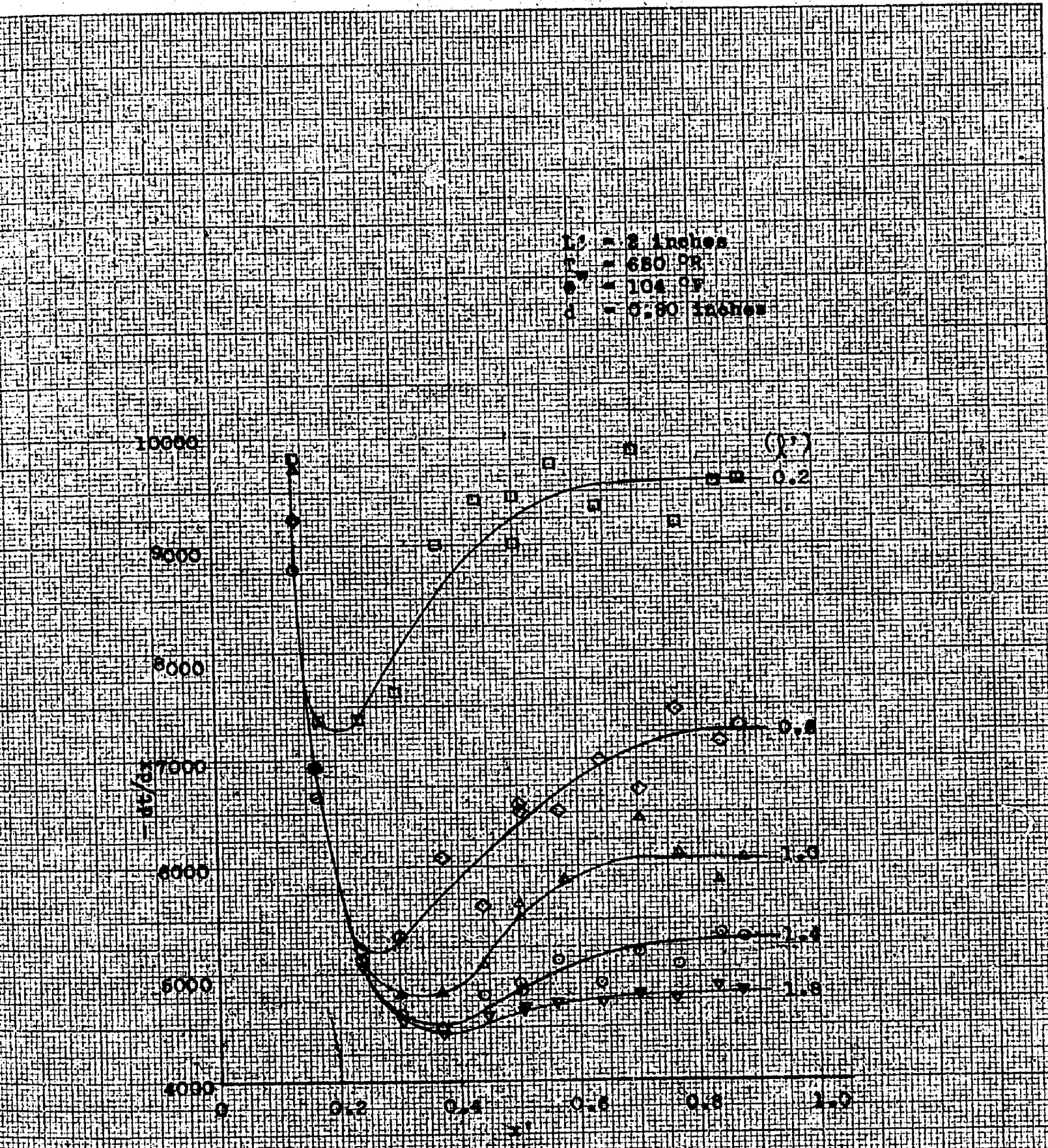

VARIATION OF TEMPERATURE GRADIENT WITH DISTANCE BETWEEN MODEL AND DUCT FOR VARIOUS DISTANCES FROM BOTTOM OF MODEL

FIGURE 46.

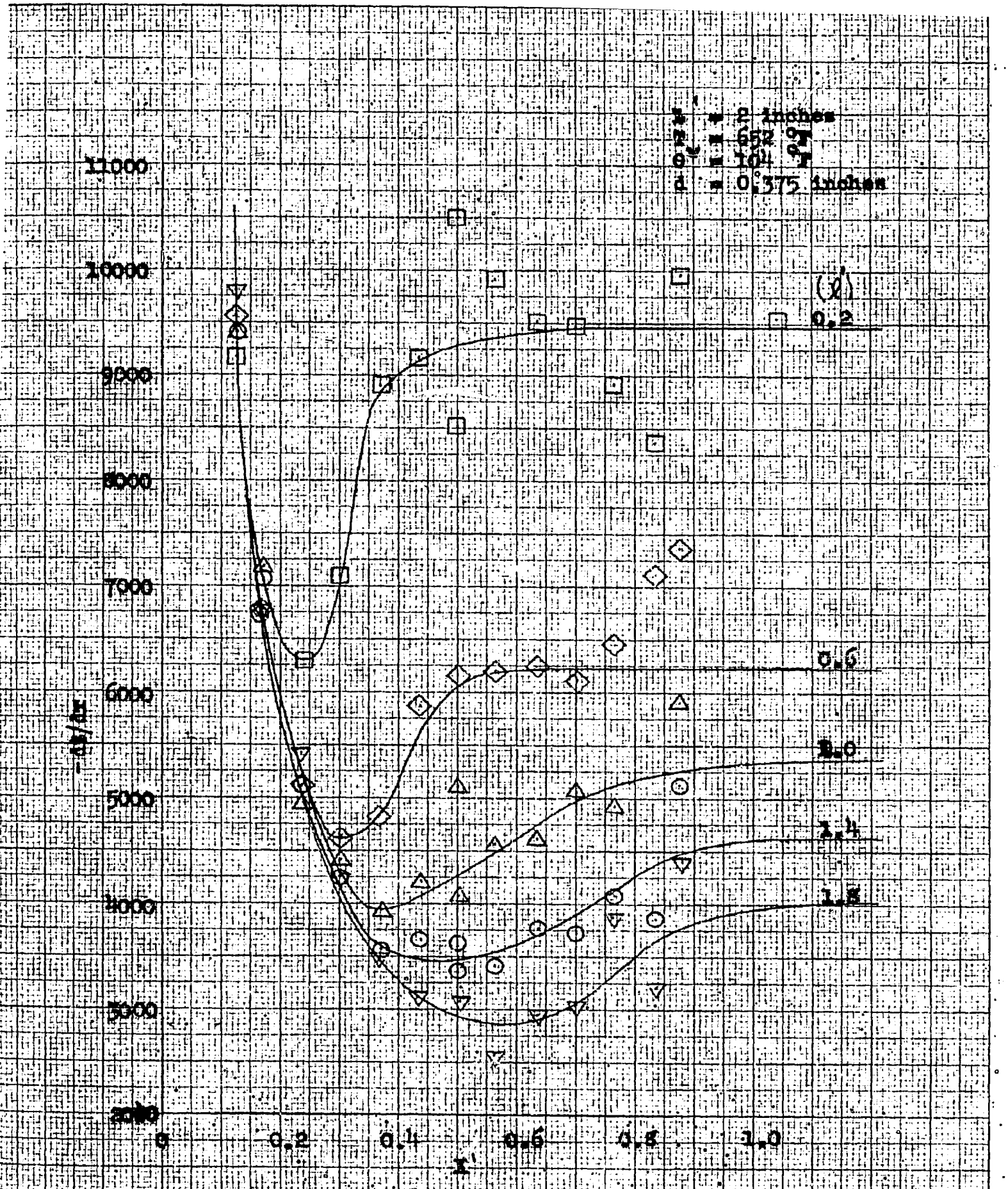

VARIATION OF TEMPERATURE GRADIENT WITH DISTANCE BETWEEN MODEL AND DUCT FOR VARIOUS DISTANCES FROM BOTTOM OF MODEL.

FIGURE 16

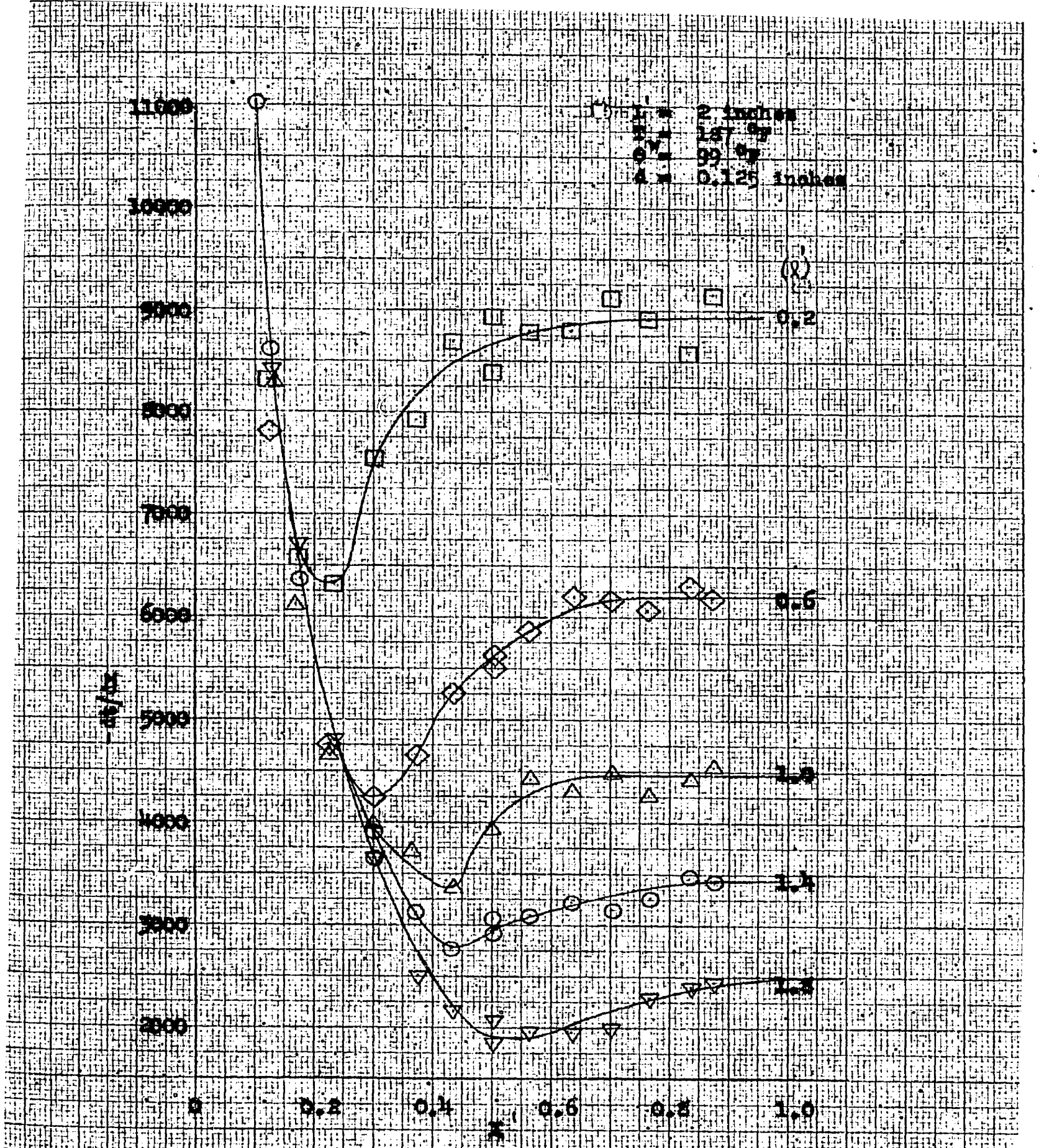

VARIATION OF TEMPERATURE GRADIENT WITH DISTANCE BETWEEN PLATE AND DUCT FOR VARIOUS DISTANCES FROM BOTTOM OF PLATE

FIGURE 47

APPENDIX V

TABLE OF TEMPERATURE GRADIENTS OBTAINED FROM FAIRED CURVES IN APPENDIX IV WITH CORRESPONDING POINT NUSSELT NUMBERS AND GRASHOF NUMBERS

TABLE 4

L' = 4.0 inches
d = 1.86 inches

x'	ℓ	Θ	T_w	-dt/dx	Nu_T	Gr
0.15	0.033	50	588	4250	2.830	2.60×10^3
		74	610	6000	2.700	3.17×10^3
		94	638	7250	2.568	3.39×10^3
	0.0917	50	588	4000	7.336	5.42×10^4
		74	610	5630	6.977	6.60×10^4
		94	638	6850	6.682	7.05×10^4
	0.1667	50	588	4000	13.340	3.26×10^5
		74	610	5780	13.021	3.96×10^5
		94	638	7000	12.414	4.24×10^5
	0.2417	50	588	3960	19.143	9.93×10^5
		74	610	5780	18.879	1.21×10^6
		94	638	6800	17.485	1.29×10^6
	0.3167	50	588	4050	25.653	2.82×10^6
		74	610	5350	22.522	3.44×10^6
		94	638	6530	22.000	3.68×10^6
0.20	0.033	50	588	3210	2.134	2.60×10^3
		74	610	5140	2.313	3.17×10^3
		94	638	6690	2.370	3.39×10^3
	0.0917	50	588	3180	5.832	5.42×10^4
		74	610	4740	5.874	6.60×10^4
		94	638	5970	5.824	7.05×10^4
	0.1667	50	588	3170	10.569	3.26×10^5
		74	610	4680	10.543	3.96×10^5
		94	638	5830	10.339	4.24×10^5
	0.2417	50	588	3110	15.034	9.93×10^5
		74	610	4780	15.612	1.21×10^6
		94	638	5620	14.451	1.29×10^6
	0.3167	50	588	3120	19.762	2.82×10^6
		74	610	4350	18.312	3.44×10^6
		94	638	5500	18.530	3.68×10^6

Table 4, continued

L = 4.0 inches
d = 1.86 inches

x'	ℓ	θ	T_w	$-dt/dx$	Nu_T	Gr
0.30	0.033	50	588	2920	1.945	2.60×10^3
		74	610	5210	2.344	3.17×10^3
		94	638	6400	2.267	3.39×10^3
	0.0917	50	588	2600	4.768	5.42×10^4
		74	610	4040	5.006	6.60×10^4
		94	638	5370	5.239	7.05×10^4
	0.1667	50	588	2470	8.235	3.26×10^5
		74	610	3780	8.515	3.96×10^5
		94	638	4990	8.849	4.24×10^5
	0.2417	50	588	2300	11.118	9.93×10^5
		74	610	3700	12.085	1.21×10^6
		94	638	4650	11.956	1.29×10^6
	0.3167	50	588	2310	14.632	2.82×10^6
		74	610	3520	14.818	3.44×10^6
		94	638	4430	14.925	3.68×10^6
0.50	0.033	50	588	3450	2.298	2.60×10^3
		74	610	5700	2.565	3.17×10^3
		94	638	7050	2.497	3.39×10^3
	0.0917	50	588	2680	4.915	5.42×10^4
		74	610	4130	5.118	6.60×10^4
		94	638	5500	5.365	7.05×10^4
	0.1667	50	588	2250	7.502	3.26×10^5
		74	610	3390	7.637	3.96×10^5
		94	638	4870	8.636	4.24×10^5
	0.2417	50	588	2020	9.765	9.93×10^5
		74	610	3130	10.223	1.21×10^6
		94	638	4400	11.314	1.29×10^6
	0.3167	50	588	2020	12.795	2.82×10^6
		74	610	3050	12.840	3.44×10^6
		94	638	4130	13.914	3.68×10^6

Table 4, continued

$L' = 4.0$ inches
$d = 1.86$ inches

x'	ℓ	⊖	T_w	-dt/dx	Nu_T	Gr
0.75	0.033	50	588	3500	2.331	2.60×10^3
		74	610	5800	2.610	3.17×10^3
		94	638	7250	2.568	3.39×10^3
	0.0917	50	588	2820	5.172	5.42×10^4
		74	610	4350	5.390	6.60×10^4
		94	638	5700	5.561	7.05×10^4
	0.1667	50	588	2270	7.568	3.26×10^5
		74	610	3500	7.884	3.96×10^5
		94	638	4940	8.761	4.24×10^5
	0.2417	50	588	2130	10.296	9.93×10^5
		74	610	3120	10.190	1.21×10^6
		94	638	4500	11.571	1.29×10^6
	0.3167	50	588	2160	13.681	2.82×10^6
		74	610	3120	13.134	3.44×10^6
		94	638	4400	14.824	3.68×10^6
1.0	0.033	50	588	3500	2.331	2.60×10^3
		74	610	5800	2.610	3.17×10^3
		94	638	7250	2.568	3.39×10^3
	0.0917	50	588	2820	5.172	5.42×10^4
		74	610	4380	5.428	6.60×10^4
		94	638	5700	5.561	7.05×10^4
	0.1667	50	588	2270	7.568	3.26×10^5
		74	610	3650	8.222	3.96×10^5
		94	638	4940	8.761	4.24×10^5
	0.2417	50	588	2180	10.538	9.93×10^5
		74	610	3140	10.256	1.21×10^6
		94	638	4500	11.571	1.29×10^6
	0.3167	50	588	2180	13.808	2.82×10^6
		74	610	3130	13.176	3.44×10^6
		94	638	4400	14.824	3.68×10^6

Table 4, continued

L' = 4.0 inches
d = 0.8 inch

x'	ℓ	θ	T_w	-dt/dx	Nu_T	Gr
0.15	0.0333	48.8	587.3	4050	2.764	2.55×10^3
		74	617	5750	2.588	3.19×10^3
		100.5	640.6	7660	2.538	3.58×10^3
		112.5	659.5	10250	3.034	3.53×10^3
	0.0917	48.8	587.3	4050	7.610	5.33×10^4
		74	617	5850	7.249	6.69×10^4
		100.5	640.6	8100	7.391	7.48×10^4
		112.5	659.5	8750	7.132	7.93×10^4
	0.1667	48.8	587.3	3920	13.391	3.18×10^5
		74	617	5620	12.660	3.99×10^5
		100.5	640.6	7550	12.523	4.47×10^5
		112.5	659.5	8750	12.966	4.41×10^5
	0.2417	48.8	587.3	3700	18.326	9.74×10^5
		74	617	6330	18.366	1.22×10^6
		100.5	640.6	7450	17.917	1.37×10^6
		112.5	659.5	8900	19.121	1.35×10^6
	0.3167	48.8	587.3	3700	24.012	2.19×10^6
		74	617	5620	24.052	2.74×10^6
		100.5	640.6	7200	22.689	3.07×10^6
		112.5	659.5	8350	23.506	3.03×10^6
0.20	0.0333	48.8	587.3	3330	2.272	2.55×10^3
		74	617	4620	2.079	3.19×10^3
		100.5	640.6	6710	2.223	3.58×10^3
		112.5	659.5	8480	2.510	3.53×10^3
	0.0917	48.8	587.3	3230	6.069	5.33×10^4
		74	617	4400	5.452	6.69×10^4
		100.5	640.6	6520	5.949	7.48×10^4
		112.5	659.5	7320	5.967	7.93×10^4
	0.1667	48.8	587.3	3050	10.419	3.18×10^5
		74	617	4320	9.732	3.99×10^5
		100.5	640.6	6420	10.649	4.47×10^5
		112.5	659.5	7170	10.624	4.41×10^5
	0.2417	48.8	587.3	2900	14.363	9.74×10^5
		74	617	4410	14.404	1.22×10^6
		100.5	640.6	6210	14.935	1.37×10^6
		112.5	659.5	7250	15.558	1.35×10^6
	0.3167	48.8	587.3	2810	18.236	2.19×10^6
		74	617	4050	17.332	2.74×10^6
		100.5	640.6	5780	18.214	3.07×10^6
		112.5	659.5	6660	16.749	3.03×10^6

Table 4, continued

L' = 4.0 inches
d = 0.8 inch

x'	$\mathcal{L}$	Θ	T_w	-dt/dx	Nu_T	Gr
0.30	0.0333	48.8	587.3	2990	2.040	2.55×10^3
		74	617	4400	1.980	3.19×10^3
		100.5	640.6	6120	2.028	3.58×10^3
		112.5	659.5	7250	2.146	3.53×10^3
	0.0917	48.8	587.3	2560	4.810	5.33×10^4
		74	617	3460	4.287	6.69×10^4
		100.5	640.6	5290	4.827	7.48×10^4
		112.5	659.5	6600	5.380	7.93×10^4
	0.1667	48.8	587.3	2250	7.686	3.18×10^5
		74	617	3450	7.772	3.99×10^5
		100.5	640.6	5120	8.493	4.47×10^5
		112.5	659.5	6100	9.039	4.41×10^5
	0.2417	48.8	587.3	2240	11.094	9.74×10^5
		74	617	3410	11.138	1.22×10^6
		100.5	640.6	4860	11.688	1.37×10^6
		112.5	659.5	5880	12.633	1.35×10^6
	0.5167	48.8	587.3	2120	13.758	2.19×10^6
		74	617	3200	13.695	2.74×10^6
		100.5	640.6	4620	14.559	3.07×10^6
		112.5	659.5	5470	15.399	3.03×10^6
0.50	0.0333	48.8	587.3	3560	2.433	2.55×10^3
		74	617	5000	2.253	3.19×10^3
		100.5	640.6	7600	2.517	3.58×10^3
		112.5	659.5	8650	2.563	3.53×10^3
	0.0917	48.8	587.3	2450	4.600	5.33×10^4
		74	617	3750	4.690	6.69×10^4
		100.5	640.6	5870	5.350	7.48×10^4
		112.5	659.5	7300	5.950	7.93×10^4
	0.1667	48.8	587.3	2150	7.330	3.18×10^5
		74	617	3300	7.430	3.99×10^5
		100.5	640.6	5050	8.370	4.47×10^5
		112.5	659.5	5890	8.917	4.41×10^5
	0.2417	48.8	587.3	1900	9.400	9.74×10^5
		74	617	2750	8.992	1.22×10^6
		100.5	640.6	4450	10.708	1.37×10^6
		112.5	659.5	5240	11.483	1.35×10^6
	0.3167	48.8	587.3	1700	11.017	2.19×10^6
		74	617	2550	10.925	2.74×10^6
		100.5	640.6	4050	12.578	3.07×10^6
		112.5	659.5	4750	13.683	3.03×10^6

Table 4, continued

$L' = 4.0$ inches
$d = 0.8$ inch

x'	ℓ	Θ	T_w	$-dt/dx$	Nu_T	Gr
0.75	0.0333	48.8	587.3	3860	2.633	2.55×10^3
		74	617	5590	2.517	3.19×10^3
		100.5	640.6	8000	2.650	3.58×10^3
		112.5	659.5	9750	2.892	3.53×10^3
	0.0917	48.8	587.3	2850	5.350	5.33×10^4
		74	617	4230	5.242	6.69×10^4
		100.5	640.6	6070	5.533	7.48×10^4
		112.5	659.5	7880	6.417	7.93×10^4
	0.1667	48.8	587.3	2420	8.267	3.18×10^5
		74	617	3750	8.450	3.99×10^5
		100.5	640.6	5280	8.750	4.47×10^5
		112.5	659.5	6150	9.333	4.41×10^5
	0.2417	48.8	587.3	2110	10.442	9.74×10^5
		74	617	3160	10.317	1.22×10^6
		100.5	640.6	4700	11.308	1.37×10^6
		112.5	659.5	5480	12.033	1.35×10^6
	0.3167	48.8	587.3	1970	12.792	2.19×10^6
		74	617	2700	11.558	2.74×10^6
		100.5	640.6	4130	13.017	3.07×10^6
		112.5	659.5	5180	14.883	3.03×10^6
1.0	0.0333	48.8	587.3	3900	2.667	2.55×10^3
		74	617	5350	2.408	3.19×10^3
		100.5	640.6	8050	2.667	3.58×10^3
		112.5	659.5	9950	2.958	3.53×10^3
	0.0917	48.8	587.3	2980	5.600	5.33×10^4
		74	617	4350	5.392	6.69×10^4
		100.5	640.6	6100	5.567	7.48×10^4
		112.5	659.5	8000	6.517	7.93×10^4
	0.1667	48.8	587.3	2500	8.533	3.18×10^5
		74	617	3750	8.450	3.99×10^5
		100.5	640.6	5240	8.767	4.47×10^5
		112.5	659.5	6200	9.217	4.41×10^5
	0.2417	48.8	587.3	2210	10.950	9.74×10^5
		74	617	3350	10.950	1.22×10^6
		100.5	640.6	4900	11.792	1.37×10^6
		112.5	659.5	5500	11.892	1.35×10^6
	0.3167	48.8	587.3	2100	13.617	2.19×10^6
		74	617	3030	13.050	2.74×10^6
		100.5	640.6	4770	15.042	3.07×10^6
		112.5	659.5	5250	14.883	3.03×10^6

Table 4, continued

L' = 4.0 inches
d = 0.375 inch

x'	ℓ	Θ	T_w	-dt/dx	Nu_T	Gr
0.15	0.0333	48	587.5	3850	2.671	2.33×10^3
		73	620	5750	2.623	3.00×10^3
		103	648	8250	2.667	3.40×10^3
	0.0917	48	587.5	3920	7.489	4.85×10^4
		73	620	5620	7.060	6.24×10^4
		103	648	7450	6.633	7.06×10^4
	0.1667	48	587.5	3550	12.328	2.92×10^5
		73	620	5670	12.720	3.75×10^5
		103	648	7750	12.543	4.25×10^5
	0.2417	48	587.5	3250	16.365	8.90×10^5
		73	620	5750	19.038	1.14×10^6
		103	648	8360	19.618	1.30×10^6
	0.3167	48	587.5	3950	26.062	2.52×10^6
		73	620	5670	24.598	3.25×10^6
		103	648	7620	23.429	3.68×10^6
0.20	0.0333	48	587.5	3050	2.116	2.33×10^3
		73	620	5000	2.381	3.00×10^3
		103	648	6580	2.127	3.40×10^3
	0.0917	48	587.5	2920	5.578	4.85×10^4
		73	620	4600	5.779	6.24×10^4
		103	648	6420	5.716	7.06×10^4
	0.1667	48	587.5	2350	8.161	2.92×10^5
		73	620	3480	7.947	3.75×10^5
		103	648	5140	8.319	4.25×10^5
	0.2417	48	587.5	2000	10.071	8.90×10^5
		73	620	2940	9.734	1.14×10^6
		103	648	4810	11.250	1.30×10^6
	0.3167	48	587.5	1290	8.511	2.52×10^6
		73	620	2030	8.807	3.25×10^6
		103	648	2920	8.978	3.68×10^6

Table 4, continued

$L' = 4.0$ inches
$d = 0.375$ inch

x'	ℓ	Θ	T_w	$-dt/dx$	Nu_T	Gr
0.30	0.0333	48	587.5	2720	1.887	2.33×10^3
		73	620	4370	1.993	3.00×10^3
		103	648	5360	1.733	3.40×10^3
	0.0917	48	587.5	2320	4.452	4.85×10^4
		73	620	3680	4.623	6.24×10^4
		103	648	5250	4.674	7.06×10^4
	0.1667	48	587.5	2190	7.606	2.92×10^5
		73	620	3400	7.764	3.75×10^5
		103	648	4820	7.801	4.25×10^5
	0.2417	48	587.5	2080	10.474	8.90×10^5
		73	620	3120	10.330	1.14×10^6
		103	648	4450	10.442	1.30×10^6
	0.3167	48	587.5	2010	13.262	2.52×10^6
		73	620	3020	13.102	3.25×10^6
		103	648	4030	12.391	3.68×10^6
0.50	0.0333	48	587.5	3260	2.261	2.33×10^3
		73	620	5460	2.491	3.00×10^3
		103	648	7440	2.405	3.40×10^3
	0.0917	48	587.5	2330	4.451	4.85×10^4
		73	620	3460	4.372	6.24×10^4
		103	648	5610	4.995	7.06×10^4
	0.1667	48	587.5	2050	7.119	2.92×10^5
		73	620	3240	7.399	3.75×10^5
		103	648	4920	7.963	4.25×10^5
	0.2417	48	587.5	1800	9.064	8.90×10^5
		73	620	2610	8.641	1.14×10^6
		103	648	4120	9.668	1.30×10^6
	0.3167	48	587.5	1270	8.379	2.52×10^6
		73	620	1920	8.330	3.25×10^6
		103	648	2990	9.193	3.68×10^6

Table 4, continued

$L' = 4.0$ inches
$d = 0.375$ inch

x'	ℓ	θ	T_w	$-dt/dx$	Nu_T	Gr
0.75	0.0333	48	587.5	3550	2.463	2.33×10^3
		73	620	5530	2.523	3.00×10^3
		103	648	7950	2.570	3.40×10^3
	0.0917	48	587.5	2640	5.043	4.85×10^4
		73	620	3950	4.962	6.24×10^4
		103	648	6700	5.965	7.06×10^4
	0.1667	48	587.5	2350	8.161	2.92×10^5
		73	620	3480	7.947	3.75×10^5
		103	648	5140	8.319	4.25×10^5
	0.2417	48	587.5	2000	10.071	8.90×10^5
		73	620	2940	9.734	1.14×10^6
		103	648	4810	11.250	1.30×10^6
	0.3167	48	587.5	1290	8.511	2.52×10^6
		73	620	2030	8.807	3.25×10^6
		103	648	2920	8.978	3.68×10^6
1.0	0.0333	48	587.5	3570	2.477	2.33×10^3
		73	620	5530	2.523	3.00×10^3
		103	648	7950	2.570	3.40×10^3
	0.0917	48	587.5	2650	5.063	4.85×10^4
		73	620	4030	5.062	6.24×10^4
		103	648	6980	6.214	7.06×10^4
	0.1667	48	587.5	2400	8.335	2.92×10^5
		73	620	3530	8.061	3.75×10^5
		103	648	5175	8.375	4.25×10^5
	0.2417	48	587.5	2100	10.574	8.90×10^5
		73	620	3000	9.933	1.14×10^6
		103	648	5040	11.827	1.30×10^6
	0.3167	48	587.5	1400	9.633	2.52×10^6
		73	620	2290	9.935	3.25×10^6
		103	648	3640	11.192	3.68×10^6

Table 4, continued

$L' = 4.0$ inches
$d = 0.125$ inch

x'	ℓ	θ	T_w	$-dt/dx$	Nu_T	Gr
0.15	0.033	51	593	4150	2.710	2.690×10^3
		77	619	6000	2.595	3.150×10^3
		108	652.5	-	-	3.510×10^3
	0.0917	51	593	3930	7.066	5.600×10^4
		77	619	5820	6.931	6.550×10^4
		108	652.5	8070	6.852	7.300×10^4
	0.1667	51	593	4000	13.074	3.360×10^5
		77	619	5850	12.659	3.940×10^5
		108	652.5	9500	14.663	4.390×10^5
	0.2417	51	593	4180	19.810	1.025×10^6
		77	619	5900	18.520	1.202×10^6
		108	652.5	8050	18.016	1.340×10^6
	0.3167	51	593	4260	24.454	2.910×10^6
		77	619	6270	25.788	3.420×10^6
		108	652.5	8070	23.664	3.800×10^6
0.20	0.033	51	593	3470	2.266	2.690×10^3
		77	619	4850	2.097	3.150×10^3
		108	652.5	7820	2.411	3.510×10^3
	0.0917	51	593	3170	5.700	5.600×10^4
		77	619	4650	5.538	6.550×10^4
		108	652.5	6850	5.816	7.300×10^4
	0.1667	51	593	3120	10.198	3.360×10^5
		77	619	4620	9.998	3.940×10^5
		108	652.5	6600	10.187	4.390×10^5
	0.2417	51	593	3110	14.739	1.025×10^6
		77	619	4500	14.125	1.202×10^6
		108	652.5	6360	14.234	1.340×10^6
	0.3167	51	593	3200	19.871	2.910×10^6
		77	619	4860	19.989	3.420×10^6
		108	652.5	6400	18.767	3.800×10^6

Table 4, continued

$L' = 4.0$ inches
$d = 0.125$ inch

x'	ℓ	Θ	T_w	$-dt/dx$	Nu_T	Gr
0.30	0.033	51	593	3120	2.037	2.690×10^3
		77	619	4420	1.911	3.150×10^3
		108	652.5	6570	2.026	3.510×10^3
	0.0917	51	593	2060	3.704	5.600×10^4
		77	619	3790	4.514	6.550×10^4
		108	652.5	5370	4.560	7.300×10^4
	0.1667	51	593	2420	7.910	3.360×10^5
		77	619	3520	7.617	3.940×10^5
		108	652.5	5120	7.903	4.390×10^5
	0.2417	51	593	2130	10.094	1.025×10^6
		77	619	3180	9.982	1.202×10^6
		108	652.5	4570	10.228	1.340×10^6
	0.3167	51	593	1860	11.550	2.910×10^6
		77	619	2900	11.927	3.420×10^6
		108	652.5	4110	12.052	3.800×10^6
0.50	0.033	51	593	3490	2.279	2.690×10^3
		77	619	5420	2.344	3.150×10^3
		108	652.5	8330	2.568	3.510×10^3
	0.0917	51	593	2610	4.693	5.600×10^4
		77	619	3910	4.656	6.550×10^4
		108	652.5	6150	5.222	7.300×10^4
	0.1667	51	593	2280	7.452	3.360×10^5
		77	619	3120	6.752	3.940×10^5
		108	652.5	5030	7.764	4.390×10^5
	0.2417	51	593	1830	8.673	1.025×10^6
		77	619	3520	11.049	1.202×10^6
		108	652.5	3930	8.795	1.340×10^6
	0.3167	51	593	900	5.589	2.910×10^6
		77	619	1360	5.594	3.420×10^6
		108	652.5	2000	5.865	3.800×10^6

Table 4, continued

$L' = 4.0$ inches
$d = 0.125$ inch

x'	ℓ	θ	T_w	$-dt/dx$	Nu_T	Gr
0.75	0.033	51	593	3710	2.422	2.690×10^3
		77	619	5680	2.456	3.150×10^3
		108	652.5	8560	2.639	3.510×10^3
	0.917	51	593	2900	5.214	5.600×10^4
		77	619	4170	4.966	6.550×10^4
		108	652.5	6920	5.876	7.300×10^4
	0.1667	51	593	2280	7.452	3.360×10^5
		77	619	3470	7.509	3.940×10^5
		108	652.5	5630	8.690	4.390×10^5
	0.2417	51	593	2000	9.478	1.025×10^6
		77	619	2790	8.758	1.202×10^6
		108	652.5	4510	10.093	1.340×10^6
	0.3167	51	593	1090	6.769	2.910×10^6
		77	619	1250	5.141	3.420×10^6
		108	652.5	1950	5.718	3.800×10^6
1.0	0.033	51	593	3710	2.422	2.690×10^3
		77	619	5680	2.456	3.150×10^3
		108	652.5	8550	2.636	3.510×10^3
	0.0917	51	593	2900	5.214	5.600×10^4
		77	619	4210	5.014	6.550×10^4
		108	652.5	7000	5.943	7.300×10^4
	0.1667	51	593	2280	7.452	3.360×10^5
		77	619	3500	7.574	3.940×10^5
		108	652.5	5600	8.644	4.390×10^5
	0.2417	51	593	2000	9.478	1.025×10^6
		77	619	2920	9.166	1.202×10^6
		108	652.5	4910	10.989	1.340×10^6
	0.3167	51	593	1130	7.017	2.910×10^6
		77	619	1250	5.141	3.420×10^6
		108	652.5	2250	6.598	3.800×10^6

Table 4, continued

$L' = 2.0$ inches
$d = 1.8$ inches

x'	ξ	θ	T_w	$-dt/dx$	Nu_T	Gr
0.15	0.0167	108	653	7600	1.170	4.500×10^2
	0.0500	108	653	7600	3.520	7.210×10^3
	0.0833	108	653	7600	5.860	5.560×10^4
	0.1167	108	653	7600	7.650	1.528×10^5
	0.1500	108	653	7600	10.550	3.240×10^5
0.20	0.0167	108	653	6900	1.060	4.500×10^2
	0.0500	108	653	6250	2.890	7.210×10^3
	0.0833	108	653	6250	4.820	5.560×10^4
	0.1167	108	653	6250	6.300	1.523×10^5
	0.1500	108	653	6250	8.680	3.240×10^5
0.30	0.0167	108	653	7700	1.181	4.500×10^2
	0.0500	108	653	5650	2.620	7.210×10^3
	0.0833	108	653	5080	3.920	5.560×10^4
	0.1167	108	653	5080	5.120	1.528×10^5
	0.1500	108	653	5250	7.300	3.240×10^5
0.50	0.0167	108	653	9100	1.400	4.500×10^2
	0.0500	108	653	6720	3.115	7.210×10^3
	0.0833	108	653	5650	4.360	5.560×10^4
	0.1167	108	653	5130	5.170	1.528×10^5
	0.1500	108	653	4970	6.900	3.240×10^5
0.75	0.0167	108	653	9530	1.463	4.500×10^2
	0.0500	108	653	6910	3.200	7.210×10^3
	0.0833	108	653	5980	4.610	5.560×10^4
	0.1167	108	653	5400	5.440	1.528×10^5
	0.1500	108	653	5230	7.260	3.240×10^5
1.0	0.0167	108	653	9530	1.463	4.500×10^2
	0.0500	108	653	6910	3.200	7.210×10^3
	0.0833	108	653	5980	4.610	5.560×10^4
	0.1167	108	653	5400	5.440	1.528×10^5
	0.1500	108	653	5240	7.270	3.240×10^5

$L' = 2.0$ inches
$d = 0.8$ inch

Table 4, continued

x'	ℓ	Θ	T_w	$-dt/dx$	Nu_T	Gr
0.15	0.0167	70	615	5330	1.325	3.66×10^2
		104	650	7750	1.242	4.35×10^2
	0.0500	70	615	5330	3.978	5.94×10^3
		104	650	7750	3.726	7.05×10^3
	0.0833	70	615	5330	6.629	4.57×10^4
		104	650	7750	6.210	5.43×10^4
	0.1167	70	615	5330	9.281	1.25×10^5
		104	650	7750	8.696	1.49×10^5
	0.1500	70	615	5330	11.933	2.67×10^5
		104	650	7750	11.176	3.17×10^5
0.20	0.0167	70	615	4520	1.124	3.66×10^2
		104	650	7200	1.153	4.35×10^2
	0.0500	70	615	4170	3.112	5.94×10^3
		104	650	5820	2.798	7.05×10^3
	0.0833	70	615	4170	5.186	4.57×10^4
		104	650	5820	4.664	5.43×10^4
	0.1167	70	615	4170	7.261	1.25×10^5
		104	650	5820	6.530	1.49×10^5
	0.1500	70	615	4170	9.336	2.67×10^5
		104	650	5820	8.392	3.17×10^5
0.30	0.0167	70	615	4270	1.062	3.66×10^2
		104	650	8400	1.346	4.35×10^2
	0.0500	70	615	3300	2.463	5.94×10^3
		104	650	5330	2.563	7.05×10^3
	0.0833	70	615	3120	3.880	4.57×10^4
		104	650	4800	3.846	5.43×10^4
	0.1167	70	615	2960	5.154	1.25×10^5
		104	650	4630	5.195	1.49×10^5
	0.1500	70	615	3120	6.985	2.67×10^5
		104	650	4630	6.676	3.17×10^5

Table 4, continued

L' = 2.0 inches
d = 0.8 inch

x'	ℓ	Θ	T_w	-dt/dx	Nu_T	Gr
0.50	0.0167	70	615	5800	1.443	3.66×10^2
		104	650	9450	1.514	4.35×10^2
	0.0500	70	615	4020	3.000	5.94×10^3
		104	650	6570	3.159	7.05×10^3
	0.0833	70	615	3380	4.204	4.57×10^4
		104	650	5580	4.471	5.43×10^4
	0.1167	70	615	3020	5.259	1.25×10^5
		104	650	4900	5.498	1.49×10^5
	0.1500	70	615	2680	6.000	2.67×10^5
		104	650	4790	6.907	3.17×10^5
0.75	0.0167	70	615	6190	1.474	3.66×10^2
		104	650	9640	1.544	4.35×10^2
	0.0500	70	615	4450	3.178	5.94×10^3
		104	650	7230	3.476	7.05×10^3
	0.0833	70	615	3780	4.500	4.57×10^4
		104	650	6070	4.864	5.43×10^4
	0.1167	70	615	3330	5.550	1.25×10^5
		104	650	5250	5.890	1.49×10^5
	0.1500	70	615	3250	6.965	2.67×10^5
		104	650	5080	7.325	3.17×10^5
1.0	0.0167	70	615	6260	1.491	3.66×10^2
		104	650	9640	1.544	4.35×10^2
	0.0500	70	615	4450	3.178	5.94×10^3
		104	650	7250	3.486	7.05×10^3
	0.0833	70	615	3790	4.512	4.57×10^4
		104	650	6070	4.864	5.43×10^4
	0.1167	70	615	3390	5.650	1.25×10^5
		104	650	5320	5.969	1.49×10^5
	0.1500	70	615	3300	7.072	2.67×10^5
		104	650	5160	7.441	3.17×10^5

Table 4, continued

$L' = 2.0$ inches
$d = 0.375$ inch

x'	ℓ	θ	T_w	$-dt/dx$	Nu_T	Gr
0.15	0.0167	104	652	7500	1.200	4.300×10^2
	0.0500	104	652	7500	3.600	6.960×10^3
	0.0833	104	652	7500	6.020	5.370×10^4
	0.1167	104	652	7500	8.400	1.473×10^5
	0.1500	104	652	7500	10.800	3.130×10^5
0.20	0.0167	104	652	6550	1.047	4.300×10^2
	0.0500	104	652	5900	2.840	6.960×10^3
	0.0833	104	652	5900	4.730	5.370×10^4
	0.1167	104	652	5900	6.600	1.473×10^5
	0.1500	104	652	5900	8.500	3.130×10^5
0.30	0.0167	104	652	7050	1.126	4.300×10^2
	0.0500	104	652	4650	2.240	6.960×10^3
	0.0833	104	652	4300	3.450	5.370×10^4
	0.1167	104	652	4100	4.590	1.473×10^5
	0.1500	104	652	4070	5.850	3.130×10^5
0.50	0.0167	104	652	9320	1.490	4.300×10^2
	0.0500	104	652	6050	2.910	6.960×10^3
	0.0833	104	652	4250	3.410	5.370×10^4
	0.1167	104	652	3470	3.880	1.473×10^5
	0.1500	104	652	2950	4.250	3.130×10^5
0.75	0.0167	104	652	9470	1.512	4.300×10^2
	0.0500	104	652	6230	2.995	6.960×10^3
	0.0833	104	652	5100	4.090	5.370×10^4
	0.1167	104	652	4060	4.550	1.473×10^5
	0.150[illegible]	104	652	3250	4.670	3.130×10^5
1.0	0.0167	104	652	9470	1.512	4.300×10^2
	0.0500	104	652	6230	2.995	6.960×10^3
	0.0833	104	652	5350	4.290	5.370×10^4
	0.1167	104	652	4620	5.170	1.473×10^5
	0.1500	104	652	3470	5.710	3.130×10^5

Table 4, continued

$L' = 2.0$ inches
$d = 0.125$ inch

x'	ℓ	θ	T_w	-dt/dx	NuT	Gr
0.15	0.0167	99	647	7300	1.225	4.200×10^2
	0.0500	99	647	7300	3.685	6.800×10^3
	0.0833	99	647	7300	6.150	5.240×10^4
	0.1167	99	647	7300	8.600	1.440×10^5
	0.1500	99	647	7300	11.030	3.060×10^5
0.20	0.0167	99	647	6350	1.065	4.200×10^2
	0.0500	99	647	5550	2.800	6.800×10^3
	0.0833	99	647	5550	4.670	5.240×10^4
	0.1167	99	647	5550	6.550	1.440×10^5
	0.1500	99	647	5550	8.400	3.060×10^5
0.30	0.0167	99	647	7500	1.260	4.200×10^2
	0.0500	99	647	4250	2.150	6.800×10^3
	0.0833	99	647	3970	3.340	5.240×10^4
	0.1167	99	647	3870	4.570	1.440×10^5
	0.1500	99	647	3700	5.600	3.060×10^5
0.50	0.0167	99	647	8680	1.458	4.200×10^2
	0.0500	99	647	5600	2.830	6.800×10^3
	0.0833	99	647	3950	3.320	5.240×10^4
	0.1167	99	647	2980	3.520	1.440×10^5
	0.1500	99	647	1950	2.960	3.060×10^5
0.75	0.0167	99	647	8920	1.497	4.200×10^2
	0.0500	99	647	6200	3.130	6.800×10^3
	0.0833	99	647	4480	3.775	5.240×10^4
	0.1167	99	647	3300	3.900	1.440×10^5
	0.1500	99	647	2250	3.410	3.060×10^5
1.0	0.0167	99	647	8920	1.497	4.200×10^2
	0.0500	99	647	6200	3.130	6.800×10^3
	0.0833	99	647	4480	3.775	5.240×10^4
	0.1167	99	647	3450	4.070	1.440×10^5
	0.1500	99	647	2500	3.780	3.060×10^5

AUTOBIOGRAPHY

I, David Jenks Masson, was born in Lorain, Ohio, May 8, 1920. I received my secondary school education in the public schools of the city of Lorain, Ohio. My undergraduate training was obtained at The Ohio State University, from which I received the degree Bachelor of Mechanical Engineering in 1943. Also from The Ohio State University, I received the degree Master of Science in 1946. In 1947, I received an appointment as Instructor in Mechanical Engineering in The Ohio State University where I specialized in the Department of Mechanical Engineering. I held this position for five years while completing the requirements for the degree Doctor of Philosophy.